université de BORDEAUX

THÈSE PRÉSENTÉE

POUR OBTENIR LE GRADE DE

DOCTEUR DE

L'UNIVERSITÉ DE BORDEAUX

ÉCOLE DOCTORALE SCIENCES CHIMIQUES

SPÉCIALITÉ POLYMERES

Par **Mohd Azmil MOHD NOOR**

STABILISATION D'EMULSIONS DE PICKERING HUILE-DANS-EAU PAR DES NANOCRISTAUX DE CELLULOSE POUR L'ENCAPSULATION ET LA PROTECTION CONTRE L'OXYDATION

STABILISATION OF OIL-IN-WATER PICKERING EMULSIONS WITH CELLULOSE NANOCRYSTALS FOR ENCAPSULATION AND OXIDATIVE PROTECTION

Sous la direction de : Gilles SEBE et Chrystel FAURE

Soutenue le 1 octobre 2024

Membres du jury :

M. CRAMAIL Henri	Professeur, Université de Bordeaux	Président
Mme CAPRON Isabelle	Directrice de recherche, INRAE Nantes	Rapporteure
Mme DRELICH Audrey	Maître de Conférences, UTC, Compiègne	Rapporteure
Mme JOSEPH Cécile	Ingénieure de recherche, ITERG	Examinatrice
M. SEBE Gilles	Maître de Conférences, Université de Bordeaux	Co-directeur
Mme. FAURE Chrystel	Professeure, Bordeaux INP	Co-directrice
M. AZIZUL HASAN Zafarizal Aldrin	Directeur, Malaysian Palm Oil Board	Invité

Titre : Stabilisation d'emulsions de Pickering huile-dans-eau par des nanocristaux de cellulose pour l'encapsulation et la protection contre l'oxydation

Résumé :

Dans ce travail de thèse, des émulsions de Pickering stabilisées par des nanocristaux de cellulose (NCCs) modifiés chimiquement ou non, ont été préparées à partir de différentes huiles & concentrations en sel, et étudiées en termes de stabilité, couverture de surface, propriétés d'encapsulation/relargage et protection contre l'oxydation. Quelle que soit l'huile utilisée, une relation linéaire entre l'inverse du diamètre des gouttes et la concentration en NCCs a été observée, en accord avec le mécanisme de coalescence limitée attendu pour les émulsions de Pickering. La couverture de surface par les particules autour des gouttes a été estimée en calculant le pourcentage de couverture C et l'aire de surface spécifique S, à partir de la pente du domaine de coalescence limitée. Une relation linéaire entre C (ou S) et la force ionique a pu être démontrée, ce qui permet d'envisager un control de la couverture de surface par les particules, à partir de la concentration en sel. Après incorporation du resvératrol (RSV) dans la phase interne de l'émulsion, l'utilisation de sel ne s'est plus avérée nécessaire pour stabiliser l'émulsion, le paramètre C étant maintenant corrélé avec la concentration en RSV plutôt qu'avec la force ionique, les molécules de RSV agissant comme co-stabilisants à l'interface. Les expériences de relargage ont montré une relation linéaire entre le taux de libération interfacial et la couverture de surface autour des gouttes. Enfin, les émulsions huile de lin-dans-eau stabilisées à partir de NCCs non modifiés ont montré une certaine protection contre l'oxydation lipidique en comparaison avec le SDS. Les propriétés protectrices des CNCs ont plus tard été encore améliorées, en fonctionnalisant la surface des nanoparticules avec la polydopamine, à partir d'un simple procédé aqueux.

Mots clés : Nanocristaux de cellulose, émulsion de Pickering, resvératrol, encapsulation, oxydation lipidique

---

Laboratoire de Chimie des Polymères Organiques

[LCPO, UMR 5629, 16 avenue Pey Berland 33607 PESSAC]

Institut de Chimie et Biologie des Membranes et des Nano-objets

[CBMN, UMR 5248, Allée de Geoffroy St Hilaire 33607 PESSAC]

Title : Stabilisation of oil-in-water Pickering emulsions with cellulose nanocrystals for encapsulation and oxidative protection

Abstract :

In this Ph.D. work, oil-in-water (O/W) Pickering emulsions stabilized by unmodified and chemically modified cellulose nanocrystals (CNCs) were prepared using different oils & salt concentrations, and investigated in terms of stability, surface coverage, encapsulation/release properties, and oxidative protection. Regardless of the oil investigated, a linear dependence of the inverse droplet diameter on CNCs concentration was observed, in line with the limited coalescence process expected for Pickering emulsions. The surface coverage by the particles around the droplets was estimated by calculating the coverage percentage C and specific surface area S, based on the slope of the limited coalescence domain. A linear dependency of C and S with the ionic strength was demonstrated, showing that the surface coverage by the particles can be monitored by the salt concentration. When resveratrol (RSV) was incorporated in the internal phase of the emulsion, salt was not required anymore to stabilize the emulsion and the C value was now correlated to the RSV concentration instead of the ionic strength, the RSV molecules acting as co-stabilizers at the interface. Release experiments showed a linear dependency of the interfacial release rate with the surface coverage around the droplets. Finally, the linseed oil-in-water emulsions stabilized with unmodified CNCs, were shown to partially protect the oil from lipid oxidation in comparison to SDS. The protective properties of the CNCs were later further improved, by functionalizing the nanoparticles surface with polydopamine, using a simple process in water.

Keywords : Cellulose nanocrystals, Pickering emulsion, resveratrol, encapsulation, lipid oxidation

---

Laboratoire de Chimie des Polymères Organiques

[LCPO, UMR 5629, 16 avenue Pey Berland 33607 PESSAC]

Institut de Chimie et Biologie des Membranes et des Nano-objets

[CBMN, UMR 5248, Allée de Geoffroy St Hilaire 33607 PESSAC]

Summary

Acknowledgements 1

List of abbreviations 5

General introduction 6

Chapter I. State-of-the-art 10

A. Pickering emulsions 10

B. Cellulose nanocrystals (CNCs) 19

C. Utilization of the CNCs as Pickering particles 32

D. Encapsulation and delivery of resveratrol (RSV) 39

E. Oxidative instability of oil-in-water emulsions 49

F. Conclusion on the literature review 58

Chapter II. Materials and methods 69

A. Preparation and characterisation of the Pickering particles 69

B. Characterisation of the CNCs dispersions 80

C. Pickering emulsification and RSV incorporation 82

D. Characterisation of the Pickering emulsions 83

E. Quantification of RSV by UV-vis spectroscopy 84

F. Evaluation of RSV uptake 86

G. Release profiles of incorporated RSV and evaluation of the interfacial rate constant ... 86

H. Release of interfacial RSV by addition of SDS 87

I. Evaluation of lipid oxidation by the conjugated dienes method 88

Chapter III. Formulation of the Pickering emulsions 93

A. Investigations with hexadecane as model oil 93

B. Investigations with other oils 104

C. Conclusions 113

Chapter IV. Incorporation of resveratrol in CNCs-stabilised emulsions and release study ..117

A. Incorporation of resveratrol 117

B. Co-stabilising properties of resveratrol at the oil-water interface 122

C. Release profiles of incorporated RSV 130

D. Conclusions 135

Chapter V. Oxidative stabilisation of linseed oil emulsions 138

A. Protocol 138

B. Oxidative stability of the emulsions stabilized with the unmodified CNCs 139

C. Oxidative stability of the emulsions stabilized with chemically modified CNCs..... 146

D. Conclusions 150

General conclusions and perspectives 152

Acknowledgements

First of all, I would like to thank my supervisors, Dr. Gilles SÈBE and Prof. Dr. Chrystel FAURE, for this Ph.D. opportunity and guidance throughout the Ph.D. study.

I am very thankful to all the committee members of Ph.D. defence: Prof. Dr. Henri CRAMAIL, Dr. Isabelle CAPRON, Dr. Audrey DRELICH and Dr. Cecile JOSEPH. Thank you for the insightful and inspiring discussions. I also would like to thank my Ph.D. follow-up committee members: Prof. Dr. Laurent POUYSEGU and Dr. Jean-Paul Douliez.

I would like to express my gratitude to Malaysian Palm Oil Board for the financial support. Many thanks to Dr. Zafarizal Aldrin AZIZUL HASAN as my MPOB supervisor, Ms. Razmah GHAZALI and Dr. Nur Aainaa Syahirah RAMLI as my direct superiors in MPOB, as well as Dr. Tuan Noor Maznee TUAN ISMAIL, Dr. LIM Wen Huei and Dr. Elina HISHAMUDDIN as my mentors during this Ph.D. study. I will not forget the staffs in MPOB training unit for their bureaucratic assistance. Ab Halim AB JALAL for sending the samples from Malaysia. Fellow colleagues in QNS Group, QEA Unit, AOTD and MPOB. Ms. Fadzlina ABDULLAH for helping me out.

I also appreciate very much the support from the University of Bordeaux, EDSC and CNRS, as well as the warm welcome from both laboratories: LCPO (Director: Prof. Dr. Sébastien LECOMMANDOUX) and CBMN (Director: Dr. Sophie LECOMTE).

I am very thankful for my talented labmates in LCPO and CBMN. These amazing lab mates always motivated and encouraged me throughout my three years in the lab:

- My officemates: Yelin HOU, Solène MEYNAUD and Christian

- ❑ The ‘Emulsional’ team: Christy HSIN-Chen Chen and Yelin HOU (Sorry Christy, I used the term first since I got to viva first 😉)
- ❑ Dr. Dharshana
- ❑ Helpful chat: Zakir AMIROV
- ❑ Technical support: Olivier SANDRE, Sylvain BOURASSEAU, Amélie, Frédérique HAM-PICHAVANT, Paul MARQUE, Emmanuel IBARBOURE, Léna ALEMBIK, Cédric LE COZ
- ❑ Big office: Dr. Jessie JACOB, Dr. Jérémy, Dr. Jamie, Dr. Clémence Casenave, Tiphaine, Dr. Yunhui WANG
- ❑ N0: Amaury Furet
- ❑ Lab next door: Romain, Lou, Maeva
- ❑ Dr. Mostafa BADRLEDIN
- ❑ Sweet couple: Dr. Dijwar YILMAZ, Dr. Clémence SCHWARTZMANN
- ❑ Helpful N2: Dr. Anouk Martin, Elise Courtecuisse, Hannah Beauseroy
- ❑ Cheerful environment: Alban CHARLIER
- ❑ Cohort Spring 2021: Manon CARRE, Dr. Quentin Jaussaud, Sifan Ji, Corentin Verilhac
- ❑ Chinese team: Yupei Ma, Dr. Huikang YANG, Yue Yu, Dongxu Zhou
- ❑ N1: Dr. Bárbara Farías, Nichollas Guimarães Jaques, Nadia SINGRAFF, Dr. Assia Stiti
- ❑ CBMN: Christelle HARSCOAT-SCHIAVO, Raphaelle SAVOIRE, Julien MONTEIL, Emmanuelle POQUE
- ❑ Antoine BERNASQUE, Lucie PERIE, Alix GOMBAERT, twin sisters
- ❑ Administration personnels: Séverine SAINT-DRENANT, Émilie LALANDE, Claude LE PIERRES, Anderson MENDONCA MEDEIROS
- ❑ Acceuil, cleaners

Special thanks go to Estelle MORVAN (IECB) for the NMR analyses, and to Isabelle SVAHN (Bordeaux Imaging Cente, UAR 3420 CNRS US4 INSERM) for the cryo-SEM analyses.

Last but not least, I would like to take this opportunity to thank CAF Gironde for the diverse support, without which, my 3 year-stay in Bordeaux would have been different.

Special dedication

This thesis is dedicated to my other half, Nurul Shafrah SHAHARIL. I would split my thesis into two if I could and would share it with you. And also, our *qurrata a'yun* (قُرَّةَ أَعْيُنٍ) Iyad, Emir and Ayman. Thank you for keeping me company in Bordeaux during these 3 years. We did really enjoy the short stay in the southwestern part of France, and we went through the hardship together.

Mama and ayah for believing in me. Looking after the house in Dengkil, Malaysia. Mira, Jack and Ajim, my brothers and sister: I really hope you are inspired by the efforts that we have made.

Mak and abah for never stopped supporting. Brothers and sisters-in-law.

My late auntie Mak Ngah (Rokiah ABU, ex-MPOB) for showing very good example. She was the reason why I got the research officer post in AOTD, MPOB.

Families:

Kg Pandan, Bik Ros, Bik Farah, Uncle

Malaccans and Singaporeans

Motivations from Dr. Vahid SENDIJAREVIC and Dr. Hazimah ABU HASSAN. They believed in me right from the day they met me in AOTD, MPOB and have never since stopped pushing me to achieve the highest level in my life. They are my tutors, my superiors, my peers, my elders and my friends all the time.

Zailan ABU BAKAR for the moral boost.

List of abbreviations

BCNFs	Bacterial cellulose nanofibrils
C	Surface coverage
CD	Conjugated dienes
CNC-Cin	Cinnamoyl-modified cellulose nanocrystals
CNC-Oct	Octanoate-modified cellulose nanocrystals
CNC-PDA	Polydopamine-coated cellulose nanocrystals
CNCs	Cellulose nanocrystals
CNFs	Cellulose nanofibrils
CP-MAS NMR	Cross-polarization magic-angle-spinning nuclear magnetic resonance
CRF	Cumulative fractional release
CTAB	Cetyltrimethylammonium bromide
DLS	Dynamic light scattering
DMAB	Didecyldimethylammonium bromide
DMF	Dimethylformamide
DMSO	Dimethyl sulfoxide
DODA	Dioctadecyldimethylammonium bromide
DS	Degree of substitution
DS_{Surf}	Surface degree of substitution
D(3,2)	Surface-averaged diameter
D(4,3)	Volume-averaged diameter
EE	Encapsulation efficiency
HR	Hydrodynamic radius
IV	Iodine value
NaCl	Sodium chloride
OSA	Octenyl succinic anhydride
O/W	Oil-in-water
P	Uniformity
pAV	p-Anisidine value
PDA	Polydopamine
PDI	Polydispersity index
PMMA	Poly(methyl methacrylate)
PV	Peroxide value
RSV	Resveratrol
S	Specific surface area
SCFA	Short-chain fatty acid
SDS	Sodium dodecyl sulphate
SEM	Scanning electron microscope
TBARs	Thiobarbituric acid reactive substances value
TEMPO	2,2,6,6-tetramethylpiperidine-1-oxyl
U	Uptake
W/O	Water-in-oil

General introduction

Pickering emulsions, *i.e.* particle-stabilised emulsion, have gained a renewed interest quite recently since their early disclosure in 1907 by Ramsden and Pickering. They share similarities with the conventional surfactant-based emulsions, yet they offer enhanced long-term stability, good biocompatibility and tunable properties. Many inorganic and organic particles have already proved to be efficient Pickering stabilizers for most common oils, but the utilisation of biopolymers is increasingly considered, due to their greener potential.

Cellulose nanocrystals (CNCs) are particularly attractive in this regard, as they are bio-sourced, biodegradable, sustainable and biocompatible. The efficiency of the CNCs as Pickering stabilizer has been already demonstrated, but is conditioned by a fine control of the hydrophilic/hydrophobic balance at the CNCs surface and the electrostatic repulsion between negatively charged CNCs through screening by addition of salt. Up to now, most of the studies reporting on the role of salt compared the properties of emulsions produced with or without salt, but the impact of salt concentration on the droplets surface coverage by the CNCs has never been really investigated. Additionally, the ability to control the release of an active molecule through CNCs-stabilized emulsions is essential for drug delivery applications. Owing to their low toxicity and biocompatibility, nanocellulose-based Pickering emulsions (*i.e.* stabilized by CNCs, nanofibrillated cellulose or bacterial cellulose) are indeed good candidates to encapsulate active molecules or oils, for applications in food or cosmetics.

Among the active molecules that could benefit from a protective encapsulation by CNC-based emulsions, resveratrol (RSV, a natural polyphenolic phytoalexin) is a good model candidate, as its utilisation in pharmaceutical, cosmetics and food industry is limited by its poor water solubility, high chemical instability and low oral bioavailability. Its encapsulation in Pickering emulsions stabilized by modified starch or lignin has been recently envisaged, but the

utilization of CNCs-based systems remains unexplored. Moreover, the relationship between release kinetics and surface coverage has still not been addressed to our knowledge.

The improvement of the oxidative stability of polyunsaturated oils (*e.g.* linseed oil) in oil–in–water (O/W) emulsion systems is also of great concern for the food and pharmaceutical industries. The oxidative stability in Pickering emulsions has been suggested to be higher than in conventional emulsions, due to the physical barrier form by the particles at the O/W interface. Yet, fundamental studies with CNCs systems are rare, and possible improvements by particles functionalization with active moieties (antioxidant, photoreactive...) still need to be explored.

In this Ph.D. project, oil-in-water (O/W) Pickering emulsions stabilized by unmodified and modified CNCs were prepared using different oils and salt concentrations, and investigated in terms of stability, surface coverage, encapsulation/release properties, and oxidative protection.

The first main objective was to investigate how the surface coverage by the CNCs at the O/W interface can be controlled, and how the later affects the interfacial release kinetics of a model active molecule (RSV) incorporated in the oil droplets.

The second objective was to explore the potential of unmodified and modified CNCs, to stabilize a highly oxidable O/W emulsion based on linseed oil, and protect it against lipid oxidation.

This Ph.D. project is a collaboration between the Malaysian Palm Oil Board (MPOB, Malaysia), the *Laboratoire de Chimie des Polymères Organiques* (LCPO, *Université de Bordeaux*, France) and the *Institut de Chimie et Biologie des Membranes et des Nano-objets* (CBMN, *Université de Bordeaux*, France).

This thesis is divided in five chapters:

The first chapter (Chapter I) describes the state-of-the-art in the field. Pickering emulsions and cellulose nanocrystals are first presented, followed by an overview on the encapsulation and delivery of RSV. This chapter ends with a paragraph on the oxidative instability of O/W emulsions.

Chapter II is an experimental section dedicated to the description of the materials, protocols and characterisation methods used throughout this thesis.

Chapter III is devoted to the formulation of CNCs-stabilized Pickering emulsions, first with hexadecane as model oil, then with various commercial oils.

Chapter IV details the incorporation of RSV in the CNCs-stabilized Pickering emulsions prepared with hexadecane, its impact on the O/W interface, and the release profile of this system.

The final chapter (Chapter V) reports on the oxidative protection of O/W Pickering emulsions stabilized with unmodified and modified CNCs, prepared with a highly oxidable oil (linseed oil).

Chapter I. State-of-the-art

A. Pickering emulsions

Pickering emulsions are emulsion systems stabilised by solid colloidal particles in the micro- or nanometer range, pioneered by Ramsden (Ramsden, 1904) and Pickering (Pickering, 1907). In these systems, the stabilization of emulsion droplets takes place through the adsorption of solid particles at the surface of emulsion droplets, instead of surfactants like in the case of classical emulsions (Figure I-1). The strong anchoring of the particles at the oil/water interface is the result of the partial wetting of the solid particles by water and oil.

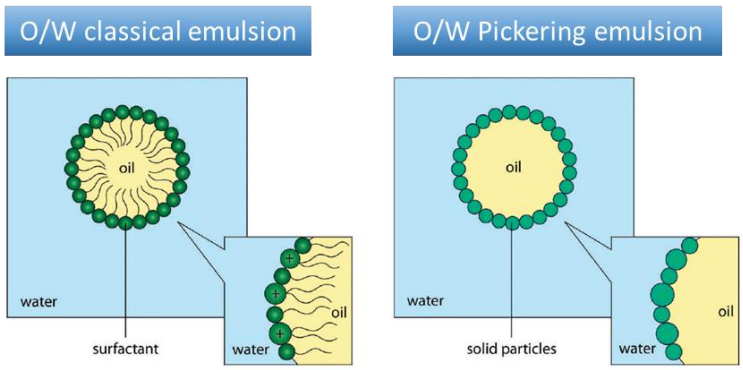

Figure I-1. Schematic illustration of classical and Pickering emulsions (Marto et al., 2016).

Pickering emulsions are commonly prepared using homogenization methods such as rotor-stator homogenization, high-pressure homogenization and sonication, in order to provide sufficient energy to overcome the energy barrier of particle adsorption (Wu and Ma, 2016). The availability of particles at the interface between the oil and aqueous phases offers high resistance to coalescence, low toxicity, and possible stimuli-responsiveness compared to classical emulsions stabilized by surfactants. The solid particles also provide a rigid shell around the droplets, which can protect sensitive compounds from the surrounding environment. These advantages of Pickering emulsions render them appealing for several applications fields,

such as food, cosmetics, pharmaceutical and biomedicine, where chemical surfactants often show adverse effects.

1. Pickering particles

Many types of particles of different morphology (size and shape) and chemical nature (inorganic or organic) have already proved to be efficient Pickering stabilizers for most common oils (Wu and Ma, 2016). The size of the particles is particularly important as smaller particles form a denser layer around the droplets and lower the interfacial tension more effectively than the bigger ones (Qi et al., 2014). Spherical particles are the most studied in the literature, but the stabilization efficiency of rods, fibres, cubes and platelets is increasingly regarded (Figure I-2).

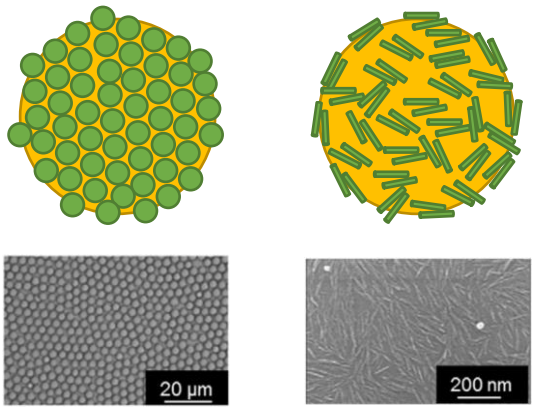

Figure I-2. Comparison of the layer formed by spheres (top left) and rods (top right) at the oil/water interface of a stabilized droplet. Optical microscopic image of spherical latex particles with a diameter of 3.5 µm (bottom left). Scanning electron microscope (SEM) image of rod-shaped cotton nanocelluloses 175 nm long and 10 nm wide (Capron et al., 2017).

Regarding the nature of the Pickering stabilizers, inorganic particles have been the most investigated up to now, *e.g.* silica nanoparticles, nanoclays (montmorillonite and laponite), or paramagnetic nanoparticles (iron-based for instance) (Chevalier and Bolzinger, 2013). These

inorganic particles have many advantages, such as a regular shape, good availability, adjustable size and narrow size distribution, but they lack biodegradability.

More recently, biopolymers (polymers produced by living organisms, which include proteins and polysaccharides), have been utilized to stabilise Pickering emulsions, due to their potentially greener and more sustainable potential (Dupont et al., 2021). Both plant-based (soy and zein) and animal-based (casein, whey, lactoglobulin and bovine serum albumin) protein nanoparticles are particularly efficient to stabilize both oil-in-water (O/W) and water-in-oil (W/O) emulsions, and can be used in synergy with polysaccharides in the form of complexes. Polysaccharides particles (*e.g.* cellulose, chitin, chitosan and starch) are also increasingly considered (in particular cellulose nanocrystals or nanofibrils), as they satisfy the increasing demand for sustainable and environmentally friendly emulsifiers (see Part B) (Fujisawa et al., 2017).

2. Particles wettability and energy of adsorption

Unlike surfactant-based emulsions, Pickering emulsions are characterised by the irreversible adsorption of the particles at the oil/water interfaces (Wiley, 1954). The wettability of the particulate emulsifiers is the key parameter governing the type (O/W or W/O) and stability of the emulsion (Aveyard et al., 2003; Binks and Lumsdon, 2000); it is expressed by the contact angle θ_{ow} that the particles make at the oil-water interface (Figure I-3). Hydrophilic particles, which display more affinity for the water phase ($\theta_{ow} < 90°$), are favouring O/W emulsions, whereas hydrophobic particles, which display more affinity for the oil phase ($\theta_{ow} > 90°$) are favouring W/O emulsions.

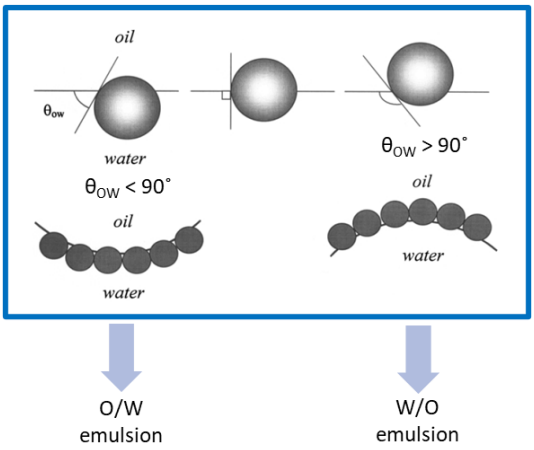

Figure I-3. Impact of the particle's contact angle on the type of emulsion formed (Aveyard et al., 2003).

The energy of attachment of a particle to a fluid-fluid interface is related to both the contact angle θ_{ow} and the oil/water interfacial tension γ_{ow}. Assuming that the particle is spherical and small enough so that the effect of gravity is negligible (typically when the particles size is in the nanometer range), the energy E required to remove the particle from the interface into one of the bulk phases, is given by Equation I-1.

$$E = \pi r^2 \gamma_{ow} (1 \pm cos\theta_{ow})^2 \qquad \textit{Equation I-1}$$

in which r is the particle radius, γ_{ow} is the oil/water interfacial tension, θ_{ow} is the contact angle that the particles make at the oil-water interface; when $\theta_{ow} < 90°$ (hydrophilic particles), the sign inside the bracket is negative and the particle is removed into water, while when $\theta_{ow} > 90°$ (hydrophobic particles) the sign inside the bracket is positive and the particle is removed into oil.

When rod-like particles instead of spheres are adsorbed at the interface, Equation I-1 is modified to account for the surface in contact with the interface (Capron et al., 2017). Assuming that the particles adsorb on their larger surface, the energy E required to remove the particle from the interface is now given by Equation I-2.

$$E = ld\gamma_{ow}(1 \pm cos\theta_{ow}) \qquad \textit{Equation I-2}$$

where l is the length and d is the width of the rods in contact with the interface, γ_{ow} is the oil/water interfacial tension, θ_{ow} is the contact angle that the particles make at the oil-water interface.

According to Equation I-1 and Equation I-2, particles of intermediate wettability ($\theta_{ow} = 90°$), give extremely stable emulsions (higher energy of attachment), while highly hydrophobic ($\theta_{ow} >> 90°$) or highly hydrophilic ($\theta_{ow} << 90°$) particles do not form stable emulsions.

To modulate the particle wettability, surface modification is often envisaged, either by chemical grafting or adsorption of different types of macromolecules (Binks and Lumsdon, 1999). Silica is one of the earliest commercial stabilising particles. Bare silica particles are generally unable to stabilize Pickering emulsions prepared with common oils because the particles are totally wetted by water. Grafting organosilanes to the surface of silica enables the control of the hydrophilic/hydrophobic balance of the silica surface, *i.e.* its wetting by both water and oil (Barthel, 1995). These fumed silica particles are currently being produced commercially by international manufacturers.

3. Destabilization mechanisms

Emulsions can be destabilized by various mechanisms (Figure I-4) (Gauthier and Capron, 2021).

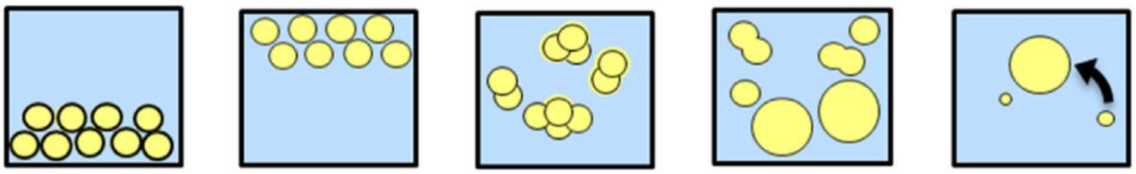

Figure I-4. Schematic representation of emulsion destabilization processes leading to phase separation (Gauthier and Capron, 2021).

Creaming and sedimentation (precipitation) are reversible processes as long as the drop interfaces do not fuse, but the droplets concentrate locally. Precipitation velocity follows Stokes' law (Equation I-3). According to the Stokes' law, the smaller the droplets, the slower the creaming or the sedimentation will be.

$$\upsilon = -\frac{2gr^2(\rho_2 - \rho_1)}{9\eta} \qquad \textit{Equation I-3}$$

where υ is the precipitation velocity, g is the gravitational force equivalent, r is the droplet radius, ρ_1 is the continuous phase density, ρ_2 is the dispersed phase density and η is the continuous phase viscosity.

Flocculation can be caused by attractive interactions between the stabilizing particles; droplets aggregate but their interfaces do not merge. Flocculation is a reversible process.

Coalescence corresponds to the merging of droplets to form a bigger droplet. Contrary to flocculation, the phenomenon is always irreversible and eventually leads to phase separation.

Ostwald ripening is controlled by the solubility of the dispersed phase in the continuous phase. Molecules are transferred from small to large droplets due to their different Laplace pressures, *via* the continuous phase. This phenomenon is governed by the Laplace's law (Equation I-4).

$$\Delta P = \gamma_{ow}\left(\frac{1}{r_1} + \frac{1}{r_2}\right) = \frac{2\gamma_{ow}}{r} \qquad \textit{Equation I-4}$$

where ΔP is the pressure difference (Pa) between the inside and the outside of the droplet, γ_{ow} is the interfacial tension (in $N.m^{-1}$), and r_1 and r_2 are the radii of curvature (m), which equal to r, the radius for a spherical droplet.

Once stabilized, Pickering emulsions are sensitive to creaming, sedimentation, or flocculation, but particles being irreversibly adsorbed, the steric repulsion prevents the droplets to merge, therefore, coalescence and Ostwald ripening are limited.

4. Limited coalescence

Limited coalescence is a process characteristic of Pickering emulsions, in which the partially-covered droplets produced during vigorous stirring experience coalescence events that reduce the total interfacial area between oil and water. During the limited coalescence process, the droplets coalesce until the oil/water interface is sufficiently covered (Arditty et al., 2003). The total interfacial area is progressively reduced, while the degree of coverage by the irreversibly adsorbed particles increases, which is reflected by a linear relationship between the inverse average drop diameter and the amount of added solid particles (Figure I-5). An interfacial film is subsequently formed, which inhibits coalescence and kinetically stabilises the droplets (Whitesides and Ross, 1995; Wiley, 1954). The coalescence process generates droplets with a well-defined characteristic size and relatively narrow droplet size distribution.

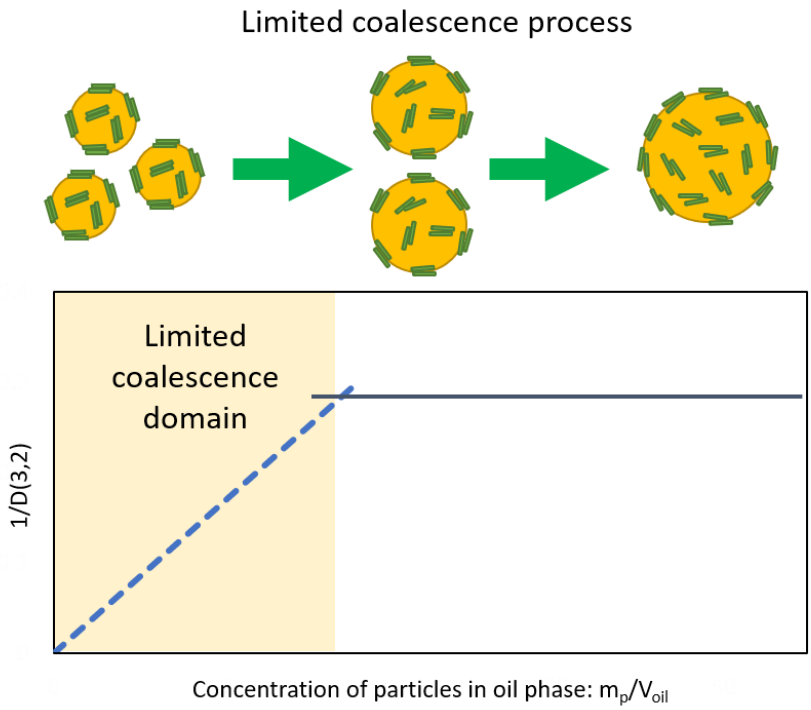

Figure I-5. Evolution of 1/D(3,2) as a function particles concentration during the limited coalescence process.

At higher particles concentrations, the proportionality does not hold anymore; the drop diameter does not decrease any longer with the increasing particles concentration. At this point, the introduction of more particles at the interface induces densification of the interfacial layer.

5. Specific surface area and surface coverage

a. Specific surface area

Assuming that all particles are permanently anchored at the oil/water interface around the droplets, the degree of coverage by the particles can be characterised by the specific surface area S (in m^2 per g of particles), defined as the ratio between the total available surface area and the total mass of particles m_p, *i.e.* the area that can be stabilized by 1 g of particles (Arditty et al., 2003). Knowing that the coalescence is arrested when a particular degree of surface

coverage is reached, the final state of adsorption characterised by S is always the same and independent of the total amount of solid particles (in the limited coalescence domain). It is established that the inverse of the average droplet diameter (1/D) varies with the total mass of particles (m_p) and specific surface area as in Equation I-5 (Arditty et al., 2003).

$$\frac{1}{D} = \frac{S}{6} \times \frac{m_p}{V_{oil}} \qquad \textit{Equation I-5}$$

The specific surface area S can therefore be estimated from the slope of the limited coalescence domain of Figure I-5.

b. Surface coverage

In another report of the same authors, the surface coverage C, expressed as the fraction of droplet interfacial area covered by the particles, was proposed as a parameter to characterise the packing density of spherical particles at the oil/water interface (Gautier et al., 2007). The authors showed that C could be estimated from the droplet size D, according to Equation I-6.

$$\frac{1}{D} = \frac{m_p}{4C\rho_p d_p V_{oil}} \qquad \textit{Equation I-6}$$

where ρ_p is the density of the particle, d_p the diameter and V_{oil} the volume of the oil phase.

For monodisperse spherical particles with hexagonal close-packed structure, C should be around 0.9. If C < 0.9 , this indicates that the particles are not closely packed at the droplet surface, while a larger value of C suggests that the droplets are covered by multiple layers or aggregates of particles at the interface (Destribats et al., 2014).

This equation was later adapted to parallelepipedal particles (cellulose nanocrystals (CNCs)) by the group of Isabelle Capron (Kalashnikova et al., 2011, 2013; Cherhal et al., 2016), who then proposed the following Equation I-7 for the evaluation of C, assuming that the particles are lying flat on their larger surface at the oil/water interface.

$$C = \frac{m_p D}{6h\rho_p V_{oil}}$$ *Equation I-7*

where m_p is the total mass of particles, D is the average diameter of the droplets, h is the thickness of particles, ρ_p is the density of particles, and V_{oil} is the volume of oil included in the emulsion after centrifugation.

It should be noted that Equation I-7 assumes that CNCs do not form aggregates. If CNCs are aggregated, Equation I-7 leads to an overestimation of the actual coverage. C is also highly dependent on the accuracy of the h value, which may vary significantly as a function of the technique used for its evaluation (Grachev et al., 2024). In contrast to C, the specific surface area S does not depend on the geometry and the state of aggregation of CNCs, making it a more accurate parameter. Both S and C values are inversely proportional and related through the Equation I-8:

$$C\ (\%) = \frac{100}{Sh\rho_p}$$ *Equation I-8*

B. Cellulose nanocrystals (CNCs)

1. Cellulose in plants

Cellulose is the most abundant renewable resources on the earth (Ji and Wang, 2023). It can represent up to 50% of the plant material, along with hemicelluloses and lignin (Figure I-6) (Grishkewich et al., 2017).

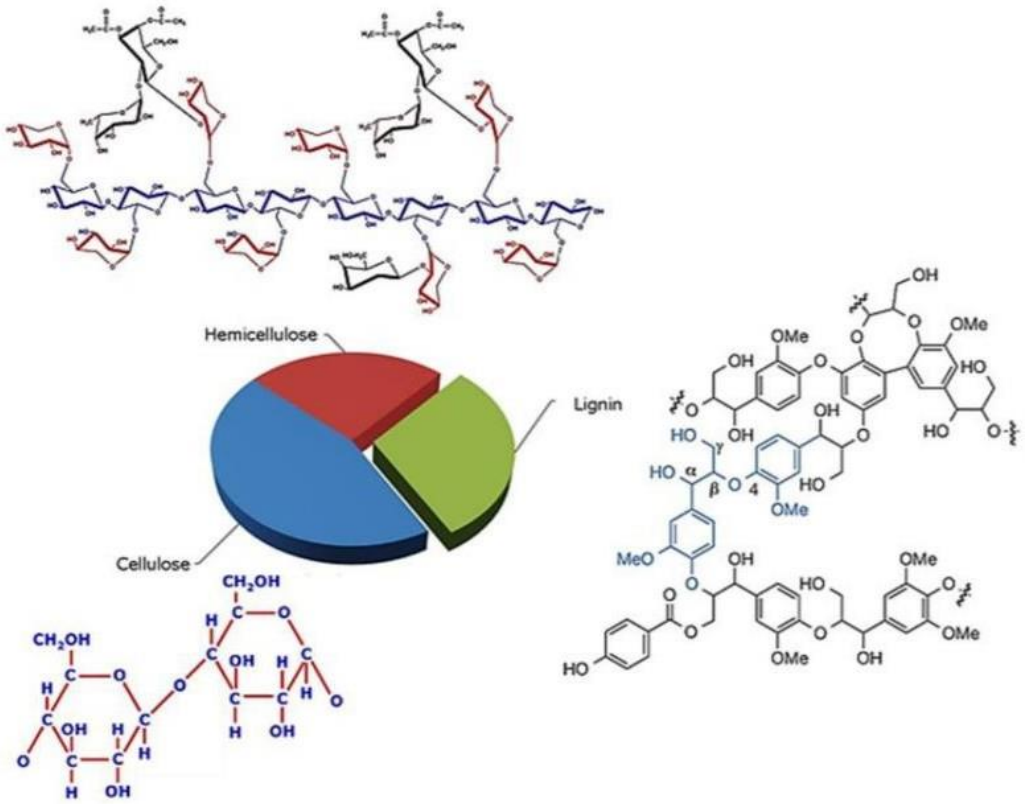

Figure I-6. Simplified chemical structures of cellulose, hemicellulose, and lignin and its composition in plant materials (Akash, 2015).

Cellulose is a linear long-chained polymer consisting of disaccharide anhydrous-D-glucopyranose units linked by 1-4 glucosidic bonds (Figure I-7) (Moon et al., 2011). Each cellulose chain has two different end groups: a chemically reducing functionality (hemiacetal unit), and a non-reducing end with a pendant hydroxyl group.

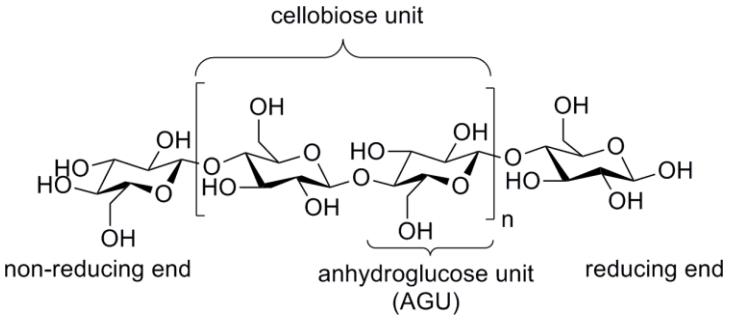

Figure I-7. Molecular structure of cellulose chains.

Cellulosic chains have a degree of polymerization of up to 15 000 anhydroglucose units (AGUs). Cellulose is the main reinforcement phase in trees (wood), plants (*e.g.* cotton), some marine creatures (tunicates), algae and bacteria (some bacteria secrete cellulose fibrils creating an external network structure). In trees and plants, cellulose chains are associated by hydrogen bonding to produce elementary fibrils that bundle together to form microfibrils, which in turn form macro-fibrils then cellulosic fibres (Figure I-8).

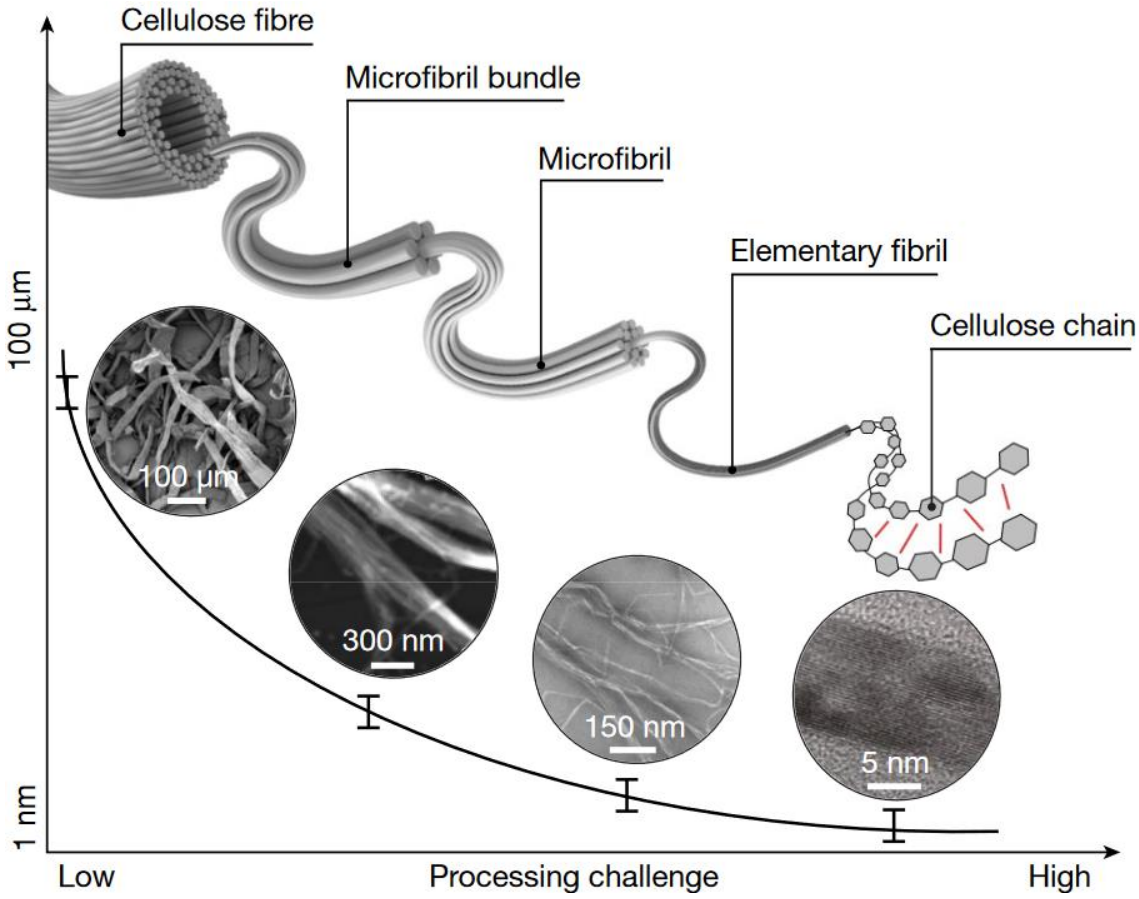

Figure I-8. Schematic description of the hierarchical structure and manufacturing challenge of fibrillated cellulose (T. Li et al., 2021).

The microfibrils are composed of both ordered (crystalline) and disordered (amorphous) domains (Figure I-9), the degree of crystallinity varying from 40 to 70% depending on the natural source and the extraction procedure. The crystalline structure of native cellulose is a composite of two crystalline phases called Iα (triclinic) and Iβ (monoclinic); cellulose from

plants being majorly composed of Iβ phase, cellulose from microorganisms (bacteria, seaweed) of Iα phase.

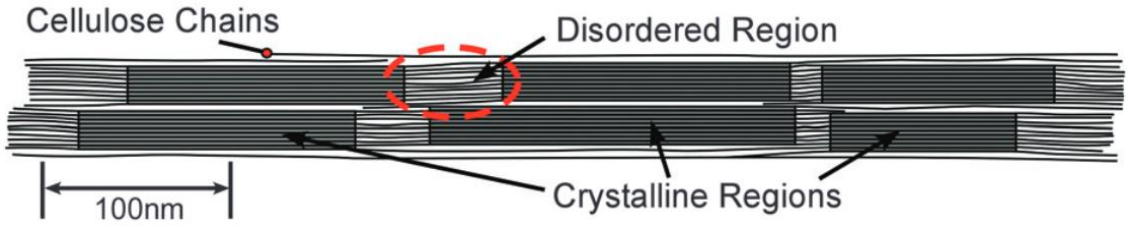

Figure I-9. Idealized cellulose microfibril showing one of the suggested configurations of the crystalline and amorphous regions (Moon et al., 2011).

In the glucose ring of cellulose, all the hydroxyl groups (OH) are equatorial and the methine groups (CH) are axial, leading to hydrophilic sites parallel to the ring plane and hydrophobic site perpendicular to this plan (Nishiyama et al., 2002). The OH-O hydrogen bonding dominates the cellulose intra-sheet interactions, while the weaker CH-O and van der Waals interactions are responsible for the inter-sheet bonding (Figure I-10).

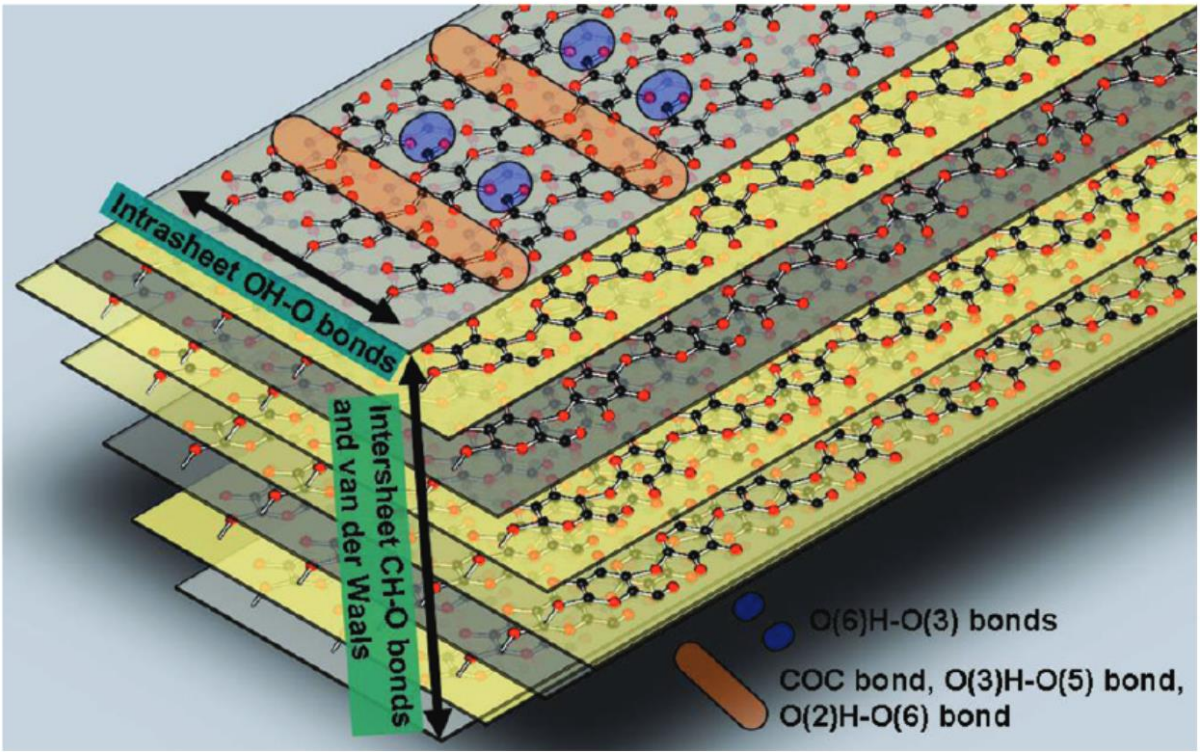

Figure I-10. Schematic illustration of hydrogen bonding directions and the layered structure in cellulose Iβ (Li and Renneckar, 2011).

2. Nanocelluloses

a. Isolation and structure

Nanocelluloses are generally extracted from the source materials in a two-step process. The source material is firstly subjected to a purification and homogenization pre-treatment in order to completely or partially remove the matrix materials (mostly hemicellulose and lignin in the case of wood and plants) and isolate the cellulosic fibres. These fibres are subsequently treated mechanically or chemically to produce cellulose nanofibrils (CNFs) or cellulose nanocrystals (CNCs), respectively. Another type of nanocellulose, referred here as bacterial cellulose nanofibrils (BCNFs), can be also produced by bio-synthesis. These three types of

nanocelluloses differ by their morphology and physical properties due to the cellulose source materials and the extraction processes (Table I-1) (Klemm et al., 2018).

Table I-1. Comparison of CNCs, CNFs and BCNFs morphology and physical properties (Klemm et al., 2018).

Characteristics	**CNFs**	**CNCs**	**BCNFs**
Example of SEM images	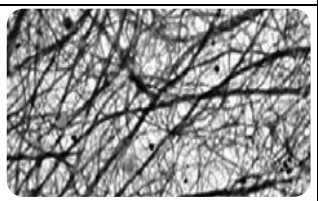	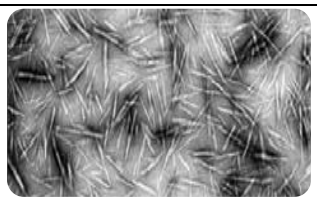	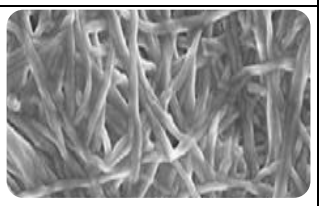
Physical appearance	Inter-connected network	Nano-rods	Nano-ribbons
Diameter	5 – 50 nm	5 – 20 nm	20 – 100 nm
Length	1 – 5 µm	50 – 500 nm	1 – 5 µm
Crystallinity	Primarily Iβ – lowest degree of crystallinity	Primarily Iβ, sometimes Iα – medium degree of crystallinity	Iα (shell) and Iβ (core) – highest degree of crystallinity

CNFs are nanofibrils produced by mechanical processes, such as high-pressure homogenization, grinding/refining, cryo-crushing, high intensity ultrasonication or micro-fluidization, assisted or not by chemical or enzymatic treatments. These nanofibrils have a high aspect ratio (5 – 50 nm wide, 1 – 5 µm in length), and contain both amorphous and crystalline regions.

CNCs are rod-like particles obtained after acid hydrolysis (generally with sulfuric acid) or oxidation (generally with TEMPO) of cellulose fibres or CNFs. CNCs have a relatively high aspect ratio (3 – 5 nm wide, 50 – 500 nm in length) and are highly crystalline (54 – 88%).

BCNFs are nano-ribbons produced by various bacteria that have been separated from the bacterial bodies and growth medium. The resulting microfibrils are in the micrometer range in length, have a high aspect ratio, and a morphology which depends on the bacteria used and culturing conditions.

b. Properties and applications

Nanocelluloses display remarkable physical and chemical properties, which enable their use in a wide range of applications (Figure I-11) (Thomas et al., 2018). Nanocelluloses retain the desirable properties for which cellulose is known, including low density, non-toxicity, and high biodegradability. In addition, nanocelluloses exhibit unique properties, such as high mechanical strength, reinforcing capabilities, and tuneable self-assembly in aqueous media, arising from its unique shape, size, surface chemistry, and high degree of crystallinity. Nanotechnology involving these cellulosic substrates has generated tremendous attention during the past few decades. Chemical, biochemical, and mechanical methods provide ways to modify nanocellulose, yielding enhanced properties such as energy conservation, barrier properties, flame retardancy, mechanical strength and reinforcing capabilities; thus, greatly expanding traditional applications of wood. Nanocelluloses have a Young's modulus in the range 20− 50 GPa and a surface area of several hundreds of square meters per gram, meaning that many new promising properties and applications can result.



Figure I-11. Applications of nanocellulosic materials (Thomas et al., 2018).

3. Isolation of cellulose nanocrystals (CNCs)

CNCs, also known as nanocrystalline cellulose or cellulose nanowhiskers, are conventionally isolated from cellulose fibrils of wood pulp, cotton, natural fibres, microcrystalline cellulose *etc.* by hydrolysis of part of the cellulose chains with strong acids, in order to selectively remove the amorphous domains (Habibi et al., 2010b). Sulfuric acid has been extensively used for CNCs extraction, but hydrochloric acid, phosphoric and hydrobromic acids, have also been reported for such purposes. When the CNCs are prepared by hydrolysis in hydrochloric acid, their ability to disperse is limited and their aqueous suspensions tend to flocculate as the particles are not charged. On the other hand, when sulfuric acid is used as a hydrolysing agent (the most employed method), it reacts partly with the surface hydroxyl groups of the CNCs to yield negatively-charged sulphate half-ester groups (Figure I-12), which enables the good

dispersion of the CNCs in water. However, the CNCs prepared by hydrolysis in sulfuric acid present lower thermal stability due to the production of sulfuric acid with temperature which accelerates the cellulose depolymerization process (Uetani et al., 2014).

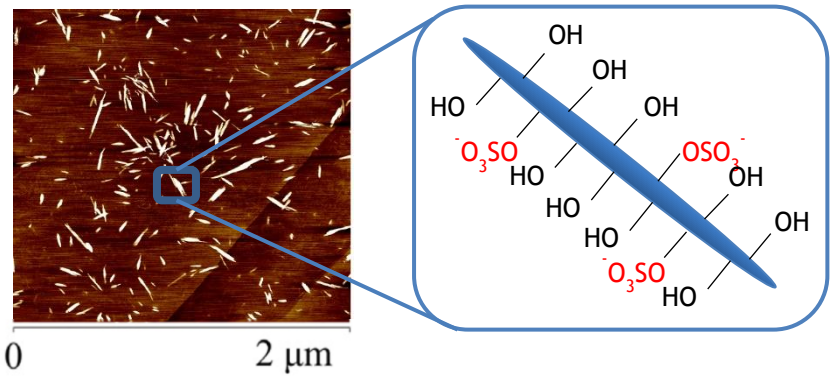

Figure I-12. Topography image taken using atomic force microscopy of pristine CNCs (Brand et al., 2017) and the schematic illustration of a CNC rod (inset).

4. Surface tailoring of the CNCs by chemical functionalization

To widen the field of application of the CNCs, it is often necessary to tailor the CNCs surface by chemical functionalization, to control the dispersive, interfacial and self-assembling properties, or to introduce novel functionalities. Due to the abundance of hydroxyl groups at the surface of CNCs, various covalent reactions can be performed, but non-covalent surface modification, including the use of adsorbing surfactants and polymer coating, can be also envisaged.

a. Covalent grafting

i. Common reactions

Superficial hydroxyl groups of CNCs provide sites for covalent grafting of different moieties, *via* oxidation, amination, acylation, polymer grafting, among others (Figure I-13) (Habibi,

2014). The modifications are usually performed in order to impart additional functions (stimuli-responsiveness, fluorescence, electronic, magnetic, catalytic and optical properties) or increase hydrophobicity (Tang et al., 2017).

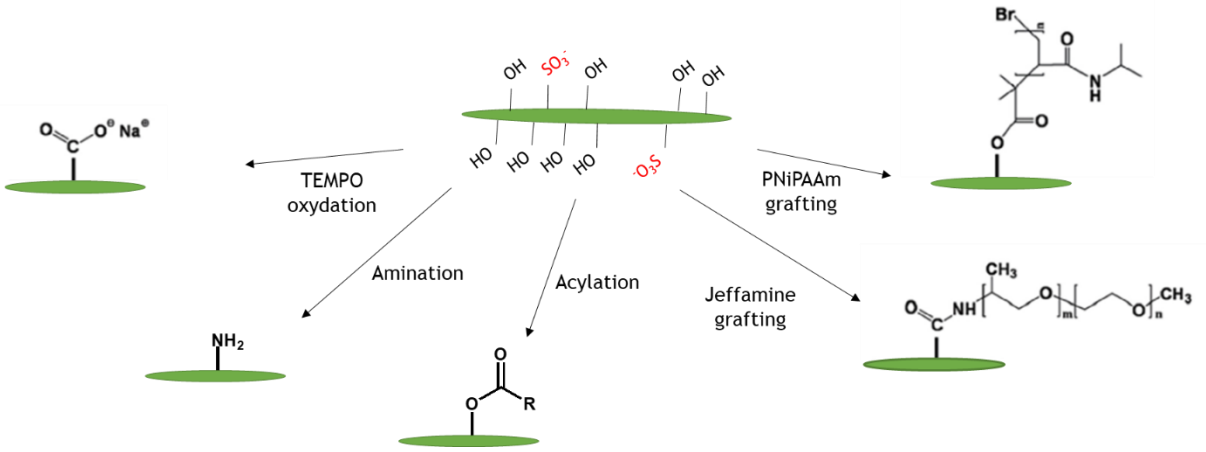

Figure I-13. Possible chemical pathways for the covalent grafting of different moieties at the CNCs surface (Habibi, 2014).

ii. Acylation with functional vinyl esters

Modification of hydroxyl groups present at the surface of CNCs through esterification is widely used due to its ease and straightforwardness (Eyley and Thielemans, 2014). The esterification by acylating agents, such as acid chlorides or anhydrides has been the most investigated. However, these reactions concurrently release hydrohalic or carboxylic acids by-products, which may adversely impact the nanocellulose structure and/or contaminate the nanoparticle surface.

Among the alternative methods, the acylation approach based on the transesterification of functional vinyl esters is particularly attractive as it allows the grafting of a wide variety of functionalities in mild conditions, using potassium carbonate as catalyst (Figure I-14) (Brand et al., 2017). The vinyl alcohol formed as a by-product quickly tautomerizes to acetaldehyde and the equilibrium is naturally shifted toward the ester formation.

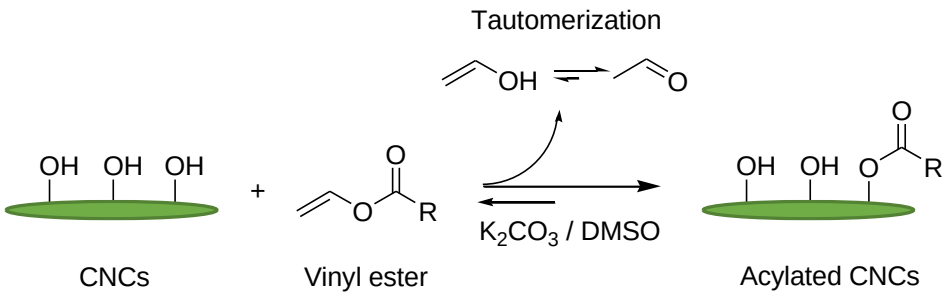

Figure I-14. Reaction scheme for the acylation of CNCs using a vinyl ester as acetylating agents.

Another advantage of this acylation method is linked to the high reactivity of vinyl esters towards sterically-hindered alcohols, presumably because the reaction involves an acylium ion; but like with other esterifications, anhydrous conditions are generally required to avoid the hydrolysis of the vinyl ester. The acylation of CNCs has been carried out in anhydrous dimethylformamide (DMF) or dimethyl sulfoxide (DMSO) in the presence of potassium carbonate as catalyst to graft acetyl moieties (Çetin et al., 2009; Werner et al., 2017; Dhuiège et al., 2018), acyl chains of various length (from 2 to 18 carbons) (Dudefoi et al., 2022), benzoyle groups (Brand et al., 2017), cinnamoyle groups (Sèbe et al., 2013; Planes et al., 2016; Brand et al., 2017), methacryloyl groups (Nielsen et al., 2010), as well as adipate, chloroacetate and trifluoroacetate functions (Brand et al., 2017).

b. Non-covalent modifications

i. Adsorption of surfactants

The most common method used in non-covalent surface modification of CNCs is the adsorption of surfactants, through electrostatic interactions, hydrogen bonds or van der Waals forces (Habibi et al., 2010b; Tardy et al., 2017).

For instance, Heux et al. modified the CNCs surface with surfactants consisting of mono- and di-esters of phosphoric acid having alkylphenol tails (Heux et al., 2000). Bondeson et al. adsorbed an anionic surfactant (Beycostat A B09) to improve the dispersion of the CNCs in

polylactic acid (Bondeson and Oksman, 2007). Kim et al. (Kim et al., 2009) and Rojas et al. (Rojas et al., 2009) both adsorbed nonionic surfactants (sorbitan monostearate) to disperse the CNCs in polystyrene-based composites. Cationic surfactants such as dioctadecyldimethylammonium bromide showed particularly strong electrostatic interactions with the anionic CNCs (Habibi et al., 2010a). We can also mention the adsorption of saccharide-based amphiphilic block copolymers on CNCs by Zhou et al, which allowed improving their dispersion in non-polar solvents (Zhou et al., 2009).

ii. Coating with polydopamine

In a recent approach, polydopamine (PDA) has been used as an innovative coating to modify the surface of the CNCs through non-covalent interactions. PDA is a melanin-like naturally inspired polymer and is a mimetic mussel adhesive protein, due to its unique chemical structure with catechol and amine groups, which makes it an excellent coating for almost any type of material surfaces (Liebscher et al., 2013; Liu et al., 2014; Barclay et al., 2017; Liu et al., 2019; Samyn, 2021). PDA displays numerous outstanding properties of naturally occurring melanin, which can impart additional functions to the coated material, such as fluorescence, UV-absorption, paramagnetism, antioxidant and radical scavenging activity, electrical conductivity, metal ions chelating activity and redox activity (Liu et al., 2014). It also possesses excellent biocompatibility.

The solution oxidation method is the most widely used protocol for the production of PDA. Its monomer, dopamine (commercially available dopamine hydrochloride is typically used), can be oxidized and spontaneously self-polymerized under alkaline conditions in water (pH > 7.5) with oxygen as the oxidant. A colour change from colourless to pale brown occurs, and finally turning to deep brown with passing time. The oxidation involves the formation of intermediate quinones, which are chemically instable and react through intermolecular cyclization into a

dihydroxyindole intermediate, which further polymerizes and assembles into a PDA network (Figure I-15).

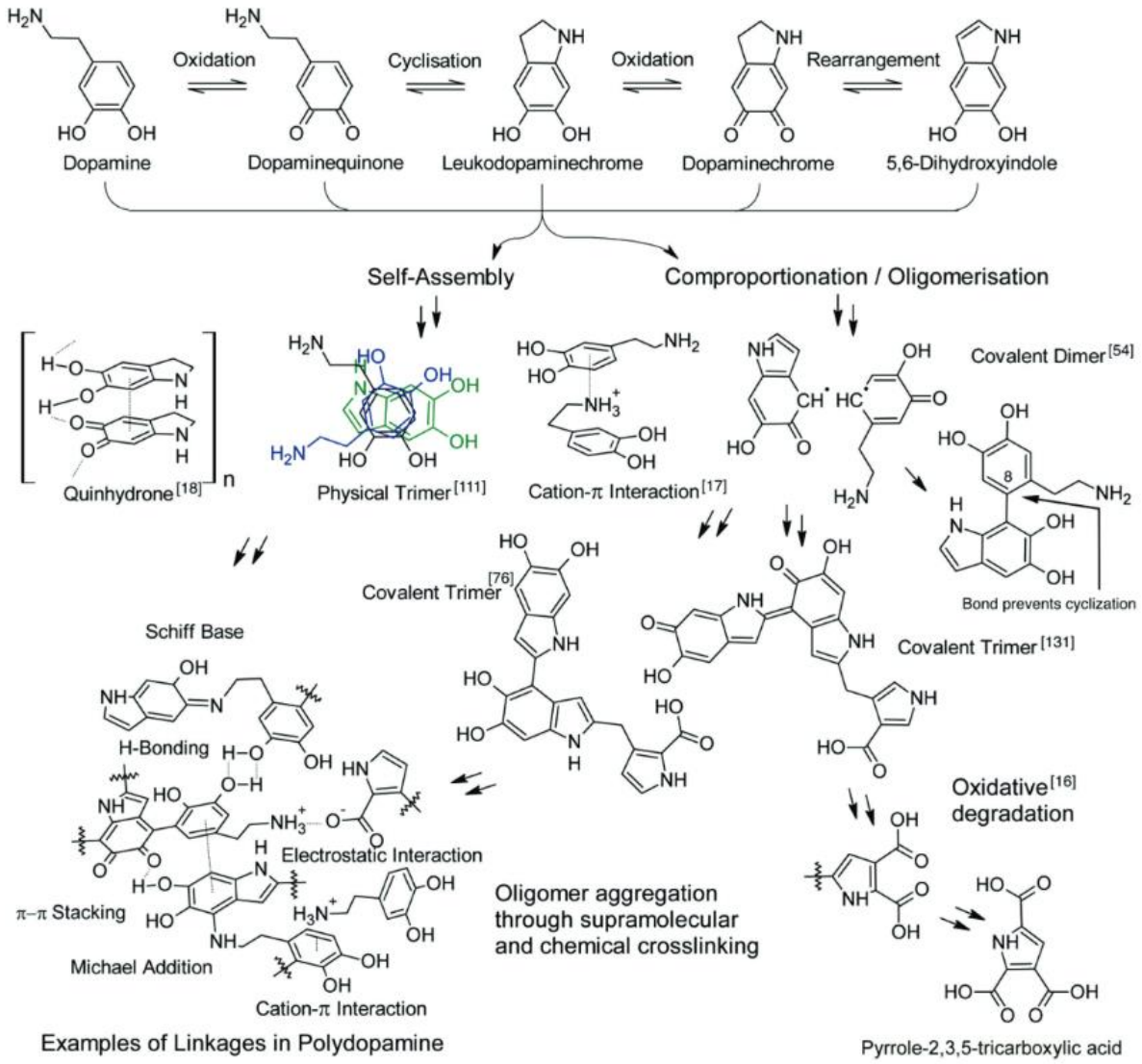

Figure I-15. Oxidative self-polymerization mechanism of dopamine under alkaline conditions with radical-induced reactions forming instable intermediates, which polymerize and assemble into polydopamine linkages (Barclay et al., 2017).

The mechanism of attachment of PDA on the organic and inorganic substrates remains poorly understood, but the presence of both catechol and amine groups seems critical. The adhesion with the substrate seems to result from of a variety of interactions such as π-π stacking, van der Waals forces, hydrophobic associations, hydrogen bonds or electrostatic interactions

(Barclay et al., 2017). With the CNCs, the method has been recently applied to graft PEG (Zheng et al., 2021), prepare Janus particles (Sun et al., 2022), crosslink nanofiber mats (Yang et al., 2020), immobilize cellulase (Qin et al., 2023) or graft polymers by SI-ATRP (Hou et al., 2024). In general, the PDA coating does not modify the geometrical nanoscale morphology of the CNCs.

C. Utilization of the CNCs as Pickering particles

In recent studies, CNCs have demonstrated good performances as Pickering stabilizers for oil-in-water emulsions, in their pristine form or after chemical functionalization of their surface.

1. Pristine CNCs

The crystalline structure of the CNCs confers them with an amphiphilic character, which makes them suitable for Pickering stabilization (Capron et al., 2017). It is suggested that a flat and more hydrophobic crystalline plane exists where extensive hydrogen bonding could take place. The (200) crystalline plane of the CNCs (Iβ allomorph), with a surface covered by a rich layer of CH methine groups, induces preferential orientation at the interface of the CNCs along this face (Figure I-16). This hydrophobic crystalline plane is responsible for the wettability of CNCs at the O/W interface, and its accessibility to oil droplets thus favours the formation of thermodynamically stable emulsions (Kalashnikova et al., 2012).

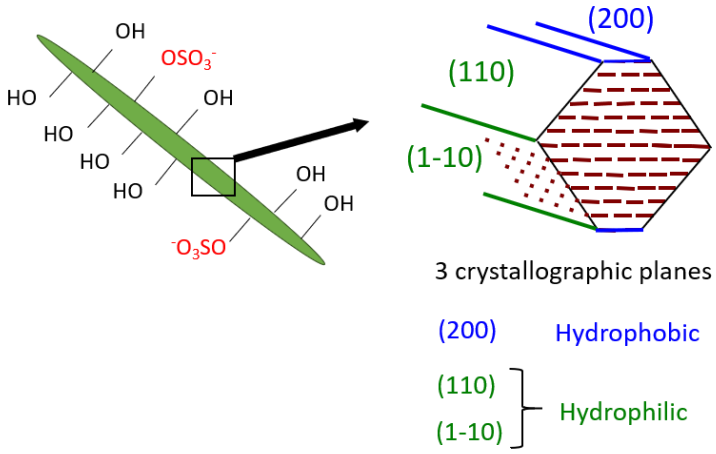

Figure I-16. Schematic representation of the crystallographic structure of the CNCs (Iβ allomorph), exposing the hydrophobic edge (200).

The stability of the emulsions is however generally conditioned by the addition of salt during the emulsification process. Indeed, the CNCs produced *via* sulfuric acid hydrolysis bear negatively charged sulphate half-ester groups, which promote repulsions at the interface, limiting the surface coverage and, consequently, leading to unstable emulsions. These repulsive forces can be however modulated through charge screening by counter ions (*e.g.* by adding salts), which enhances CNCs adsorption and surface coverage by lowering the interparticle and particle–interface electrostatic repulsions (Bergfreund et al., 2019; Bertsch et al., 2018).

As an alternative to salt addition, the surface charge density can also be modulated by desulfation treatments, as a surface charge density superior than 0.03 e/nm^2 cannot anchor efficiently at the oil/water interface (Cherhal et al., 2016; Kalashnikova et al., 2012). However, the desulfation of CNCs can lead to aggregated CNCs and a thicker and more heterogeneous surface at the oil/water interface (Figure I-17).

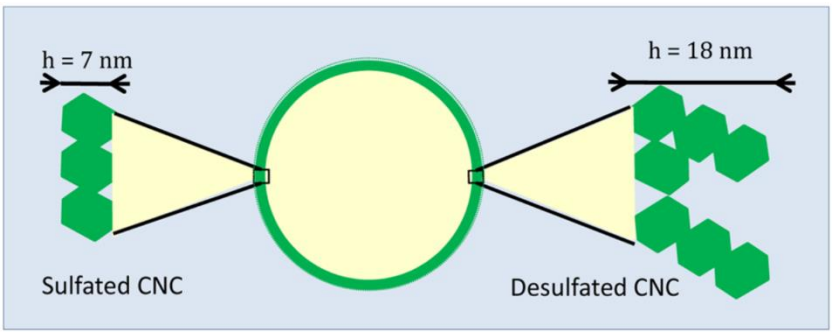

Figure I-17. Schematic representation illustrating the oil/water interface with the CNCs totally wetted by the aqueous phase; a thicker interface is obtained with desulphated CNCs, due to particles aggregation (Cherhal et al., 2016).

In the literature, CNCs have been used to stabilise emulsions of different edible oils, such as corn oil (Ni et al., 2020), sunflower oil (Zhang et al., 2020), coconut oil (Hedjazi and Razavi, 2018) and palm oil (Wang et al., 2016). Hedjazi and Razavi related the stability of the emulsions with the droplet coverage (Hedjazi and Razavi, 2018).

2. Hydrophobized CNCs

The strong hydrophilic character of the unmodified CNCs can also be mitigated by grafting hydrophobic moieties on the surface. The modification can be achieved through physical adsorption of cationic surfactants such as alkyl ammonium surfactants didecyldimethylammonium bromide (DMAB) and cetyltrimethylammonium bromide (CTAB) (Hu et al., 2015a). In addition, the use of water-soluble polymers, *e.g.* hydroxyethyl cellulose or methyl cellulose, enables a better control of the droplet size in comparison to systems with pristine CNCs solely (Hu et al., 2015b).

More sophisticated surface modifications have been envisaged in order to prepare functional emulsions. The covalent grafting of poly(N-isopropylacrylamide) or poly[2-(dimethylamino)ethyl methacrylate for instance, provided temperature-sensitive or pH-

responsive properties to the emulsions, respectively (Tang et al., 2014; Zoppe et al., 2012), while magneto-responsive properties were obtained with iron-modified CNCs (Fe_3O_4-CNC) (Low et al., 2017).

Surface modification is also generally required to prepare W/O or multiple emulsions (Carrillo et al., 2015; Cunha et al., 2014). Dudefoi et al. prepared either O/W or W/O Pickering emulsions by partially hydrophobizing CNCs with acyl groups of various chain lengths and surface degree of substitution (DS_{Surf}) (Dudefoi et al., 2022). Whatever the DS_{Surf}, CNCs grafted with linear acyl chains of 2 to 6 carbons led to the exclusive formation of direct O/W emulsions with hexadecane (Figure I-18). Distinctively, both O/W and W/O emulsions could be obtained when the linear chain contained 8 carbons or more, at low and high DS_{Surf}, respectively.

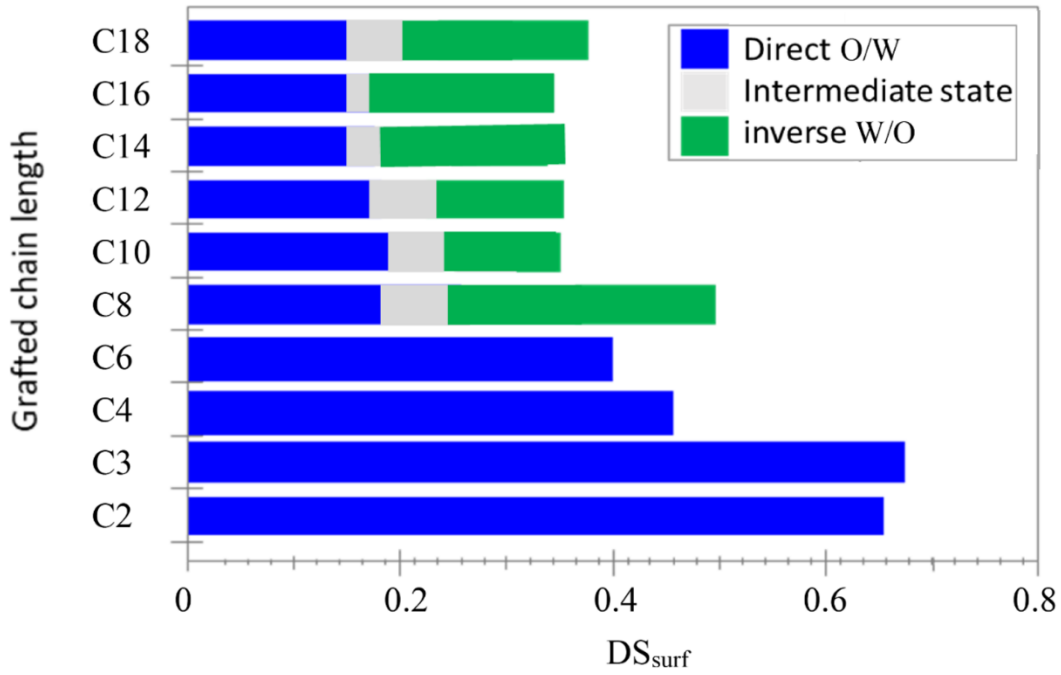

Figure I-18. Type of emulsion obtained in the experimental conditions as a function of DS_{Surf} and number of carbons in the grafted chain. Direct and inverse emulsions are obtained with W/O = 80/20 and 20/80 v/v, respectively. The intermediate state corresponds to a situation where both oil and water droplets are present in the medium according to the microscopic observations.

3. Encapsulation of active molecules in CNCs-stabilised Pickering emulsions

In this context, Pickering emulsions stabilized with CNCs are increasingly considered as a valuable mean to encapsulate active molecules or oils owing in particular to the low toxicity and biocompatibility of cellulose (Fujisawa et al., 2017; Q. Li et al., 2021). The utilization of pristine CNCs has been envisaged in a few cases, but most of the investigations in this area have been performed with modified CNCs.

Pristine CNCs have been used to encapsulate essential oils (cinnamaldehyde, eugenol and limonene) and prepare emulsions with antibacterial properties (Mikulcová et al., 2016). The antimicrobial oil content was as high as 40% weight fraction of the emulsion and the encapsulation efficiency (EE) ranged from 79 to 100%. The antibacterial properties of the emulsions were tested against different bacterial strains, representing a wide range of the major food-borne pathogens (*e.g. E. coli, Salmonella* and *P. aeruginosa*). It was demonstrated that the antibacterial effect is primarily controlled by the oil encapsulated in droplets, while the impact of free or non-encapsulated oil was only marginal.

In another study, CNCs extracted from sisal fibre were used to stabilize emulsions of dichloromethane containing curcumin (a hydrophobic bioactive polyphenol compound) and poly(methyl methacrylate) (PMMA), to later produce curcumin-loaded PMMA particles after evaporation of the solvent (Figure I-19) (Liu et al., 2018). The EE of curcumin in the PMMA@SCNC composite microspheres reached up to 72%. The authors reported a rapid initial release of the curcumin located at the external surface of the composite microspheres, followed by a slower release of the inner molecules.

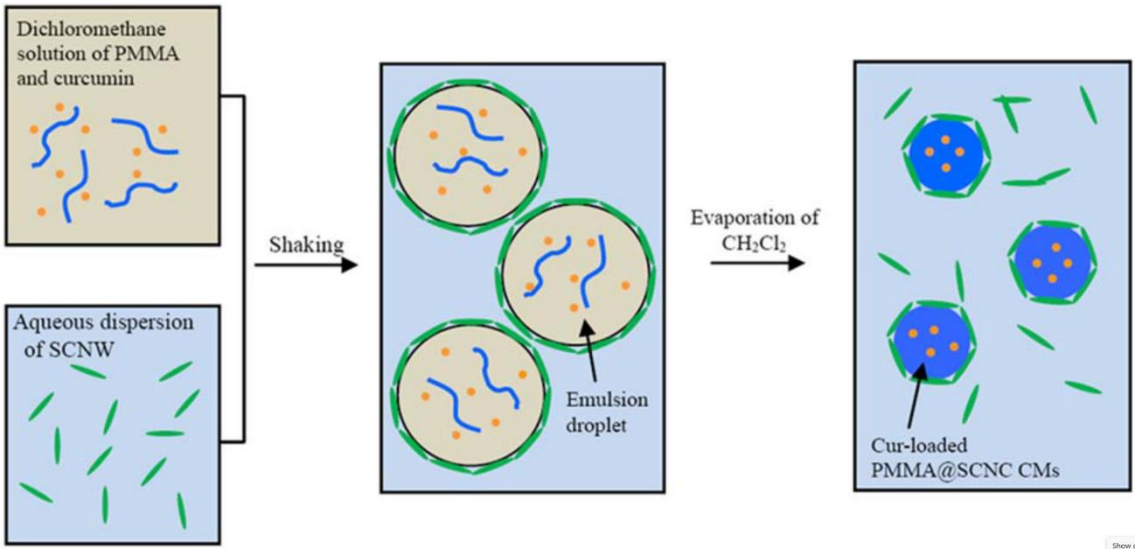

Figure I-19. Schematic illustration of the fabrication of curcumin-loaded PMMA-CNC composite microspheres (Liu et al., 2018).

Amine-modified CNCs have also been employed to encapsulate curcumin isolated from *Curcuma longa* (turmeric), leading to a sustained release of the molecule, and excellent in vitro cytotoxicity (Asabuwa Ngwabebhoh et al., 2018). The EE in the oil phase, which consisted in a mixture of medium chain triglyceride and Tween 80, was 90%. The release percentage at pH 7.4 was 10% after 24 h, and 76% after 8 days. In vitro cytotoxicity studies performed with human cell lines (L929 fibroblast cells and MCF-7 breast cancer cells) demonstrated the potential of the emulsion to promote preferential killing of cancer cells instead of normal cells.

More recently, cationic CNCs were coupled with anionic diosgenin-alginate conjugates, and the particles obtained were used as Pickering stabilizers to form hydrocolloid nanocarriers for the delivery of quinalizarin, a poor water soluble drug (Figure I-20) (Ilkar Erdagi et al., 2020). The cationic CNCs were prepared through nucleophilic addition of alkali-activated hydroxyl groups of CNCs to the epoxy moiety of 2,3-epoxypropyl trimethylammonium chloride. After encapsulation (EE was 62%), a sustained drug release was noted. In vitro cytotoxicity assays revealed excellent anticancer activity in human lung (A549) and breast (MCF-7) cancer cell lines.

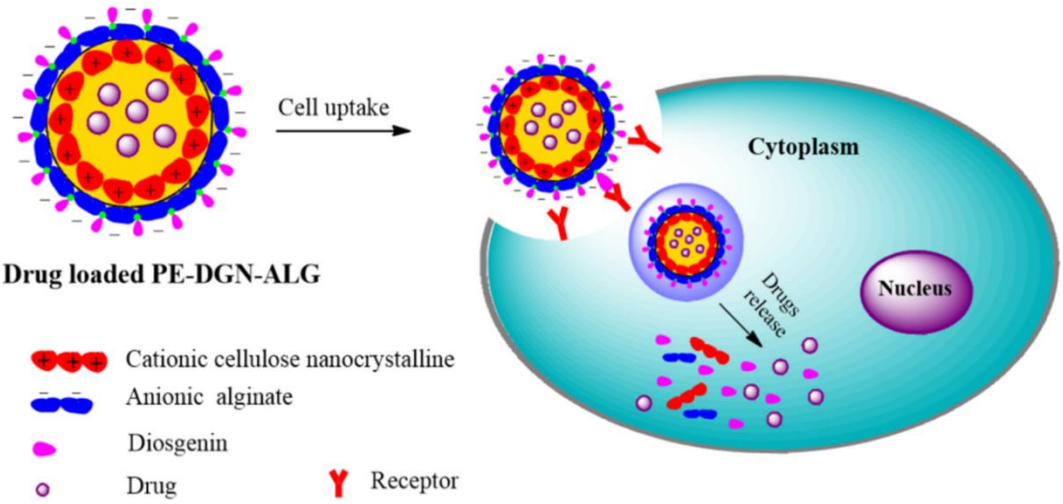

Figure I-20. Illustration of intracellular release of drug loaded PE-DGN-ALG (Ilkar Erdagi et al., 2020).

Cinnamoyl chloride-modified CNCs have been used to encapsulate both turpentine (a botanical pesticide essential oil) and 2,4-dichlorophenoxyacetic acid (2,4-D, an herbicide) (Tang et al., 2019). In this process, the herbicide was dissolved in turpentine, and the Pickering droplets were later modified with a polydopamine coating to produce microcapsules, which shell could be controlled by adjusting the amount of deposited PDA. 75% of 2,4-D was encapsulated in the microcapsules, which displayed a sustained release profile (40% of 2,4-D was released after 1 day).

Octenyl succinic anhydride-modified CNCs have been used to stabilise Pickering emulsions of short-chain fatty acids (SCFAs, including propionic and butyric acids) for targeted delivery in digestive tracts (Le et al., 2020). The emulsion droplets were prone to flocculation in the gastric environment tested, as the low pH and high ionic strength induced a reduction of the electrostatic repulsive forces between droplets. In vitro gastrointestinal digestion studies revealed that a high proportion of SCFAs remained loaded in the emulsions after intestinal digestion (55%), showing good promise for an application in colon-targeted delivery of SCFAs.

D. Encapsulation and delivery of resveratrol (RSV)

1. Properties of RSV

RSV (*trans*-RSV, 3,4′,5-*trans*-trihydroxy-stilbene, $C_{14}H_{12}O_3$, chemical structure as in Figure I-21) can be found in relatively high levels in grape skins, berries, peanuts, cocoa powder and foods derived from them (*e.g.*, juices, fermented drinks, dried fruits, jams and spreads) (Davidov-Pardo and McClements, 2014; Gambini et al., 2013; Gugleva et al., 2020). Currently classified as Class II drug in Biopharmaceutics Classification System, RSV is reported to display a wide range of therapeutic and preventive properties such as antioxidant, anticancer, anti-inflammatory, antineuralgic and cardioprotective.

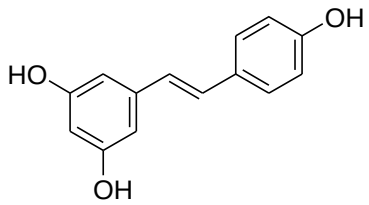

Figure I-21. Chemical structure of RSV.

These potential health benefits of RSV have led to increasing usage as a bioactive agent in foods and pharmaceuticals. RSV is extracted from natural sources and is then incorporated into capsules or tablets for use as a supplement or food products.

a. Light and chemical instability

However, RSV in solution has a limited stability under the influence of UV light, certain pH levels or certain temperatures, which can cause its *trans-cis* isomerization or degradation (Francioso et al., 2014). Unfortunately, the more stable *cis*-RSV is less biologically active.

Trans-RSV is highly photosensitive and rapidly isomerizes to *cis*-RSV (Figure I-22) when exposed to UV or visible light (Neves et al., 2012). Isomerization kinetics of this photochemical degradation is affected by the irradiation time, wavelength and temperature.

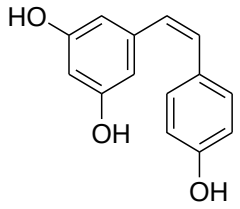

Figure I-22. cis-RSV, the isomer of trans-RSV.

Trans-RSV suffers photocatalytic degradations in the presence of a photocatalyst such as TiO_2 under UV irradiation. In such conditions, oxidation and fragmentation takes place, leading to several photoproducts, which are mainly due to successive reactions with $HO^{\bullet}$ (Silva et al., 2013). The suggested photoproducts are: (1) 3,4′,5-trihydroxydiphenylacetylene, (2) 5-(1-hydroxy-2-(4-hydroxyphenyl)ethyl)benzene-1,3diol, (3) 4-hydroxybenzaldehyde, (4) 3,5-dihydroxybenzaldehyde, (5) 2-(3,5-dihydroxyphenyl)-2-hydroxyacetic acid, and (6) 4-hydroxybenzoic acid (Figure I-23).

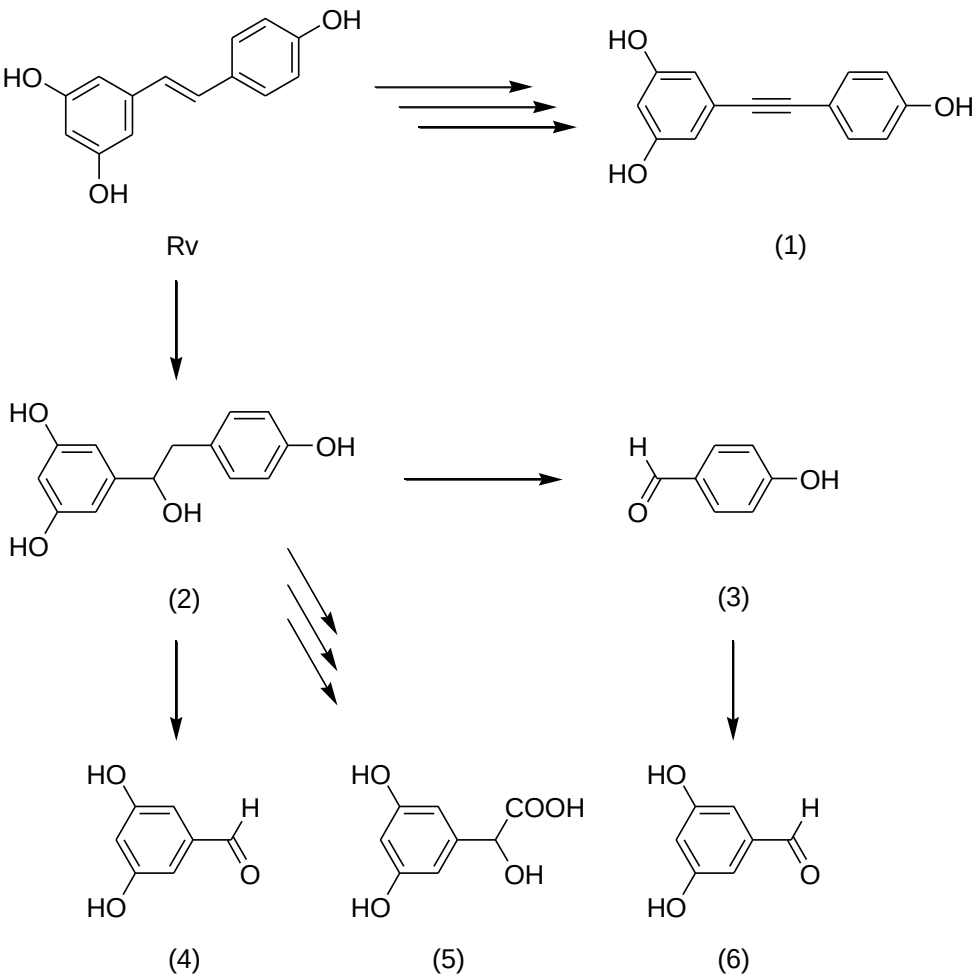

Figure I-23. Proposed photoproducts of RSV after photocatalytic degradation (Silva et al., 2013).

Concerning the impact of pH, RSV is stable at acidic pH, but start to degrade exponentially above pH 6.8 (Zupančič et al., 2015). At acidic pH, the protonated form of the phenol groups protects the molecule from radical oxidation. Above pH 6.8 on the other hand, the presence of phenate ions in the trans-RSV structure make it particularly susceptible to oxidation to phenoxy radicals. With regards to temperature, the degradation of *trans*-RSV at pH 7.4 is rapid at room temperature (50% degraded after two days), slowed down at 4 °C and prevented at -22 °C in the absence of light (Zupančič et al., 2015). It has been also reported that RSV can degrade when exposed to ultrasound cavitations, but degradation can be prevented by controlling the sonication power (Kumar et al., 2017).

b. Poor water solubility and bioavailability

The solubility of RSV is high in polar solvents such as ethanol or DMSO (50 and 16 g/L, respectively), but poor in water (at pH 7.4) (reported to be between 19.6 and 50 µg/mL at 25 °C) (Davidov-Pardo and McClements, 2014; Robinson et al., 2015; Shi et al., 2008). Variations in the water solubility were however noted as a function of pH by Zupančič et al., who measured values of 64, 61 and 50 µg/mL at pH 1.2, 6.8 and 7.4, respectively, after 72 h (Zupančič et al., 2015).

In edible oils, the solubility of RSV is generally slightly higher than in water, ranging from (44 to 162 µg/mL) (Table I-2).

Table I-2. Solubility of RSV in some edible oils.

Oils	**Solubility of RSV (µg/mL)**	**Reference**
Olive oil	44	(Hung et al., 2006)
Isopropyl myristate	49	(Juškaitė et al., 2015)
Orange oil	109	(Davidov-Pardo and McClements, 2015)
Mixture of grape seed oil and orange oil	112	(Davidov-Pardo and McClements, 2015)
Soybean oil	140	(Robinson et al., 2015)
Coconut oil	162	(Hung et al., 2006)

The bioavailability of RSV is poor, the molecule being rapidly and extensively metabolized and excreted (Neves et al., 2012; Smoliga and Blanchard, 2014). It is suggested that this polyphenol has high oral absorption, but rapid and extensive metabolism without adverse effects in both rodents and humans, resulting in only trace amounts of unchanged RSV in the systemic circulation (Boocock et al., 2007a, 2007b; Niles et al., 2006; Sale et al., 2004).

2. Encapsulation and delivery of RSV

a. Context

Consuming RSV-rich foods is the most direct approach for the intake of RSV, but this approach is unsuitable for widespread utilization due to the low bioavailability of RSV from natural sources (Murtaza et al., 2013). The amount of RSV within a natural source may vary considerably depending on species, climate, location, time of year, *etc*. It is also impractical to consume the quantity of a natural source required to have an appreciable biological effect. In addition, the RSV may be primarily located within parts of the natural source which are not normally consumed, such as the skin or seeds.

RSV can be isolated from natural sources by simple processing operations, such as crushing, grinding, solvent extraction (usually aqueous alcoholic mixtures), and separation and purification techniques. Extraction and purification usually lead to a powdered form of RSV consisting of white crystals. However, the crystals are poorly soluble in water and sediment in low viscosity fluid products (such as a beverage), leading to an undesirable appearance and the possibility that they are not consumed. Crystalline forms of RSV may also lead to an undesirable mouthfeel, such as graininess or grittiness.

For these reasons, it is often desirable to incorporate the RSV powder into a suitable delivery system. Encapsulation is a technique in which ingredients are trapped within some form of matrix. This matrix may be solid or liquid, homogenous or heterogenous, and microscopic or macroscopic. The ingredient to be entrapped is usually referred to as the “active” or “core” material, whereas the material that forms the matrix is usually referred to as the “wall”, “encapsulant”, “shell”, or “carrier” material (Madene et al., 2006). Encapsulation is primordially needed to increase the dispersibility of RSV in aqueous solutions so that it can be added to a wide variety of food products, ranging from clear beverages to bakery products.

Encapsulation is also required to protect RSV from environmental factors that promote its chemical degradation during storage, such as ultraviolet light and oxygen. Last but not least, encapsulation is necessary to enhance the oral bioavailability of RSV by increasing its solubility in gastrointestinal fluids, promoting its absorption by enterocyte cells, and reducing its metabolism prior to absorption.

b. Colloidal systems

Various colloidal systems efficient for encapsulation, protection and delivery of RSV have been recently developed (Machado et al., 2019). In the literature, colloidal delivery systems based on emulsions, liposome/niosomes, molecular inclusion complexes and biopolymer particles have been reported (Table I-3). Liposomes are spherical vesicular structures usually composed of concentric phospholipid bilayers dispersed in an aqueous environment. Niosomes are also vesicular systems that differ from liposomes due to the fact that the building blocks are non-ionic surfactants rather than phospholipids. On the other hand, molecular inclusion is a process in which a "guest" molecule is trapped within a "host" molecule due to physical forces. In addition, a variety of colloidal delivery systems can be fabricated from food-grade biopolymers, such as proteins and polysaccharides, e.g., biopolymer nanoparticles, hydrogel particles, and filled hydrogel particles. Emulsion-based encapsulations have been one of the most representative delivery systems developed for RSV during the last decade (Machado et al., 2019).

Table I-3. Examples of the different colloidal delivery systems available to encapsulate and protect RSV.

Encapsulation technology	**Encapsulation details**	**Evaluations on the encapsulated RSV**	**Reference**
Emulsion	O/W emulsions • Whey protein isolate or sodium caseinate as emulsifier • RSV was encapsulated in sunflower oil, fish oil, medium-	Spatial partition of RSV at the O/W interface	(Chen et al., 2023)

	chain triglyceride and peppermint oil		
	O/W emulsions • A mixture of soy lecithin and sugar ester as emulsifier • RSV (0.01% wt) was encapsulated in peanut oil	Chemical stability	(Donsì et al., 2011)
	$W_1/O/W_2$ emulsions • Inner aqueous phase (W_1): RSV in ethanol (0.05 g/L) • Miglyol 812 containing polyglycerol polyricinoleate (5% wt), a hydrophobic emulsifier • External aqueous phase (W2): carboxymethylcellulose, Tween 20 and 0.1 M of NaCl	Chemical stability	(Matos et al., 2015)
	$W_1/O/W_2$ emulsions • Inner aqueous phase (W_1): Tween 80 in normal saline • RSV dissolved in a lipid mixture of Geleol and Gelucire • External aqueous phase (W2): Tween 80 in normal saline	Antioxidant activity and chemical stability	(Jain et al., 2023)
Liposomes/ Niosomes	Vesicles composed of soy phosphatidylcholine, oleic acid and non-ionic surfactants (caprylyl/capryl polyglucosides or propylene glycol monolaurate) • RSV loaded in oleic acid (2 mg/ml) • Tris buffer as aqueous phase	Skin diffusion using Franz cells	(Caddeo et al., 2015)
	RSV in a mixture of Span 60, Tween 80, and cholesterol	Cytotoxic activity	(Firouzi Amandi et al., 2024)
Liposomes	Liposomes composed of phoshatidylcholine and Tween 80 propylene glycol monolaurate) • RSV loaded in ethanol • Water as aqueous phase	Skin diffusion using Franz cells	(Lafarge et al., 2022)
Molecular inclusion complexes	RSV complexed with 2-hydroxypropyl-γ-cyclodextrin in phosphate buffered saline	In vitro cytotoxicity	(Soo et al., 2016)
Biopolymer particles	Lipid microparticles coated with chitosan • RSV loaded in tristearin (lipidic material) • Hydrogenated phosphatidylcholine as surfactant	Skin diffusion using Franz cells In vivo skin penetration	(Scalia et al., 2015)

	RSV-loaded zein particles coated with alginate/chitosan complex	In vitro release (simulated gastrointestinal condition) and bio-accessibility	(Khan et al., 2019)

c. Pickering emulsion systems

Very recently, several Pickering emulsions systems have been proposed to encapsulate RSV.

RSV-loaded O/W emulsions stabilized with quinoa starch particles were prepared by Matos and co-workers (Matos et al., 2018). The starch particles were modified with octenyl succinic anhydride (OSA) (DS_{Surf} of 1.8%) to increase the particles hydrophobicity. RSV was dissolved in the oil phase composed of a mixture of Miglyol 812 and orange oil to favour the solubilization of RSV (RSV is highly soluble in orange oil). The emulsions obtained showed a mean droplet size of 50 μm (Figure I-24) and displayed an improved stability against creaming phenomena, when compared to conventional emulsions stabilised with Tween 20. EE of RSV obtained for OSA-modified starch granules emulsions was 98 ± 2%, while Tween 20 stabilized emulsions gave an EE of 63 ± 1% (Matos et al., 2018). The lower EE in the conventional emulsions is explained by RSV solubilization in the surfactant micelles in addition to oil droplets, and similar results were also observed by other authors (Davidov-Pardo and McClements, 2015). Progressive releases of RSV after four days were detected in both emulsions.

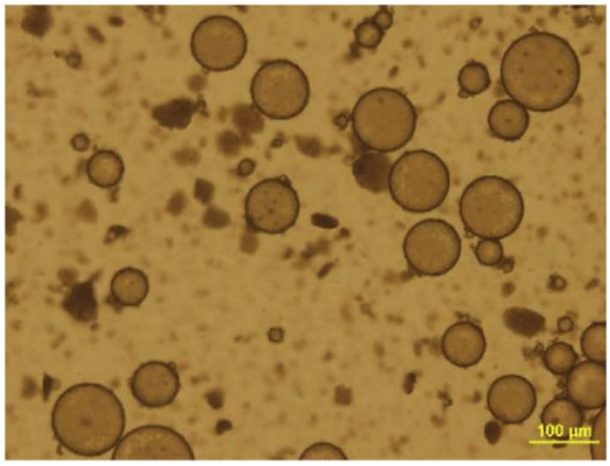

Figure I-24. Microscope image of a RSV-loaded O/W Pickering emulsion stabilized by OSA-modified Quinoa starch granules, formulated with a mixture of Miglyol 812 and orange oil as dispersed phase (Matos et al., 2018).

In another work, Pickering emulsions were stabilized by lignin-based nanoparticles (Dai et al., 2019). Thermo-responsive lignin particles were prepared by grafting poly(N-isopropylacrylamide) onto lignin, *via* atom transfer radical polymerization, and used to prepare O/W emulsions of palm oil loaded with RSV. Poly(N-isopropylacrylamide) being temperature-responsive, a decrease in droplet size was observed when the emulsion was heated at 45°C as shown in Figure I-25 (205 µm at 25 °C to 181 µm at 45 °C) The thermo-responseness of the lignin-based nanoparticles and the UV resistance of lignin (abundance of UV chromophoric groups in lignin molecules) could be combined to improve the controlled release and light stability of RSV. The results showed that the release behaviour depends strongly on the temperature (Figure I-26). It is suggested that the decreasing temperature induced a deformation of the modified lignin nanoparticles at the interface, which then led to an increase in droplet size, and the accelerated release of RSV.

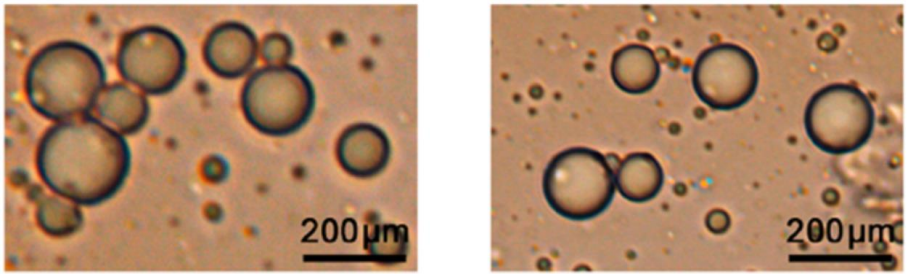

Figure I-25. Optical micrographs of emulsion droplets of palm oil loaded with RSV, stabilized by poly(N-isopropylacrylamide-grafted lignin particles, at 25 °C (left) and 45 °C (right) (Dai et al., 2019).

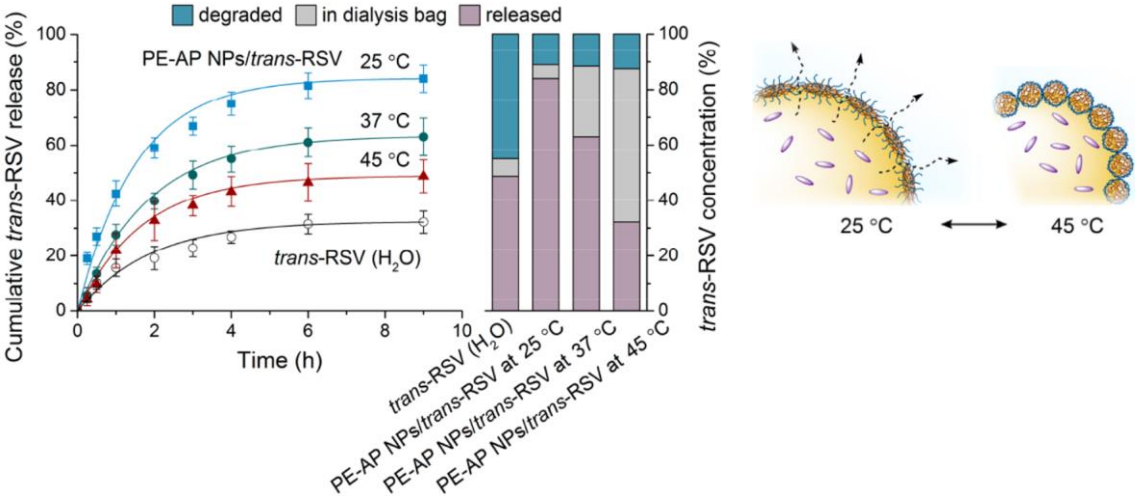

Figure I-26. Cumulative RSV release in water and from the lignin-based Pickering emulsions at different temperatures (left); schematic illustration of the thermal-controlled release of RSV at different temperatures (Dai et al., 2019).

More recently, chitosan/gum arabic nanoparticles, synthesized through ionotropic gelation, were used to stabilise RSV-loaded O/W Pickering emulsions formulated with olive oil as dispersed phase (Sharkawy et al., 2020). A high oil content was used (60% v/v), and the droplet size was found to decrease with increasing particles content (24 µm with 0.5% w/v; 17 µm with 1.5% w/v). The EE of RSV for the formulation prepared with 0.5% w/v of nanoparticles was 92.8%, whereas it was 94.5% for the emulsion prepared with 1.5% w/v of nanoparticles. It was concluded that the increase in nanoparticle concentration had no influence on RSV retention and the presence of the nanoparticles at a low concentration (0.5% w/v) was sufficient to form

a mechanical barrier at the water-oil interface, which successfully enabled RSV entrapment in the oil phase. Moreover, the RSV releases after 24 h were 53.7% and 38.5% for formulations prepared with 0.5% and 1.5% w/v of nanoparticles, respectively. The slower release from the latter could be explained by the presence of a higher amount of nanoparticles. These nanoparticles, being adsorbed at the oil droplet surfaces, have eventually reduced the rate of RSV release from the oil core.

E. Oxidative instability of oil-in-water emulsions

Despite the numerous advantages of oil-in-water (O/W) Pickering emulsions in terms of physical stability, one of the crucial factors that can deteriorate their quality during storage is lipid oxidation (Keramat et al., 2022). Lipid oxidation describes a complex reaction between unsaturated fatty acyl groups with active oxygen species. Lipid oxidation leads to product degradations, off-flavours, and other sensory alterations, which reduces consumer acceptance. Some lipid oxidation products are toxic for humans. There are many reports on bulk oil oxidations, and yet only a few studies have investigated oil oxidations in emulsions. The lipid oxidation rate in O/W emulsions is reported to be higher than in bulk oils (McClements and Decker, 2000). Lipid oxidation in O/W emulsions primarily occurs at the oil–water interface because it is the contact region between pro-oxidant compounds (dissolved in the aqueous phase) and unsaturated lipids (located in the emulsion droplets) (Chen et al., 2013). Pro-oxidant compounds, which are solubilized in the aqueous phase, include oxygen and transition metal ions. Yet, the oxidative stability in Pickering emulsions has been suggested to be higher than conventional emulsions (Keramat et al., 2022). Stabilised Pickering emulsions have solid particles irreversibly adsorbed at the interface. The particles form a thick physical barrier at the interface, which can provide higher oxidative stability.

1. Chemical composition of oils

The oils concerned in this study are composed of lipids, which include triacylglycerols (also known as triglycerides) and free fatty acids. Triacylglycerols consist of fatty acids esterified by glycerol (Figure I-27). Triacylglycerols are important storage lipids and the main constituents of vegetable oils and food lipids.

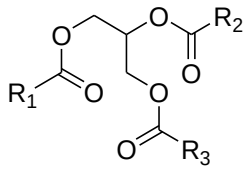

Figure I-27. Chemical structure of triacylglycerols.

Fatty acids are long chain aliphatic carboxylic acids and can be either saturated or unsaturated (Figure I-28). The fatty acids of major vegetable oils and animal fats include saturated, mono-unsaturated and poly-unsaturated fatty acids (Table I-4). The triply unsaturated α-linolenic acid ($C_{18:3}$ ω-3 fatty acid) and the doubly unsaturated linoleic acid ($C_{18:2}$ ω-6 fatty acid) are highly susceptible to oxidation due to the conjugated double bonds leading to hydroperoxides.

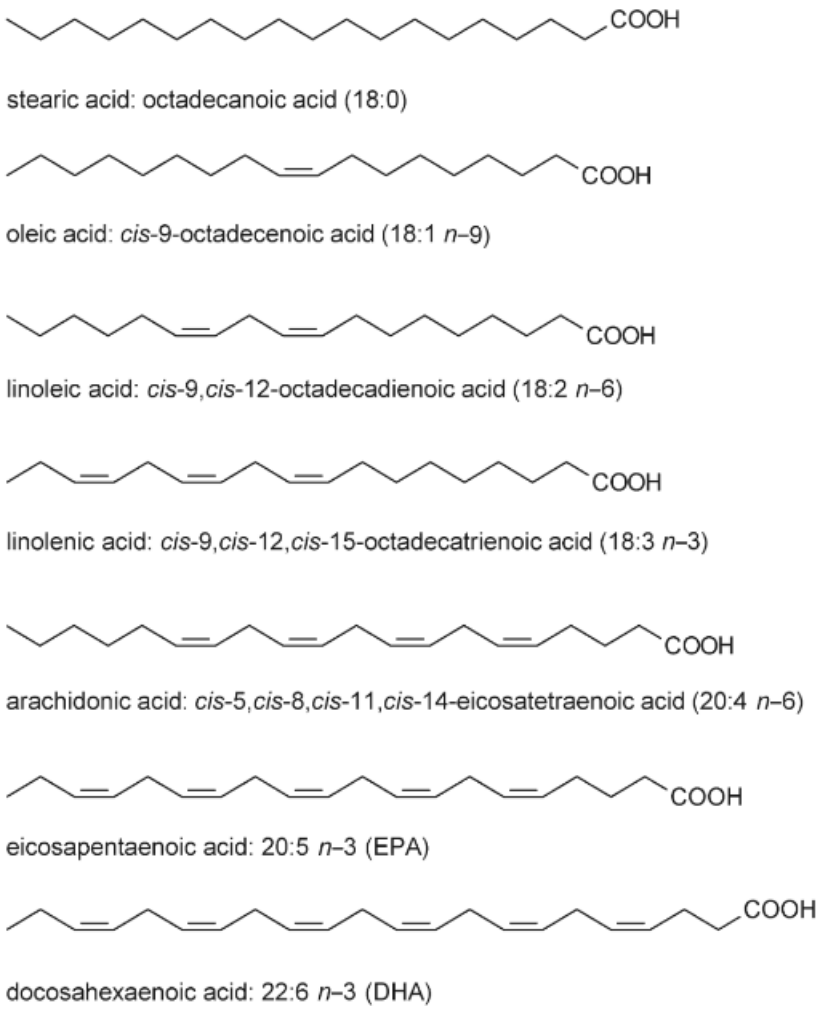

Figure I-28. Structure of saturated, mono-unsaturated and poly-unsaturated fatty acids.

Table I-4. Average fatty acid compositions of vegetable oils, animal fat and fish oil (% by weight).

Oils and fats	**16:0**	**18:0**	**18:1**	**18:2**	**18:3**	**Others**
Coconut [a]	9	3	6	1	-	81
Palm [b]	39	4	43	11	< 1	3
Olive [c]	10	2	78	7	1	2
Soybean [c]	11	4	22	53	8	2
Sunflower [c]	6	5	20	69	< 1	-
Rapeseed [c]	4	2	56	26	10	3
Linseed [d]	7	4	21	15	53	-
Beef tallow [c]	27	7	48	2	-	16
Salmon [c]	15	3	19	3	2	58

[a] (Marina et al., 2009)
[b] (Mohd Hassim, 2020)
[c] (Gunstone, 2012)

[d] (Vereshchagin and Novitskaya, 1965)

2. Lipid oxidation mechanism

Lipid oxidation takes place according to two different mechanisms: free radical autoxidation (with triplet-state oxygen) and photosensitized oxidation (with single-state oxygen) (Frankel, 2014).

a. Free radical auto-oxidation of unsaturated lipids

Auto-oxidation is the direct reaction of molecular oxygen with organic compounds under mild conditions. The auto-oxidation process of unsaturated lipids (RH) can be generally divided into three distinct stages, *i.e.* initiation, propagation, and termination (Brewer, 2011).

Initiation:

The lipid radical ($R^{\bullet}$) is usually initiated by the presence of other radical compounds, singlet state oxygen ($^1O_2$), or the decomposition of hydroperoxides (ROOH) or pigments as in Equation I-9.

$$RH \xrightarrow{Initiator} R^{\bullet} + H^{\bullet} \qquad \textit{Equation I-9}$$

Propagation:

The lipid radical ($R^{\bullet}$) reacts rapidly with molecular oxygen (biradical form in triplet state, $^3O_2$, $^{\bullet}O\text{-}O^{\bullet}$) forming peroxyl radicals (Equation I-10). This is followed by the hydrogen transfer reaction with unsaturated lipids to form hydroperoxides (Equation I-11). This oxidation occurs widely and describes the early stages of hydroperoxides formation as the primary products of lipid oxidation.

$$R^{\bullet} + O_2 \rightarrow ROO^{\bullet} \qquad \textit{Equation I-10}$$

$$ROO^{\bullet} + RH \rightarrow ROOH + R^{\bullet}$$ *Equation I-11*

Termination:

The lipid radicals accumulate at the last stages of auto-oxidation. They interact with each other to form non-radical products as in Equation I-12, Equation I-13 and Equation I-14.

$$R^{\bullet} + R^{\bullet} \rightarrow R - R$$ *Equation I-12*

$$R^{\bullet} + ROO^{\bullet} \rightarrow ROOR$$ *Equation I-13*

$$ROO^{\bullet} + ROO^{\bullet} \rightarrow ROOR + O_2$$ *Equation I-14*

Antioxidants (AH) also inhibit the chain reaction by donating hydrogen atoms ($H^{\bullet}$) to radicals (Equation I-15). The antioxidant free radical may then form a stable non-radical compound (Equation I-16).

$$ROO^{\bullet} + AH \rightarrow ROOH + A^{\bullet}$$ *Equation I-15*

$$ROO^{\bullet} + A^{\bullet} \rightarrow ROOA$$ *Equation I-16*

The auto-oxidation of monounsaturated lipid, *e.g.* methyl oleate (18:1), in the presence of triplet oxygen follows the free radical mechanism, as described earlier. It involves hydrogen abstraction at allylic carbon-8 and carbon-11 to produce two delocalised three-carbon allylic radicals (Figure I-29). Oxygen attacks at the end-carbon positions of these intermediates to produce a mixture of four allylic hydroxyperoxides containing OOH groups on carbons 8, 9, 10 and 11.

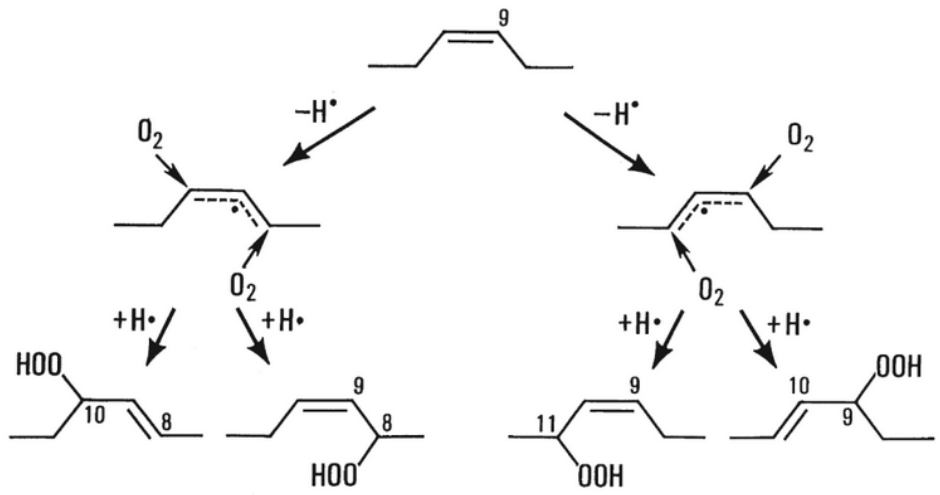

Figure I-29. Mechanism of oleate auto-oxidation (Frankel, 2014).

Polyunsaturated lipids, *i.e.* linoleate (18:2) and linolenate (18:3), are more reactive than mono-unsaturated lipids because they have at least one active bis-allylic methylene group on carbon-11 between two double bonds. In the case of linoleate, hydrogen abstraction at the carbon-11 produces a hybrid pentadienyl radical, which reacts with oxygen at the end carbon-9 and carbon-13 yielding a mixture of two conjugated diene 9- and 13-hydroperoxides (Figure I-30). The pentadienyl radical intermediate is stabilised by resonance, and the resulting dienoic hydroxyperoxides are stabilised by conjugation. This leads to the greater reactivity of polyunsaturated lipids compared to mono-unsaturated lipids.

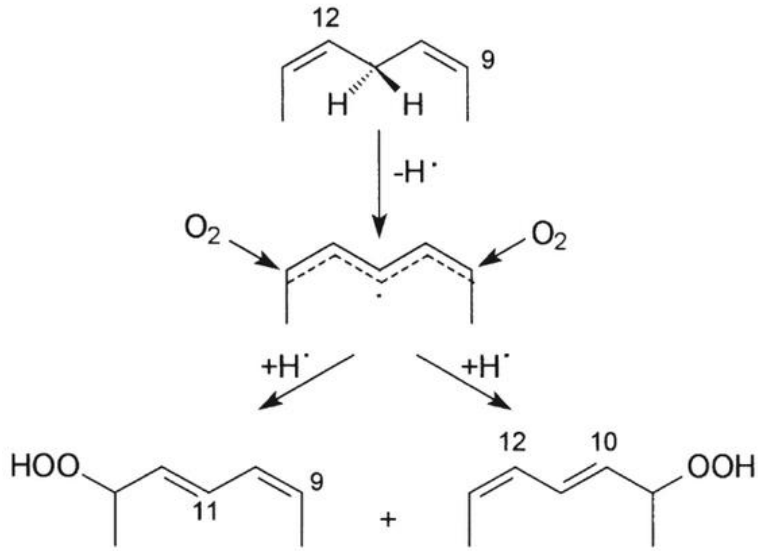

Figure I-30. Mechanism of linoleate auto-oxidation (Frankel, 2014).

In O/W emulsions, the high interfacial area increases the accessibility of oxygen dissolved in water to the oil phase, favouring the auto-oxidation process. In addition, the process of emulsification itself increases the rate of lipid oxidation through incorporation of oxygen (Mao et al., 2009) and the formation of free radicals through acoustic cavitation if sonication is applied (Jana et al., 1990).

Trace amounts of transition metal ions (M), *e.g.* iron and copper, can also accelerate the rates of lipid oxidation through two pathways (Frankel, 2014): (a) electron transfer (Equation I-17) and (b) formation of metal–oxygen complexes (M-O_2) or metal–hydroperoxide complexes (M−HOOR) that catalyse autoxidation and decomposition by one electron redox reactions (Equation I-18 and Equation I-19).

$$M^{(n+1)+} + RH \rightarrow M^{n+} + R^{\bullet} + H^{+} \qquad \textit{Equation I-17}$$

$$M^{n+} + ROOH \xrightarrow{M-O_2 \text{ or } M-HOOR} M^{(n+1)+} + RO^{\bullet} + OH^{-} \qquad \textit{Equation I-18}$$

$$M^{(n+1)+} + ROOH \xrightarrow{M-O_2 \text{ or } M-HOOR} M^{n+} + ROO^{\bullet} + H^{+} \qquad \textit{Equation I-19}$$

The reaction between transition metal ions dissolved in the aqueous phase and hydroperoxides located at oil–water interface is one of the most important mechanisms in the oxidation of Pickering O/W emulsions (Keramat et al., 2022). A schematic representation of lipid oxidation at the interfacial layer of Pickering emulsions is presented in Figure I-31. This reaction increases the dissociation of lipid hydroperoxides into alkoxy and peroxyl radicals, which further increases the lipid oxidation rate.

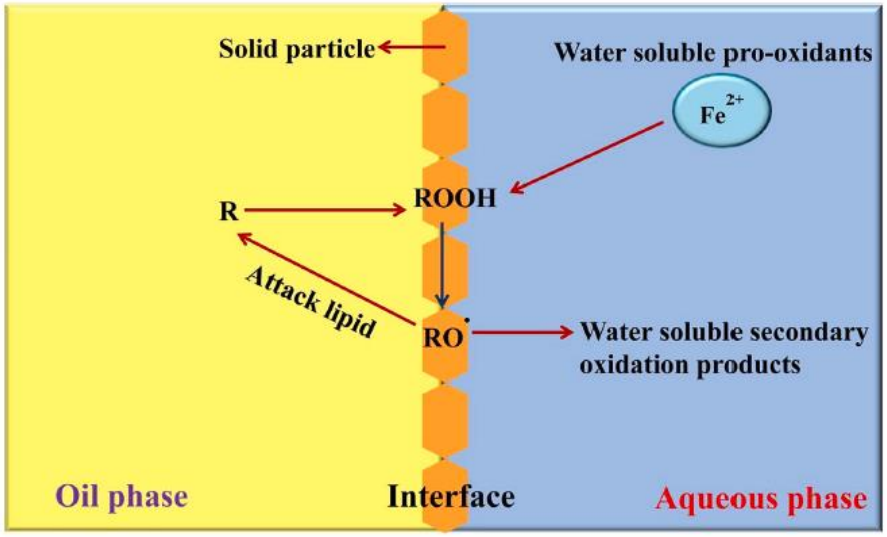

Figure I-31. Mechanism of lipid oxidation in Pickering O/W emulsion (R = unsaturated fatty acid, ROOH = fatty acid peroxide, RO• = alkoxy radical) (Keramat et al., 2022).

b. Photosensitized oxidation of unsaturated lipids

The oxidation of unsaturated lipids is accelerated by exposure to light. Photosensitized oxidation of unsaturated fatty acids proceeds in the presence of oxygen by a nonradical mechanism, different from autoxidation (Frankel, 2014). Exposure to light and a photosensitizer (such as chlorophyll) can activate the triplet oxygen ($^3O_2$) to its singlet state ($^1O_2$), by transfer of energy from the sensitizer. This singlet oxygen is then highly reactive towards the carbon-carbon double bonds of unsaturated lipids, leading to the production hydroperoxides at each unsaturated carbon, by concerted "ene" addition (Figure I-32).

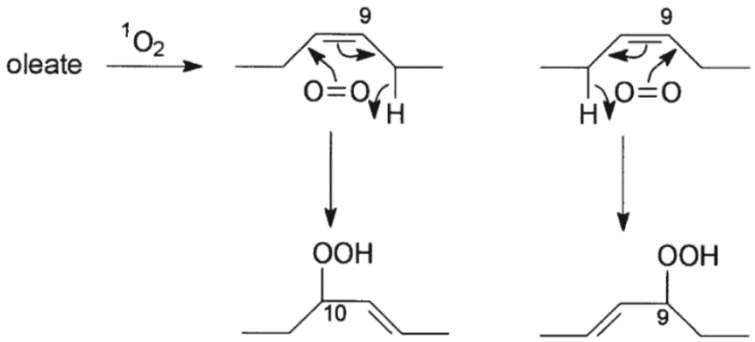

Figure I-32. Oxidation of oleate by singlet oxygen (Frankel, 2014).

3. Improvement of the oxidative stability of O/W Pickering emulsions

Solid particles with proper modifications can physically stabilise Pickering emulsions and also enhance their oxidative stability. Strategies to improve the oxidative stability of Pickering emulsions are generally based on the manipulation of the physical and chemical properties of the interfacial layer, and the increase of the viscosity of the continuous phase (Keramat et al., 2022). The physical properties of interfacial layers, such as thickness and permeability, can influence the diffusion of pro-oxidants, free radicals, and oxygen through the interfacial layer to access the oil droplets (McClements and Decker, 2000). Numerous bio-based particles, namely protein isolates, starch granules and chitosan, have been used to adjust the thickness of the interfacial layer of O/W Pickering emulsions and improve the oxidative stability of the encapsulated oil (Keramat et al., 2023). Several studies with nanocelluloses were also documented, but the formulations investigated were generally quite complex. Angkuratipakorn *et al.* studied the oxidative stability of rice bran O/W Pickering emulsions stabilized with a mixture of CNCs, gum arabic and a non-ionic surfactant, and observed an enhanced oxidative stability of the emulsions (Angkuratipakorn et al., 2017). In another study, TEMPO-oxidized bacterial cellulose was coupled with soy protein isolate nanoparticles to stabilise canola O/W

Pickering emulsions and the system exhibited lower lipid oxidation than the one stabilised solely with soy protein isolate (Zhang et al., 2019).

Besides the interfacial properties, the electrical charge of emulsion droplets can have an impact on the lipid oxidation rate. Cationic protein was reported to impede lipid oxidation through electrostatic repulsion of transition metal ions (pro-oxidants), keeping them away from the lipid droplets (Hu et al., 2003). Alternatively, antioxidants can be incorporated into the solid particles prior to the formation of Pickering emulsions, the Pickering particles acting both as emulsion stabilizers and interfacial reservoirs of antioxidants. Antioxidants, such as tannic acid and anthocyanin, have been combined with solid particles and the resulting Pickering emulsions managed to inhibit the lipid oxidation rate (Ju et al., 2020; Zhou et al., 2020).

F. Conclusion on the literature review

Throughout this literature review, it was shown that CNCs demonstrate good performances as Pickering emulsion stabilizers, in their pristine form or after chemical functionalization of their surface. The stabilisation of Pickering emulsions with pristine CNCs is however conditioned by the surface charge density, which can be modulated by salt addition or desulfation treatments. Up to now, most of the studies reporting on the role of salt compared the properties of emulsions produced with or without salt, but the impact of salt concentration on the surface coverage by the CNCs has never been really investigated.

The efficiency of the CNCs as Pickering stabilizers can also be tailored by modulating the hydrophilic/hydrophobic balance at the CNCs surface, through chemical modification by covalent or non-covalent strategies. The introduction of well-chosen functional moieties can provide at the same time additional characteristics to the CNCs. The functionalization of the

CNCs surface by transesterification of vinyl esters is particularly interesting in this regard, as it allows the grafting of a wide variety of functionalities in mild conditions, using potassium carbonate as catalyst. The surface coating by polydopamine is another attractive strategy, as it is a bio-compatible UV-absorbing and radical-scavenging material, and as such, it can help preventing the oxidation of oil emulsions stabilized by the CNCs. To our knowledge, the utilization of PDA-coated CNCs as Pickering stabilizer has not been investigated yet.

Pickering emulsions stabilized with CNCs are increasingly considered as a valuable mean to encapsulate active molecules or oils, owing in particular to the low toxicity and biocompatibility of cellulose. Resveratrol (RSV) in particular, is a naturally occurring polyphenolic antioxidant compound that would benefit from such encapsulation, its utilization in food or cosmetics being still limited by its poor water solubility, high chemical instability and low oral bioavailability. Yet, the utilization of CNCs-based systems to encapsulate and deliver RSV remains unexplored.

The improvement of the oxidative stability of polyunsaturated oils (*e.g.* linseed oil) in oil–in–water (O/W) emulsion systems is also an important challenge. The oxidative stability in Pickering emulsions has been suggested to be higher than in conventional emulsions, due to the physical barrier form by the particles at the O/W interface. Yet, fundamental studies with CNCs systems are rare, and possible improvements by particles functionalization with active moieties (antioxidant, photoreactive...) still needs to be explored.

References

Akash, B., 2015. Thermochemical depolymerization of biomass. Procedia Computer Science 52, 827–834.

Angkuratipakorn, T., Sriprai, A., Tantrawong, S., Chaiyasit, W., Singkhonrat, J., 2017. Fabrication and characterization of rice bran oil-in-water Pickering emulsion stabilized

by cellulose nanocrystals. Colloids and Surfaces A: Physicochemical and Engineering Aspects 522, 310–319. https://doi.org/10.1016/j.colsurfa.2017.03.014
Arditty, S., Whitby, C.P., Binks, B.P., Schmitt, V., Leal-Calderon, F., 2003. Some general features of limited coalescence in solid-stabilized emulsions. Eur. Phys. J. E 11, 273–281. https://doi.org/10.1140/epje/i2003-10018-6
Asabuwa Ngwabebhoh, F., Ilkar Erdagi, S., Yildiz, U., 2018. Pickering emulsions stabilized nanocellulosic-based nanoparticles for coumarin and curcumin nanoencapsulations: In vitro release, anticancer and antimicrobial activities. Carbohydrate Polymers 201, 317–328. https://doi.org/10.1016/j.carbpol.2018.08.079
Aveyard, R., Binks, B.P., Clint, J.H., 2003. Emulsions stabilised solely by colloidal particles. Advances in Colloid and Interface Science 100–102, 503–546. https://doi.org/10.1016/S0001-8686(02)00069-6
Barclay, T.G., Hegab, H.M., Clarke, S.R., Ginic-Markovic, M., 2017. Versatile Surface Modification Using Polydopamine and Related Polycatecholamines: Chemistry, Structure, and Applications. Adv Materials Inter 4, 1601192. https://doi.org/10.1002/admi.201601192
Barthel, H., 1995. Surface interactions of dimethylsiloxy group-modified fumed silica. Colloids and Surfaces A: Physicochemical and Engineering Aspects 101, 217–226.
Bergfreund, J., Sun, Q., Fischer, P., Bertsch, P., 2019. Adsorption of charged anisotropic nanoparticles at oil–water interfaces. Nanoscale Adv. 1, 4308–4312. https://doi.org/10.1039/C9NA00506D
Bertsch, P., Diener, M., Adamcik, J., Scheuble, N., Geue, T., Mezzenga, R., Fischer, P., 2018. Adsorption and interfacial layer structure of unmodified nanocrystalline cellulose at air/water interfaces. Langmuir 34, 15195–15202.
Binks, B.P., Lumsdon, S.O., 2000. Influence of Particle Wettability on the Type and Stability of Surfactant-Free Emulsions. Langmuir 16, 8622–8631. https://doi.org/10.1021/la000189s
Binks, B.P., Lumsdon, S.O., 1999. Stability of oil-in-water emulsions stabilised by silica particles. Physical Chemistry Chemical Physics 1, 3007–3016.
Bondeson, D., Oksman, K., 2007. Dispersion and characteristics of surfactant modified cellulose whiskers nanocomposites. Composite Interfaces 14, 617–630. https://doi.org/10.1163/156855407782106519
Boocock, D.J., Faust, G.E., Patel, K.R., Schinas, A.M., Brown, V.A., Ducharme, M.P., Booth, T.D., Crowell, J.A., Perloff, M., Gescher, A.J., 2007a. Phase I dose escalation pharmacokinetic study in healthy volunteers of resveratrol, a potential cancer chemopreventive agent. Cancer Epidemiology Biomarkers & Prevention 16, 1246–1252.
Boocock, D.J., Patel, K.R., Faust, G.E., Normolle, D.P., Marczylo, T.H., Crowell, J.A., Brenner, D.E., Booth, T.D., Gescher, A., Steward, W.P., 2007b. Quantitation of trans-resveratrol and detection of its metabolites in human plasma and urine by high performance liquid chromatography. Journal of Chromatography B 848, 182–187.
Brand, J., Pecastaings, G., Sèbe, G., 2017. A versatile method for the surface tailoring of cellulose nanocrystal building blocks by acylation with functional vinyl esters. Carbohydrate Polymers 169, 189–197. https://doi.org/10.1016/j.carbpol.2017.03.077
Brewer, M.S., 2011. Natural Antioxidants: Sources, Compounds, Mechanisms of Action, and Potential Applications. Comprehensive Reviews in Food Science and Food Safety 10, 221–247. https://doi.org/10.1111/j.1541-4337.2011.00156.x
Caddeo, C., Manconi, M., Cardia, M.C., Díez-Sales, O., Fadda, A.M., Sinico, C., 2015. Investigating the interactions of resveratrol with phospholipid vesicle bilayer and the

skin: NMR studies and confocal imaging. International Journal of Pharmaceutics 484, 138–145. https://doi.org/10.1016/j.ijpharm.2015.02.049
Capron, I., Rojas, O.J., Bordes, R., 2017. Behavior of nanocelluloses at interfaces. Current Opinion in Colloid & Interface Science 29, 83–95. https://doi.org/10.1016/j.cocis.2017.04.001
Carrillo, C.A., Nypelö, T.E., Rojas, O.J., 2015. Cellulose nanofibrils for one-step stabilization of multiple emulsions (W/O/W) based on soybean oil. Journal of Colloid and Interface Science 445, 166–173. https://doi.org/10.1016/j.jcis.2014.12.028
Çetin, N.S., Tingaut, P., Özmen, N., Henry, N., Harper, D., Dadmun, M., Sèbe, G., 2009. Acetylation of Cellulose Nanowhiskers with Vinyl Acetate under Moderate Conditions. Macromolecular Bioscience 9, 997–1003. https://doi.org/10.1002/mabi.200900073
Chen, B., McClements, D.J., Decker, E.A., 2013. Oxidation in Different Food Matrices, in: Lipid Oxidation. Elsevier, pp. 129–154. https://doi.org/10.1016/B978-0-9830791-6-3.50006-0
Chen, Y., Cheng, H., Liang, L., 2023. Effect of Oil Type on Spatial Partition of Resveratrol in the Aqueous Phase, the Protein Interface and the Oil Phase of O/W Emulsions Stabilized by Whey Protein and Caseinate. Antioxidants 12, 589. https://doi.org/10.3390/antiox12030589
Cherhal, F., Cousin, F., Capron, I., 2016. Structural Description of the Interface of Pickering Emulsions Stabilized by Cellulose Nanocrystals. Biomacromolecules 17, 496–502. https://doi.org/10.1021/acs.biomac.5b01413
Chevalier, Y., Bolzinger, M.-A., 2013. Emulsions stabilized with solid nanoparticles: Pickering emulsions. Colloids and Surfaces A: Physicochemical and Engineering Aspects 439, 23–34. https://doi.org/10.1016/j.colsurfa.2013.02.054
Cunha, A.G., Mougel, J.-B., Cathala, B., Berglund, L.A., Capron, I., 2014. Preparation of Double Pickering Emulsions Stabilized by Chemically Tailored Nanocelluloses. Langmuir 30, 9327–9335. https://doi.org/10.1021/la5017577
Dai, L., Li, Y., Kong, F., Liu, K., Si, C., Ni, Y., 2019. Lignin-Based Nanoparticles Stabilized Pickering Emulsion for Stability Improvement and Thermal-Controlled Release of *trans*-Resveratrol. ACS Sustainable Chem. Eng. 7, 13497–13504. https://doi.org/10.1021/acssuschemeng.9b02966
Davidov-Pardo, G., McClements, D.J., 2015. Nutraceutical delivery systems: Resveratrol encapsulation in grape seed oil nanoemulsions formed by spontaneous emulsification. Food Chemistry 167, 205–212. https://doi.org/10.1016/j.foodchem.2014.06.082
Davidov-Pardo, G., McClements, D.J., 2014. Resveratrol encapsulation: Designing delivery systems to overcome solubility, stability and bioavailability issues. Trends in Food Science & Technology 38, 88–103. https://doi.org/10.1016/j.tifs.2014.05.003
Destribats, M., Gineste, S., Laurichesse, E., Tanner, H., Leal-Calderon, F., Héroguez, V., Schmitt, V., 2014. Pickering Emulsions: What Are the Main Parameters Determining the Emulsion Type and Interfacial Properties? Langmuir 30, 9313–9326. https://doi.org/10.1021/la501299u
Dhuiège, B., Pecastaings, G., Sèbe, G., 2018. Sustainable approach for the direct functionalization of cellulose nanocrystals dispersed in water by transesterification of vinyl acetate. ACS Sustainable Chemistry & Engineering 7, 187–196.
Donsì, F., Sessa, M., Mediouni, H., Mgaidi, A., Ferrari, G., 2011. Encapsulation of bioactive compounds in nanoemulsion- based delivery systems. Procedia Food Science 1, 1666–1671. https://doi.org/10.1016/j.profoo.2011.09.246
Dudefoi, W., Dhuiège, B., Capron, I., Sèbe, G., 2022. Controlled hydrophobic modification of cellulose nanocrystals for tunable Pickering emulsions. Carbohydrate Polymer

Technologies and Applications 3, 100210. https://doi.org/10.1016/j.carpta.2022.100210
Dupont, H., Maingret, V., Schmitt, V., Héroguez, V., 2021. New Insights into the Formulation and Polymerization of Pickering Emulsions Stabilized by Natural Organic Particles. Macromolecules 54, 4945–4970. https://doi.org/10.1021/acs.macromol.1c00225
Eyley, S., Thielemans, W., 2014. Surface modification of cellulose nanocrystals. Nanoscale 6, 7764–7779. https://doi.org/10.1039/C4NR01756K
Firouzi Amandi, A., Bahmanyar, Z., Dadashpour, M., Lak, M., Natami, M., Döğüş, Y., Alem, M., Adeli, O.A., 2024. Fabrication of magnetic niosomal platform for delivery of resveratrol: potential anticancer activity against human pancreatic cancer Capan-1 cell. Cancer Cell Int 24, 46. https://doi.org/10.1186/s12935-024-03219-2
Francioso, A., Mastromarino, P., Masci, A., D'Erme, M., Mosca, L., 2014. Chemistry, stability and bioavailability of resveratrol. Medicinal Chemistry 10, 237–245. https://doi.org/10.2174/15734064113096660053
Frankel, E.N., 2014. Lipid oxidation. Elsevier.
Fujisawa, S., Togawa, E., Kuroda, K., 2017. Nanocellulose-stabilized Pickering emulsions and their applications. Science and Technology of Advanced Materials 18, 959–971. https://doi.org/10.1080/14686996.2017.1401423
Gambini, J., López-Grueso, R., Olaso-González, G., Inglés, M., Abdelazid, K., El Alami, M., Bonet-Costa, V., Borrás, C., Viña, J., 2013. [Resveratrol: distribution, properties and perspectives], Resveratrol: distribución, propiedades y perspectivas. Revista Española de Geriatría y Gerontología 48, 79–88. https://doi.org/10.1016/j.regg.2012.04.007
Gauthier, G., Capron, I., 2021. Pickering nanoemulsions: An overview of manufacturing processes, formulations, and applications. JCIS Open 4, 100036. https://doi.org/10.1016/j.jciso.2021.100036
Gautier, F., Destribats, M., Perrier-Cornet, R., Dechézelles, J.-F., Giermanska, J., Héroguez, V., Ravaine, S., Leal-Calderon, F., Schmitt, V., 2007. Pickering emulsions with stimulable particles: from highly- to weakly-covered interfaces. Phys. Chem. Chem. Phys. 9, 6455. https://doi.org/10.1039/b710226g
Grachev, V., Deschaume, O., Lang, P.R., Lettinga, M.P., Bartic, C., Thielemans, W., 2024. Dimensions of Cellulose Nanocrystals from Cotton and Bacterial Cellulose: Comparison of Microscopy and Scattering Techniques. Nanomaterials 14, 455. https://doi.org/10.3390/nano14050455
Grishkewich, N., Mohammed, N., Tang, J., Tam, K.C., 2017. Recent advances in the application of cellulose nanocrystals. Current Opinion in Colloid & Interface Science 29, 32–45.
Gugleva, V., Zasheva, S., Hristova, M., Andonova, V., 2020. Topical use of resveratrol: technological aspects. PHAR 67, 89–94. https://doi.org/10.3897/pharmacia.67.e48472
Gunstone, F.D., 2012. Fatty acid and lipid chemistry. Springer.
Habibi, Y., 2014. Key advances in the chemical modification of nanocelluloses. Chem. Soc. Rev. 43, 1519–1542. https://doi.org/10.1039/C3CS60204D
Habibi, Y., Hoeger, I., Kelley, S.S., Rojas, O.J., 2010a. Development of Langmuir−Schaeffer Cellulose Nanocrystal Monolayers and Their Interfacial Behaviors. Langmuir 26, 990–1001. https://doi.org/10.1021/la902444x
Habibi, Y., Lucia, L.A., Rojas, O.J., 2010b. Cellulose Nanocrystals: Chemistry, Self-Assembly, and Applications. Chem. Rev. 110, 3479–3500. https://doi.org/10.1021/cr900339w
Hedjazi, S., Razavi, S.H., 2018. A comparison of Canthaxanthine Pickering emulsions, stabilized with cellulose nanocrystals of different origins. International Journal of

Biological Macromolecules 106, 489–497. https://doi.org/10.1016/j.ijbiomac.2017.08.030
Heux, L., Chauve, G., Bonini, C., 2000. Nonflocculating and chiral-nematic self-ordering of cellulose microcrystals suspensions in nonpolar solvents. Langmuir 16, 8210–8212. https://doi.org/10.1021/la9913957
Hou, Y., Zhang, Z., Harrisson, S., Sèbe, G., 2024. SI-ATRP grafting of polymers from polydopamine-modified cellulose nanocrystals. Carbohydrate Polymers 341, 122346. https://doi.org/10.1016/j.carbpol.2024.122346
Hu, M., McClements, D.J., Decker, E.A., 2003. Lipid Oxidation in Corn Oil-in-Water Emulsions Stabilized by Casein, Whey Protein Isolate, and Soy Protein Isolate. J. Agric. Food Chem. 51, 1696–1700. https://doi.org/10.1021/jf020952j
Hu, Z., Ballinger, S., Pelton, R., Cranston, E.D., 2015a. Surfactant-enhanced cellulose nanocrystal Pickering emulsions. Journal of Colloid and Interface Science 439, 139–148. https://doi.org/10.1016/j.jcis.2014.10.034
Hu, Z., Patten, T., Pelton, R., Cranston, E.D., 2015b. Synergistic Stabilization of Emulsions and Emulsion Gels with Water-Soluble Polymers and Cellulose Nanocrystals. ACS Sustainable Chem. Eng. 3, 1023–1031. https://doi.org/10.1021/acssuschemeng.5b00194
Hung, C.-F., Chen, J.-K., Liao, M.-H., Lo, H.-M., Fang, J.-Y., 2006. Development and Evaluation of Emulsion-Liposome Blends for Resveratrol Delivery. j nanosci nanotechnol 6, 2950–2958. https://doi.org/10.1166/jnn.2006.420
Ilkar Erdagi, S., Ngwabebhoh, F.A., Yildiz, U., 2020. Pickering stabilized nanocellulose-alginate: A diosgenin-mediated delivery of quinalizarin as a potent cyto-inhibitor in human lung/breast cancer cell lines. Materials Science and Engineering: C 109, 110621. https://doi.org/10.1016/j.msec.2019.110621
Jain, D., Hasan, N., Zafar, S., Thakur, J., Haider, K., Parvez, S., Ahmad, F.J., 2023. Transferrin functionalized nanostructured lipid carriers for targeting Rivastigmine and Resveratrol to Alzheimer's disease: Synthesis, in vitro characterization and brain uptake analysis. Journal of Drug Delivery Science and Technology 86, 104555. https://doi.org/10.1016/j.jddst.2023.104555
Jana, A.K., Agarwal, S., Chatterjee, S.N., 1990. Membrane lipid peroxidation by ultrasound: Mechanism and implications. J Biosci 15, 211–215. https://doi.org/10.1007/BF02703887
Ji, C., Wang, Y., 2023. Nanocellulose-stabilized Pickering emulsions: Fabrication, stabilization, and food applications. Advances in Colloid and Interface Science 318, 102970. https://doi.org/10.1016/j.cis.2023.102970
Ju, M., Zhu, G., Huang, G., Shen, X., Zhang, Y., Jiang, L., Sui, X., 2020. A novel pickering emulsion produced using soy protein-anthocyanin complex nanoparticles. Food Hydrocolloids 99, 105329. https://doi.org/10.1016/j.foodhyd.2019.105329
Juškaitė, V., Ramanauskienė, K., Briedis, V., 2015. Design and Formulation of Optimized Microemulsions for Dermal Delivery of Resveratrol. Evidence-Based Complementary and Alternative Medicine 2015, 1–10. https://doi.org/10.1155/2015/540916
Kalashnikova, I., Bizot, H., Bertoncini, P., Cathala, B., Capron, I., 2013. Cellulosic nanorods of various aspect ratios for oil in water Pickering emulsions. Soft Matter 9, 952–959.
Kalashnikova, I., Bizot, H., Cathala, B., Capron, I., 2012. Modulation of Cellulose Nanocrystals Amphiphilic Properties to Stabilize Oil/Water Interface. Biomacromolecules 13, 267–275. https://doi.org/10.1021/bm201599j
Kalashnikova, I., Bizot, H., Cathala, B., Capron, I., 2011. New Pickering Emulsions Stabilized by Bacterial Cellulose Nanocrystals. Langmuir 27, 7471–7479. https://doi.org/10.1021/la200971f

Keramat, M., Ehsandoost, E., Golmakani, M.-T., 2023. Recent Trends in Improving the Oxidative Stability of Oil-Based Food Products by Inhibiting Oxidation at the Interfacial Region. Foods 12, 1191. https://doi.org/10.3390/foods12061191

Keramat, M., Kheynoor, N., Golmakani, M.-T., 2022. Oxidative stability of Pickering emulsions. Food Chemistry: X 14, 100279. https://doi.org/10.1016/j.fochx.2022.100279

Khan, M.A., Yue, C., Fang, Z., Hu, S., Cheng, H., Bakry, A.M., Liang, L., 2019. Alginate/chitosan-coated zein nanoparticles for the delivery of resveratrol. Journal of Food Engineering 258, 45–53. https://doi.org/10.1016/j.jfoodeng.2019.04.010

Kim, J., Montero, G., Habibi, Y., Hinestroza, J.P., Genzer, J., Argyropoulos, D.S., Rojas, O.J., 2009. Dispersion of cellulose crystallites by nonionic surfactants in a hydrophobic polymer matrix. Polymer Engineering & Sci 49, 2054–2061. https://doi.org/10.1002/pen.21417

Klemm, D., Cranston, E.D., Fischer, D., Gama, M., Kedzior, S.A., Kralisch, D., Kramer, F., Kondo, T., Lindström, T., Nietzsche, S., Petzold-Welcke, K., Rauchfuß, F., 2018. Nanocellulose as a natural source for groundbreaking applications in materials science: Today's state. Materials Today 21, 720–748. https://doi.org/10.1016/j.mattod.2018.02.001

Kumar, R., Kaur, K., Uppal, S., Mehta, S.K., 2017. Ultrasound processed nanoemulsion: A comparative approach between resveratrol and resveratrol cyclodextrin inclusion complex to study its binding interactions, antioxidant activity and UV light stability. Ultrasonics Sonochemistry 37, 478–489. https://doi.org/10.1016/j.ultsonch.2017.02.004

Lafarge, E., Villette, S., Cario-André, M., Lecomte, S., Faure, C., 2022. Transdermal diffusion of resveratrol by multilamellar liposomes: Effect of encapsulation on its stability. Journal of Drug Delivery Science and Technology 76, 103742. https://doi.org/10.1016/j.jddst.2022.103742

Le, H.D., Loveday, S.M., Singh, H., Sarkar, A., 2020. Gastrointestinal digestion of Pickering emulsions stabilised by hydrophobically modified cellulose nanocrystals: Release of short-chain fatty acids. Food Chemistry 320, 126650. https://doi.org/10.1016/j.foodchem.2020.126650

Li, Q., Renneckar, S., 2011. Supramolecular Structure Characterization of Molecularly Thin Cellulose I Nanoparticles. Biomacromolecules 12, 650–659. https://doi.org/10.1021/bm101315y

Li, Q., Wu, Y., Fang, R., Lei, C., Li, Y., Li, B., Pei, Y., Luo, X., ShilinLiu, 2021. Application of Nanocellulose as particle stabilizer in food Pickering emulsion: Scope, Merits and challenges. Trends in Food Science & Technology 110, 573–583. https://doi.org/10.1016/j.tifs.2021.02.027

Li, T., Chen, C., Brozena, A.H., Zhu, J.Y., Xu, L., Driemeier, C., Dai, J., Rojas, O.J., Isogai, A., Wågberg, L., Hu, L., 2021. Developing fibrillated cellulose as a sustainable technological material. Nature 590, 47–56. https://doi.org/10.1038/s41586-020-03167-7

Liebscher, J., Mrówczyński, R., Scheidt, H.A., Filip, C., Hădade, N.D., Turcu, R., Bende, A., Beck, S., 2013. Structure of Polydopamine: A Never-Ending Story? Langmuir 29, 10539–10548. https://doi.org/10.1021/la4020288

Liu, H., Zhou, C., Liu, X., Xu, Y., Geng, S., Chen, Y., Wei, C., Yu, C., 2018. PMMA@SCNC composite microspheres prepared from pickering emulsion template as curcumin delivery carriers: Research Article. J. Appl. Polym. Sci. 135, 46127. https://doi.org/10.1002/app.46127

Liu, S., Chen, Y., Liu, C., Gan, L., Ma, X., Huang, J., 2019. Polydopamine-coated cellulose nanocrystals as an active ingredient in poly(vinyl alcohol) films towards intensifying packaging application potential. Cellulose 26, 9599–9612. https://doi.org/10.1007/s10570-019-02749-7

Liu, Y., Ai, K., Lu, L., 2014. Polydopamine and Its Derivative Materials: Synthesis and Promising Applications in Energy, Environmental, and Biomedical Fields. Chem. Rev. 114, 5057–5115. https://doi.org/10.1021/cr400407a

Low, L.E., Tey, B.T., Ong, B.H., Chan, E.S., Tang, S.Y., 2017. Palm olein-in-water Pickering emulsion stabilized by Fe3O4-cellulose nanocrystal nanocomposites and their responses to pH. Carbohydrate Polymers 155, 391–399. https://doi.org/10.1016/j.carbpol.2016.08.091

Machado, N.D., Fernández, M.A., Díaz, D.D., 2019. Recent Strategies in Resveratrol Delivery Systems. ChemPlusChem 84, 951–973. https://doi.org/10.1002/cplu.201900267

Madene, A., Jacquot, M., Scher, J., Desobry, S., 2006. Flavour encapsulation and controlled release – a review. International Journal of Food Science & Technology 41, 1–21. https://doi.org/10.1111/j.1365-2621.2005.00980.x

Mao, L., Xu, D., Yang, J., Yuan, F., Gao, Y., Zhao, J., 2009. Effects of small and large molecule emulsifiers on the characteristics of β-carotene nanoemulsions prepared by high pressure homogenization. Food Technology and Biotechnology 47, 336–342.

Marina, A.M., Che Man, Y.B., Nazimah, S.A.H., Amin, I., 2009. Chemical Properties of Virgin Coconut Oil. J Americ Oil Chem Soc 86, 301–307. https://doi.org/10.1007/s11746-009-1351-1

Marto, J., Ascenso, A., Simoes, S., Almeida, A.J., Ribeiro, H.M., 2016. Pickering emulsions: challenges and opportunities in topical delivery. Expert Opinion on Drug Delivery 13, 1093–1107. https://doi.org/10.1080/17425247.2016.1182489

Matos, M., Gutiérrez, G., Iglesias, O., Coca, J., Pazos, C., 2015. Enhancing encapsulation efficiency of food-grade double emulsions containing resveratrol or vitamin B12 by membrane emulsification. Journal of Food Engineering 166, 212–220. https://doi.org/10.1016/j.jfoodeng.2015.06.002

Matos, M., Laca, A., Rea, F., Iglesias, O., Rayner, M., Gutiérrez, G., 2018. O/W emulsions stabilized by OSA-modified starch granules versus non-ionic surfactant: Stability, rheological behaviour and resveratrol encapsulation. Journal of Food Engineering 222, 207–217. https://doi.org/10.1016/j.jfoodeng.2017.11.009

McClements, D.J., Decker, E.A., 2000. Lipid Oxidation in Oil-in-Water Emulsions: Impact of Molecular Environment on Chemical Reactions in Heterogeneous Food Systems. J Food Science 65, 1270–1282. https://doi.org/10.1111/j.1365-2621.2000.tb10596.x

Mikulcová, V., Bordes, R., Kašpárková, V., 2016. On the preparation and antibacterial activity of emulsions stabilized with nanocellulose particles. Food Hydrocolloids 61, 780–792. https://doi.org/10.1016/j.foodhyd.2016.06.031

Mohd Hassim, N.A., 2020. Quality of commercial palm-based cooking oil packed in plastic pouch and polyethylene terephthalate (PET) bottle. JOPR. https://doi.org/10.21894/jopr.2020.0089

Moon, R.J., Martini, A., Nairn, J., Simonsen, J., Youngblood, J., 2011. Cellulose nanomaterials review: structure, properties and nanocomposites. Chem. Soc. Rev. 40, 3941. https://doi.org/10.1039/c0cs00108b

Murtaza, G., Latif, U., Najam-Ul-Haq, M., Sajjad, A., Karim, S., Akhtar, M., Hussain, I., 2013. Resveratrol: An active natural compound in red wines for health. Journal of Food and Drug Analysis 21, 12.

Neves, A.R., Lúcio, M., Lima, J.L.C., Reis, S., 2012. Resveratrol in medicinal chemistry: A critical review of its pharmacokinetics, drug-delivery, and membrane interactions.

Current Medicinal Chemistry 19, 1663–1681. https://doi.org/10.2174/092986712799945085
Ni, Y., Li, J., Fan, L., 2020. Production of nanocellulose with different length from ginkgo seed shells and applications for oil in water Pickering emulsions. International Journal of Biological Macromolecules 149, 617–626. https://doi.org/10.1016/j.ijbiomac.2020.01.263
Nielsen, L.J., Eyley, S., Thielemans, W., Aylott, J.W., 2010. Dual fluorescent labelling of cellulose nanocrystals for pH sensing. Chemical Communications 46, 8929–8931.
Niles, R.M., Cook, C.P., Meadows, G.G., Fu, Y.-M., McLaughlin, J.L., Rankin, G.O., 2006. Resveratrol is rapidly metabolized in athymic (nu/nu) mice and does not inhibit human melanoma xenograft tumor growth. The Journal of nutrition 136, 2542–2546.
Nishiyama, Y., Langan, P., Chanzy, H., 2002. Crystal Structure and Hydrogen-Bonding System in Cellulose Iβ from Synchrotron X-ray and Neutron Fiber Diffraction. J. Am. Chem. Soc. 124, 9074–9082. https://doi.org/10.1021/ja0257319
Pickering, S.U., 1907. Emulsions. Journal of the Chemical Society, Transactions 91, 2001–2021.
Planes, M., Brand, J., Lewandowski, S., Remaury, S., Solé, S., Le Coz, C., Carlotti, S., Sèbe, G., 2016. Improvement of the Thermal and Optical Performances of Protective Polydimethylsiloxane Space Coatings with Cellulose Nanocrystal Additives. ACS Appl. Mater. Interfaces 8, 28030–28039. https://doi.org/10.1021/acsami.6b09043
Qi, F., Wu, J., Sun, G., Nan, F., Ngai, T., Ma, G., 2014. Systematic studies of Pickering emulsions stabilized by uniform-sized PLGA particles: preparation and stabilization mechanism. Journal of Materials Chemistry B 2, 7605–7611.
Qin, T., Liu, L., Cao, H., Lu, B., Nie, S., Cheng, Z., Zhang, X., Liu, H., An, X., 2023. Polydopamine modified cellulose nanocrystals (CNC) for efficient cellulase immobilization towards advanced bamboo fiber flexibility and tissue softness. International Journal of Biological Macromolecules 253, 126734. https://doi.org/10.1016/j.ijbiomac.2023.126734
Ramsden, W., 1904. Separation of solids in the surface-layers of solutions and ‘suspensions’(observations on surface-membranes, bubbles, emulsions, and mechanical coagulation).—Preliminary account. Proceedings of the royal Society of London 72, 156–164.
Robinson, K., Mock, C., Liang, D., 2015. Pre-formulation studies of resveratrol. Drug Development and Industrial Pharmacy 41, 1464–1469. https://doi.org/10.3109/03639045.2014.958753
Rojas, O.J., Montero, G.A., Habibi, Y., 2009. Electrospun nanocomposites from polystyrene loaded with cellulose nanowhiskers. J of Applied Polymer Sci 113, 927–935. https://doi.org/10.1002/app.30011
Sale, S., Verschoyle, R., Boocock, D., Jones, D., Wilsher, N., Ruparelia, K.C., Potter, G., Farmer, P., Steward, W., Gescher, A., 2004. Pharmacokinetics in mice and growth-inhibitory properties of the putative cancer chemopreventive agent resveratrol and the synthetic analogue trans 3, 4, 5, 4′-tetramethoxystilbene. British journal of cancer 90, 736–744.
Samyn, P., 2021. Polydopamine and Cellulose: Two Biomaterials with Excellent Compatibility and Applicability. Polymer Reviews 61, 814–865. https://doi.org/10.1080/15583724.2021.1896545
Scalia, S., Trotta, V., Iannuccelli, V., Bianchi, A., 2015. Enhancement of in vivo human skin penetration of resveratrol by chitosan-coated lipid microparticles. Colloids and Surfaces B: Biointerfaces 135, 42–49. https://doi.org/10.1016/j.colsurfb.2015.07.043

Sèbe, G., Ham-Pichavant, F., Pecastaings, G., 2013. Dispersibility and Emulsion-Stabilizing Effect of Cellulose Nanowhiskers Esterified by Vinyl Acetate and Vinyl Cinnamate. Biomacromolecules 14, 2937–2944. https://doi.org/10.1021/bm400854n

Sharkawy, A., Casimiro, F.M., Barreiro, M.F., Rodrigues, A.E., 2020. Enhancing trans-resveratrol topical delivery and photostability through entrapment in chitosan/gum Arabic Pickering emulsions. International Journal of Biological Macromolecules 147, 150–159. https://doi.org/10.1016/j.ijbiomac.2020.01.057

Shi, G., Rao, L., Yu, H., Xiang, H., Yang, H., Ji, R., 2008. Stabilization and encapsulation of photosensitive resveratrol within yeast cell. International Journal of Pharmaceutics 349, 83–93. https://doi.org/10.1016/j.ijpharm.2007.07.044

Silva, C.G., Monteiro, J., Marques, R.R.N., Silva, A.M.T., Martínez, C., Canle L., M., Faria, J.L., 2013. Photochemical and photocatalytic degradation of trans-resveratrol. Presented at the Photochemical and Photobiological Sciences, pp. 638–644. https://doi.org/10.1039/c2pp25239b

Silva, Cláudia Gomes, Monteiro, J., Marques, R.R.N., Silva, A.M.T., Martínez, C., Canle L., M., Faria, J.L., 2013. Photochemical and photocatalytic degradation of trans-resveratrol. Photochem Photobiol Sci 12, 638–644. https://doi.org/10.1039/c2pp25239b

Smoliga, J., Blanchard, O., 2014. Enhancing the Delivery of Resveratrol in Humans: If Low Bioavailability is the Problem, What is the Solution? Molecules 19, 17154–17172. https://doi.org/10.3390/molecules191117154

Soo, E., Thakur, S., Qu, Z., Jambhrunkar, S., Parekh, H.S., Popat, A., 2016. Enhancing delivery and cytotoxicity of resveratrol through a dual nanoencapsulation approach. Journal of Colloid and Interface Science 462, 368–374. https://doi.org/10.1016/j.jcis.2015.10.022

Sun, Q., Xiao, L., Nie, Y., Wang, W., Bai, L., Chen, H., Yang, L., Yang, H., Wei, D., 2022. Fabrication of Janus-type nanocomposites from cellulose nanocrystals for self-healing hydrogels' flexible sensors. Colloids and Surfaces B: Biointerfaces 216, 112554. https://doi.org/10.1016/j.colsurfb.2022.112554

Tang, C., Li, Y., Pun, J., Mohamed Osman, A.S., Tam, K.C., 2019. Polydopamine microcapsules from cellulose nanocrystal stabilized Pickering emulsions for essential oil and pesticide encapsulation. Colloids and Surfaces A: Physicochemical and Engineering Aspects 570, 403–413. https://doi.org/10.1016/j.colsurfa.2019.03.049

Tang, J., Lee, M.F.X., Zhang, W., Zhao, B., Berry, R.M., Tam, K.C., 2014. Dual Responsive Pickering Emulsion Stabilized by Poly[2-(dimethylamino)ethyl methacrylate] Grafted Cellulose Nanocrystals. Biomacromolecules 15, 3052–3060. https://doi.org/10.1021/bm500663w

Tang, J., Sisler, J., Grishkewich, N., Tam, K.C., 2017. Functionalization of cellulose nanocrystals for advanced applications. Journal of Colloid and Interface Science 494, 397–409. https://doi.org/10.1016/j.jcis.2017.01.077

Tardy, B.L., Yokota, S., Ago, M., Xiang, W., Kondo, T., Bordes, R., Rojas, O.J., 2017. Nanocellulose–surfactant interactions. Current Opinion in Colloid & Interface Science 29, 57–67. https://doi.org/10.1016/j.cocis.2017.02.004

Thomas, B., Raj, M.C., B, A.K., H, R.M., Joy, J., Moores, A., Drisko, G.L., Sanchez, C., 2018. Nanocellulose, a Versatile Green Platform: From Biosources to Materials and Their Applications. Chem. Rev. 118, 11575–11625. https://doi.org/10.1021/acs.chemrev.7b00627

Uetani, K., Watanabe, Y., Abe, K., Yano, H., 2014. Influence of drying method and precipitated salts on pyrolysis for nanocelluloses. Cellulose 21, 1631–1639. https://doi.org/10.1007/s10570-014-0242-2

Vereshchagin, A.G., Novitskaya, G.V., 1965. The triglyceride composition of linseed oil. J Am Oil Chem Soc 42, 970–974. https://doi.org/10.1007/BF02632457

Wang, W., Du, G., Li, C., Zhang, H., Long, Y., Ni, Y., 2016. Preparation of cellulose nanocrystals from asparagus (Asparagus officinalis L.) and their applications to palm oil/water Pickering emulsion. Carbohydrate Polymers 151, 1–8. https://doi.org/10.1016/j.carbpol.2016.05.052

Werner, A., Schmitt, V., Sèbe, G., Héroguez, V., 2017. Synthesis of surfactant-free micro- and nanolatexes from Pickering emulsions stabilized by acetylated cellulose nanocrystals. Polym. Chem. 8, 6064–6072. https://doi.org/10.1039/C7PY01203A

Whitesides, T.H., Ross, D.S., 1995. Experimental and theoretical analysis of the limited coalescence process: stepwise limited coalescence. Journal of colloid and interface science 169, 48–59.

Wiley, R., 1954. Limited coalescence of oil droplets in coarse oil-in-water emulsions. Journal of Colloid Science 9, 427–437.

Wu, J., Ma, G., 2016. Recent Studies of Pickering Emulsions: Particles Make the Difference. Small 12, 4633–4648. https://doi.org/10.1002/smll.201600877

Yang, P., Zhang, S., Chen, X., Liu, X., Wang, Z., Li, Y., 2020. Recent developments in polydopamine fluorescent nanomaterials. Mater. Horiz. 7, 746–761. https://doi.org/10.1039/C9MH01197H

Zhang, H., Chen, Y., Wang, S., Ma, L., Yu, Y., Dai, H., Zhang, Y., 2020. Extraction and comparison of cellulose nanocrystals from lemon (Citrus limon) seeds using sulfuric acid hydrolysis and oxidation methods. Carbohydrate Polymers 238, 116180. https://doi.org/10.1016/j.carbpol.2020.116180

Zhang, X., Liu, Y., Wang, Y., Luo, X., Li, Y., Li, B., Wang, J., Liu, S., 2019. Surface modification of cellulose nanofibrils with protein nanoparticles for enhancing the stabilization of O/W pickering emulsions. Food Hydrocolloids 97, 105180. https://doi.org/10.1016/j.foodhyd.2019.105180

Zheng, T., Clemons, C.M., Pilla, S., 2021. Grafting PEG on cellulose nanocrystals via polydopamine chemistry and the effects of PEG graft length on the mechanical performance of composite film. Carbohydrate Polymers 271, 118405. https://doi.org/10.1016/j.carbpol.2021.118405

Zhou, B., Gao, S., Li, X., Liang, H., Li, S., 2020. Antioxidant Pickering emulsions stabilised by zein/tannic acid colloidal particles with low concentration. International Journal of Food Science & Technology 55, 1924–1934.

Zhou, Q., Brumer, H., Teeri, T.T., 2009. Self-Organization of Cellulose Nanocrystals Adsorbed with Xyloglucan Oligosaccharide−Poly(ethylene glycol)−Polystyrene Triblock Copolymer. Macromolecules 42, 5430–5432. https://doi.org/10.1021/ma901175j

Zoppe, J.O., Venditti, R.A., Rojas, O.J., 2012. Pickering emulsions stabilized by cellulose nanocrystals grafted with thermo-responsive polymer brushes. Journal of Colloid and Interface Science 369, 202–209. https://doi.org/10.1016/j.jcis.2011.12.011

Zupančič, Š., Lavrič, Z., Kristl, J., 2015. Stability and solubility of trans-resveratrol are strongly influenced by pH and temperature. European Journal of Pharmaceutics and Biopharmaceutics 93, 196–204. https://doi.org/10.1016/j.ejpb.2015.04.002

Chapter II. Materials and methods

A. Preparation and characterisation of the Pickering particles

1. Pristine CNCs

The CNCs used in this thesis were acquired from the University of Maine. The CNCs were isolated by sulfuric acid treatment of wood pulp and consist of negatively-charged needle-like particles of 110 ± 48 nm in length and 4.8 ± 1.1 nm in thickness, as determined by atomic force microscopy in a previous study (*Figure I-33*) (Brand et al., 2017). In aqueous suspension, the CNCs display a zeta potential of about −49 mV, induced by the presence of negative sulphate half-ester groups at the surface, due to the sulfuric acid treatment (sulfur content = 1.05 wt%).

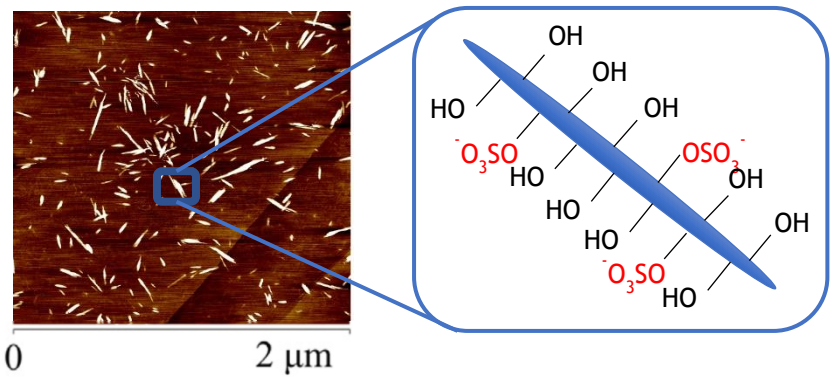

Figure I-33. Topography image taken using atomic force microscopy of pristine CNCs (Brand et al., 2017) and the schematic illustration of a CNC rod (inset).

2. Octanoyl-modified CNCs

a. Reaction mechanism

It has been shown in a previous study that octanoyl-modified CNCs could be efficiently used to stabilize O/W emulsions, as long as the surface degree of substitution (DS_{Surf}) is well

monitored (Dudefoi et al., 2022). Therefore, CNCs with different hydrophilic/hydrophobic balance at the surface were prepared by reacting the CNCs with vinyl octanoate, for various reaction times (*Figure I-34*). During the reaction, the released vinyl alcohol tautomerizes quickly to acetaldehyde, shifting the equilibrium towards the formation of the acylated product (see Chapter I, Part B.4.a.ii).

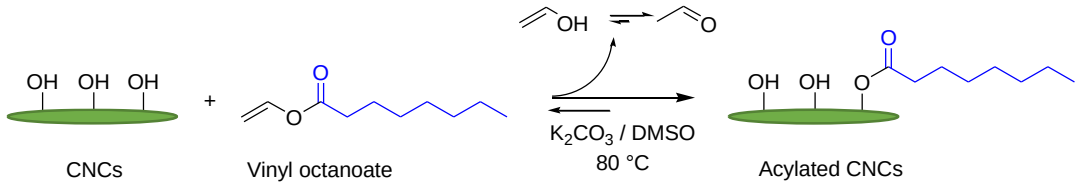

Figure I-34. Reaction scheme of the acylation of CNCs with vinyl octanoate.

b. Experimental protocols

Typically, 0.5 g of CNCs, 0.2 g of K_2CO_3 and 20 mL of DMSO were introduced in a triple-necked 100 mL flask, fitted with a condenser, and the mixture was sonicated for 1 min (Bandelin, MS72 probe, 1.5 kJ). 1 mL of vinyl octanoate was then added and the mixture was heated in an oil bath at 80 °C, and magnetically stirred at 250 rpm for different periods of time (30, 35, 45, 60 and 90 min). At the end of the reaction, the mixture was quenched with THF, and then cooled down in a water bath until room temperature was reached. Any remaining reagent or organic by-products was removed by successive washing/sedimentation steps using 1) THF, 2) ethanol and 3) acetone, and with the help of a centrifuge. The modified particles were then dialyzed in water for two days using a 1 kDa regenerated cellulose membrane and changing the water bath two times a day, to remove the K_2CO_3 catalyst. Finally, the particles were re-dispersed by sonication and freeze-dried. The modified particles obtained after 30, 35, 45, 60 and 90 min were denoted as CNC-Oct 30, CNC-Oct 35, CNC-Oct 45, CNC-Oct 60 and CNC-Oct 90, respectively.

c. Characterisation

The acylation of CNCs was monitored by recording the characteristic vibrations and chemical shifts of the grafted acyl moieties in the FT-IR and ^{13}C Cross-Polarization Magic-Angle-Spinning Nuclear Magnetic Resonance (CP-MAS NMR) spectra of the acylated products (*Figure I-35* and *Figure I-36*, respectively). The FT-IR spectra of the acylated products showed absorption bands for the stretching vibrations of the carbonyl bond at 1740 cm^{-1}, and the $-CH_2-$ and $-CH_3$ groups at 2925 and 2850 cm^{-1}, respectively.

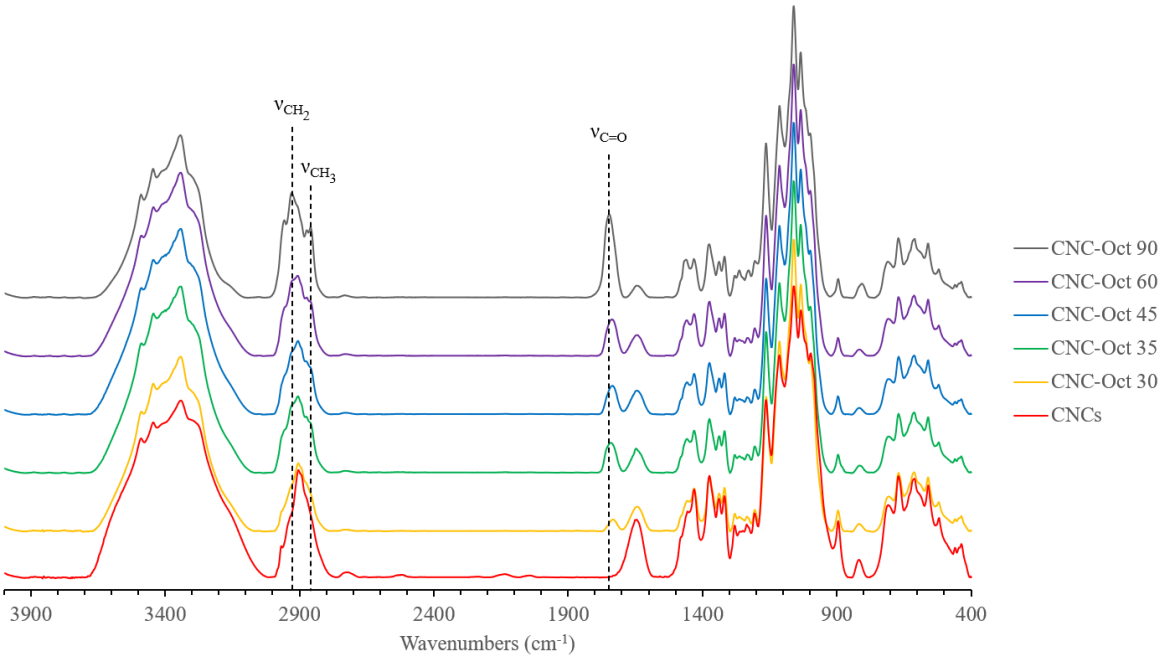

Figure I-35. FT-IR spectra of unmodified and octanoyl-modified CNCs. The FTIR spectra were normalized on the absorption band corresponding to the C-O-C link of cellulose at 1158 cm^{-1}.

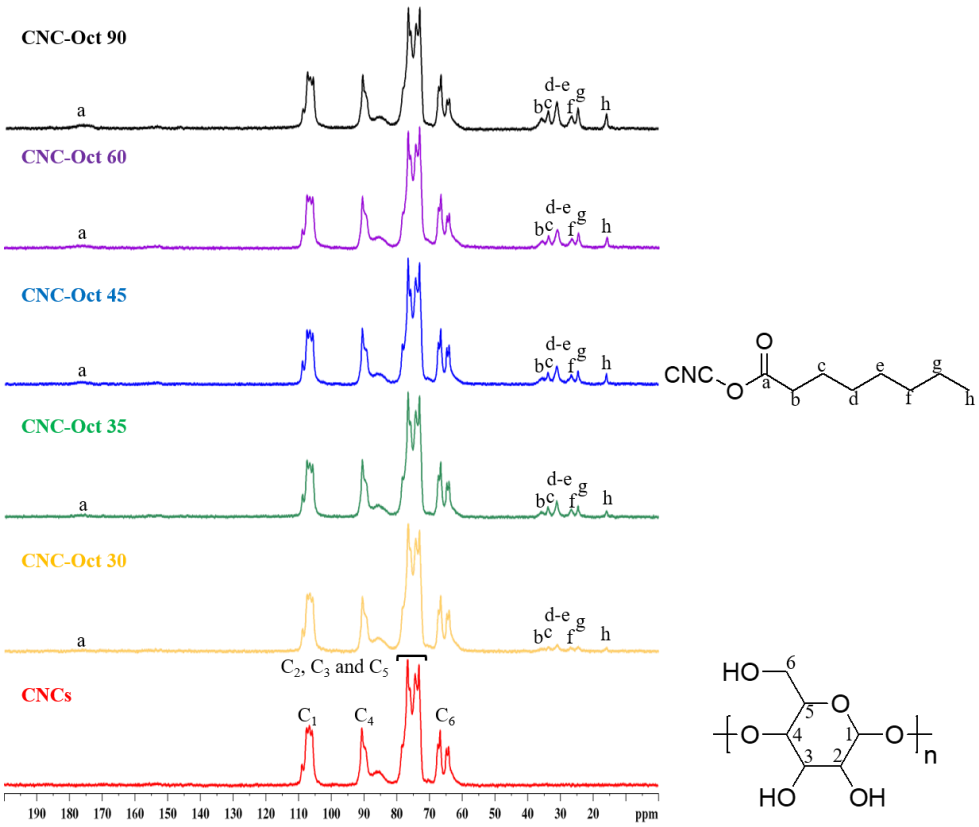

Figure I-36. ^{13}C solid-state CP-MAS NMR spectra of the unmodified and octanoyl-modified CNCs, with the assignment of the characteristic signals.

In the ^{13}C CP-MAS NMR spectra, the carbons of cellulose resonate at 108 ppm (C_1), 91 ppm (C_4 crystalline), 89 ppm (C_4 amorphous), 73–80 ppm (C_2, C_3 and C_5), 67 ppm (C_6 crystalline) and 64 ppm (C_6 amorphous), while the grafted moieties can be observed at 175 ppm (signal of the carbonyl) and in the 15 – 40 ppm region (signals of the methylene and methyl carbons). The cellulose pattern in the NMR spectra was not affected by the acylation treatments and the signals corresponding to the crystalline domains retained their sharpness, suggesting that the ester grafting was limited to the outer surface of the nanoparticles.

The average degree of substitution (DS) per anhydroglucose unit was deduced from the NMR spectra, by comparing the average integral per carbon for the grafted chain (between 15 and 40 ppm and at 175 ppm), with the integral of the C_1 carbon of cellulose used as reference as in *Equation I-20* (Dudefoi et al., 2022).

$$DS = \frac{\left(Sum\ of\ the\ integrations\ for\ the\ grafted\ chain \Big/ Number\ of\ carbons\ in\ the\ chain\right)}{Integration\ of\ the\ C_1\ of\ cellulose}$$ *Equation I-20*

The DS was then converted into a surface degree of substitution (DS_{Surf}) using *Equation I-21*, knowing that only 16.7% of the hydroxyl groups (33.4% of the total anhydroglucose unit) are located at the surface of the CNCs and hence accessible for a chemical reaction (Brand et al., 2017).

$$DS_{Surf} = \frac{DS}{0.334}$$ *Equation I-21*

The DS_{Surf} for the acylated CNCs were calculated and plotted as a function of reaction time (*Figure I-37*). The DS_{Surf} increased with the reaction time, from 0.1 to 0.4, which is in accordance with previous reports (Dudefoi et al., 2022). These acylated CNCs with different DS_{Surf} were then used to stabilise hexadecane-in-water emulsions.

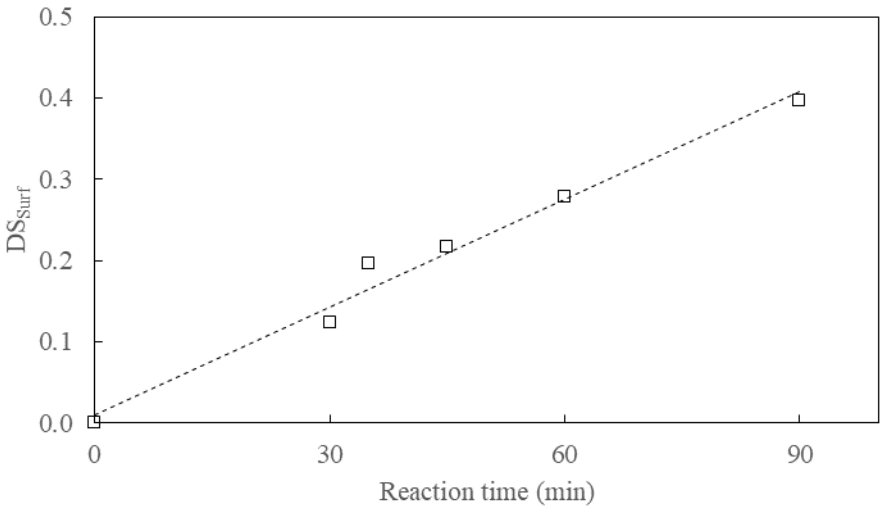

Figure I-37. Evolution of the DS_{Surf} as a function of reaction time for the different octanoyl-modified CNCs.

3. Cinnamoyl-modified CNCs

a. Reaction mechanism

The surface-modification of the CNC was also performed through acylation with vinyl cinnamate (*Figure I-38*), with the double objective to i) partially hydrophobise the CNCs surface for Pickering emulsification, and ii) introduce photoactive moieties. Indeed, it has been shown that cinnamates can undergo reversible trans-cis isomerization and/or dimerization upon UV light irradiation (*Figure I-39*) (Abrakhi et al., 2012). Their ability to dimerize is related to the carbon–carbon double bonds, which can undergo a [2+2] cycloaddition reaction. Moreover, the potential of cinnamoyl-modified CNCs to stabilize O/W Pickering emulsions has been demonstrated in a previous study (Sèbe et al., 2013).

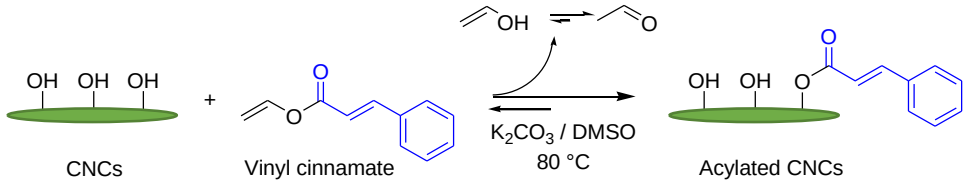

Figure I-38. Reaction scheme of the acylation of CNCs with vinyl cinnamate.

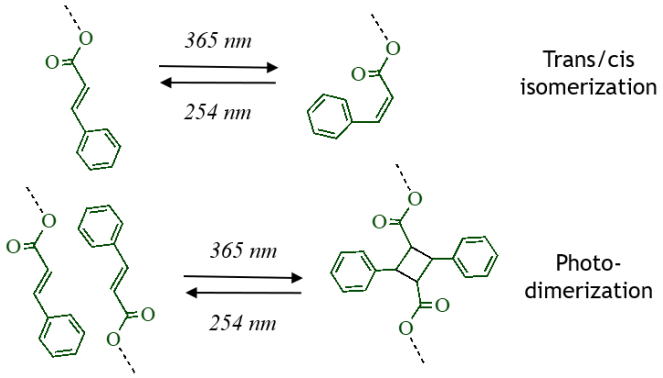

Figure I-39. Reaction scheme of trans-cis isomerization (top) and dimerization (bottom) of cinnamates under UV irradiation.

b. Experimental protocols

In the current work, 0.5 g of CNCs, 0.2 g of K_2CO_3 and 20 mL of DMSO were introduced in a triple-necked 100 mL flask, fitted with a condenser, and the mixture was sonicated for 1 min (Bandelin, MS72 probe, 1.5 kJ). 1 mL of vinyl cinnamate was then added and the mixture was heated in an oil bath at 80 °C, and magnetically stirred at 250 rpm 15 min. At the end of the reaction, the mixture was quenched with THF, and then cooled down in a water bath until room temperature was reached. Any remaining reagent or organic by-products was removed by successive washing/sedimentation steps using 1) THF, 2) ethanol and 3) acetone, and with the help of a centrifuge. The modified particles were then dialyzed in water for two days using a 1 kDa regenerated cellulose membrane and changing the water bath two times a day, to remove the K_2CO_3 catalyst. Finally, the particles were re-dispersed by sonication and freeze-dried. The modified particles obtained were denoted as CNC-Cin 15.

c. Characterisation

The grafting was confirmed by FT-IR and ^{13}C CP-MAS NMR spectroscopy. In the FT-IR spectrum, the vibrations of the grafted cinnamate groups emerged at 1715 ($\nu_{C=O}$), 1635 ($\nu_{C=C}$ exocyclic), and 770 cm^{-1} ($\nu_{=C-H}$ aromatic) (*Figure I-40*). The absorption of the exocyclic C=C bond at 1635 cm^{-1} is relatively strong due to the conjugation with the aromatic ring (Planes et al., 2016).

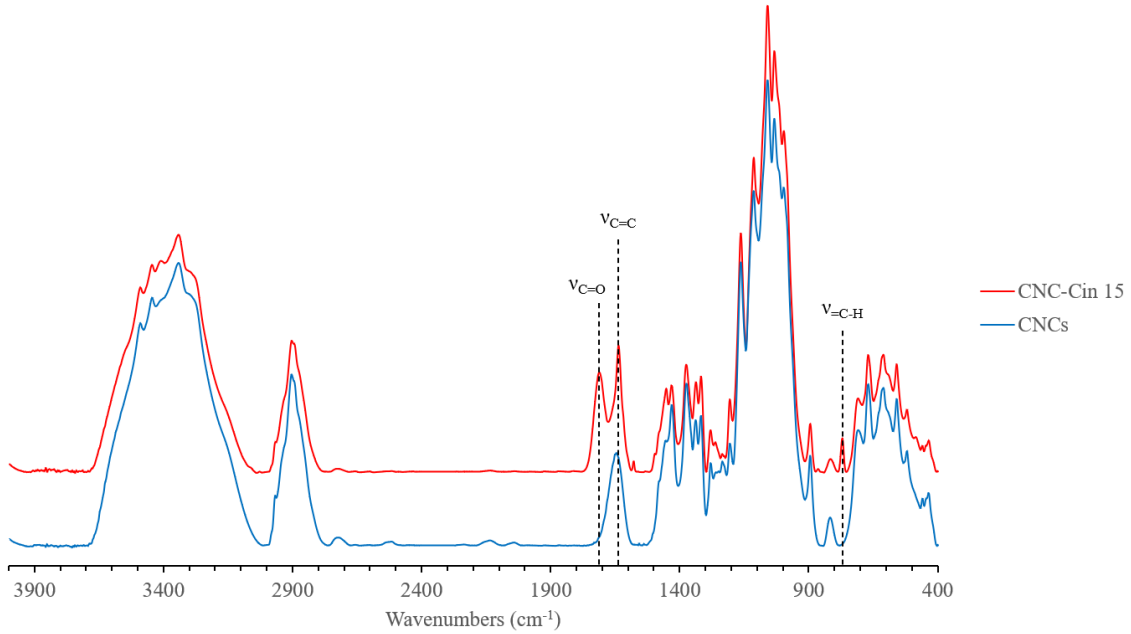

Figure I-40. FT-IR spectra of unmodified and cinnamate-modified CNCs. The FTIR spectra were normalized on the absorption band corresponding to the C-O-C link of cellulose at 1158 cm^{-1}.

In the ^{13}C CP-MAS NMR spectrum, the cinnamate group was observed in the form of weak signals at 160 ppm (C=O) and in the 120−180 ppm region (sp^2 carbons of the exocyclic C=C and aromatic ring) (*Figure I-41*). The chemical shift at around 40 ppm is related to the residual DMSO still trapped at the CNCs surface. The calculated DS_{Surf} was 0.13.

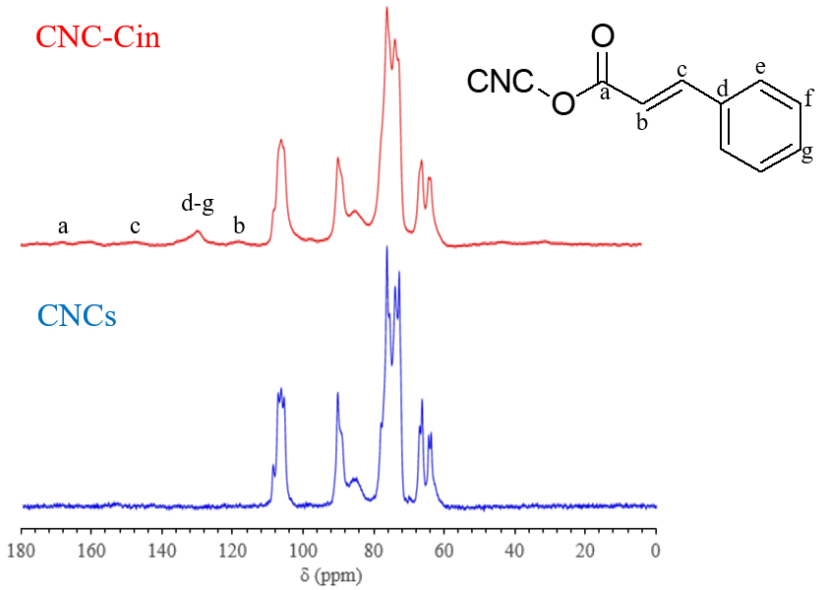

Figure I-41. ^{13}C solid-state CP-MAS NMR spectra of the unmodified and cinnamate-modified CNCs, with the assignment of the characteristic signals.

4. Polydopamine-modified CNCs

a. Reaction mechanism

In a third approach, we envisaged introducing antioxidant properties at the surface of the CNCs by coating the nanopa rticles with polydopamine (PDA) (see Chapter I, Part B.4.b.ii). Indeed, PDA is mainly composed of dihydroxyindole, indolquinone and dopamine units, which display antioxidant and radical scavenging properties (Liu et al., 2014). In collaboration with Yelin Hou (a Ph.D. candidate at LCPO), the treatment was performed by in-situ oxidative polymerization of the dopamine monomer in a Tris buffer solution (Hou et al., 2024)) (*Figure I-42*).

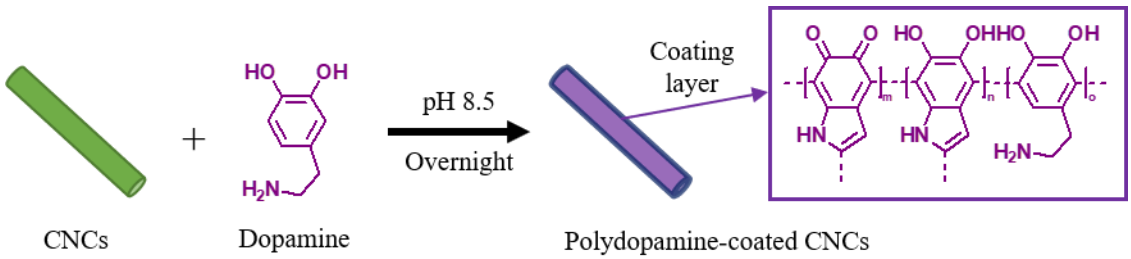

Figure I-42. Reaction scheme of the coating of the CNCs with a PDA layer, starting from dopamine.

b. Experimental protocols

0.5 g of CNCs were dispersed in 20 mL water through 1 min sonication (Bandelin, MS72 probe). 0.6 g of dopamine and 70 mL of water were then added to this suspension, which was adjusted to pH = 8.5 with 0.6 g of Tris. The mixture was stirred at room temperature for 24 h. The particles were recovered by centrifugation, washed three times with water/centrifugation cycles, then freeze-dried. The particles were denoted as CNC-PDA.

c. Characterisation

The presence of PDA at the CNCs surface was confirmed by the appearance of band at 1508 cm^{-1} in the FT-IR spectra (*Figure I-43*), corresponding to the scissoring deformation of N–H (Alzahrani et al., 2022; Liu et al., 2019).

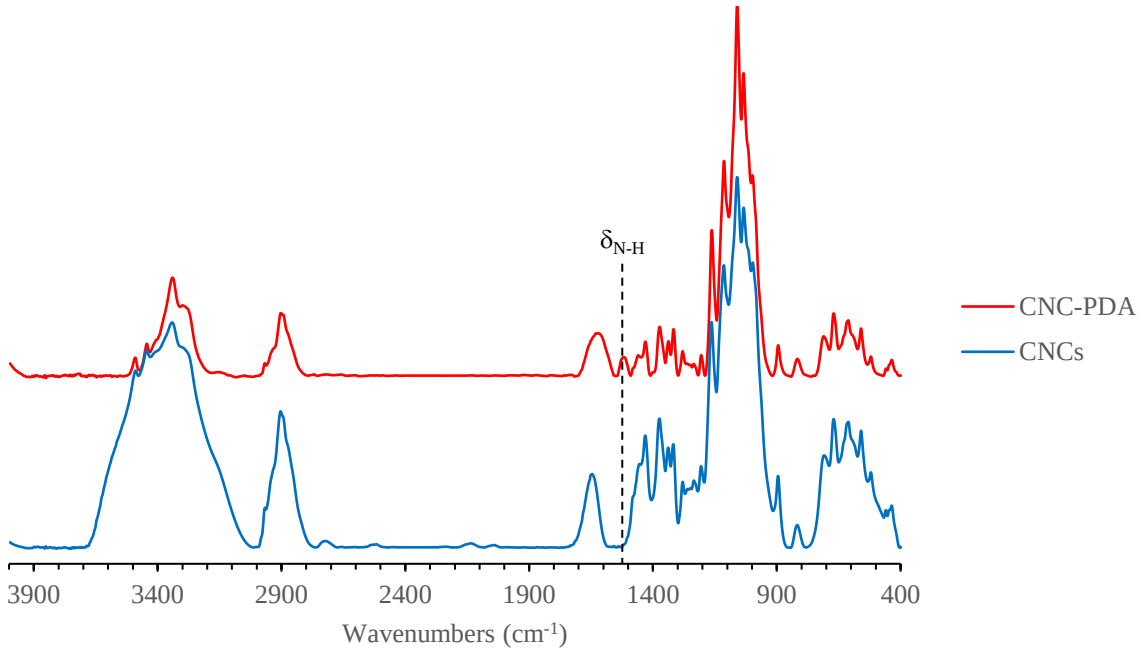

Figure I-43. FT-IR spectra of unmodified and CNC-PDA. The FTIR spectra were normalized on the adsorption band corresponding to the C-O-C link of cellulose at 1158 cm^{-1}.

Peaks characteristic of PDA were also found in the ^{13}C solid-state CP-MAS NMR spectrum (*Figure I-44*), the signals between 20 and 50 ppm being assigned to the carbon atoms of cyclic aliphatics and those between 115 and 150 ppm to the carbon atoms of the arenes (Liebscher et al., 2013).

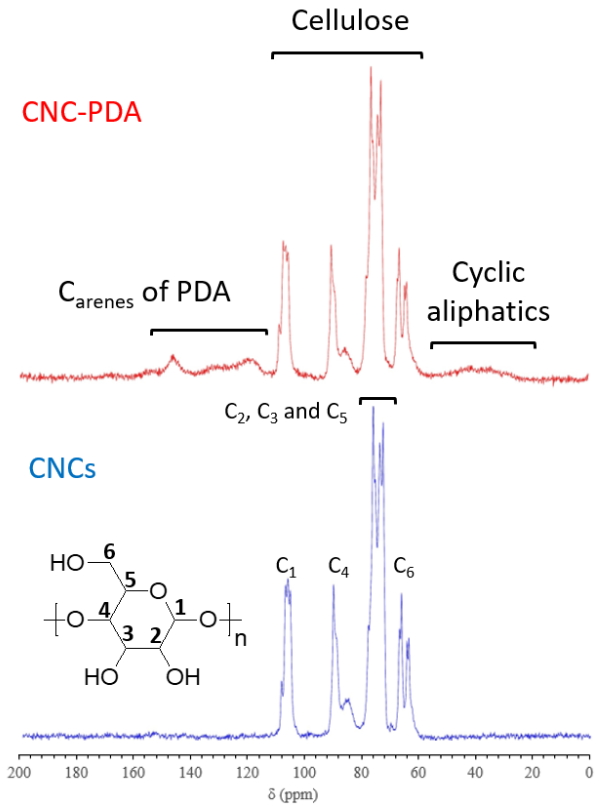

Figure I-44. ^{13}C solid-state CP-MAS NMR spectra of the unmodified and CNC-PDA, with the assignment of the characteristic signals.

B. Characterisation of the CNCs dispersions

1. Preparation of the CNCs dispersions

CNCs aqueous dispersions (1.6 mL) with various NaCl concentrations were prepared by 1 min sonication in an ice bath, using a Bandelin HD 3100 ultrasonicator equipped with a 2 mm tapered titanium probe (20 kHz frequency; sonication power of 100 W; alternation of 2 s sonication with 2 s standby).

2. Determination of hydrodynamic radius

The hydrodynamic radius (HR) and polydispersity index (PDI) of the suspended CNCs were then determined by dynamic light scattering (DLS) using a Nano ZS instrument (Malvern U.K.) working at a 90° angle detection. The HR was deduced from the autocorrelation functions using the cumulant method.

3. Quantification of the isolated CNCs dispersed in water

The amount of CNCs released in the water phase upon addition of SDS in the CNC-stabilized emulsions (Chapter IV, Part B.2) was evaluated by the phenol-sulfuric acid method, with slight modifications (Dubois et al., 1951, 1956; Saha and Brewer, 1994; Goi et al., 2019). The emulsion was centrifuged to induce creaming (1 000 rpm for 5 min at 20 °C), then the water phase containing the released CNCs was collected and freeze-dried for 2 days (BenchTop Pro freeze dryer, SP Scientific U.K.). The dried CNCs were re-dispersed in 0.5 mL of water and mixed with 0.5 mL of a 5% w/w aqueous phenol solution. Concentrated H_2SO_4 (96%) (2.5 mL) was then added, and the mixture was allowed to stand for 30 min at room temperature (no cooling was applied during this step, although heat was released). This solution was analysed by UV-Vis spectroscopy in 500 µL quartz cells (1 cm), using a Cary 100 UV–vis spectrophotometer. The CNC concentration was then determined from the absorbency measured at 490 nm, based on a calibration curve constructed with water dispersions (1.6 mL) of known CNCs concentrations (from 0 to 0.3 mg/mL) (*Figure I-45*).

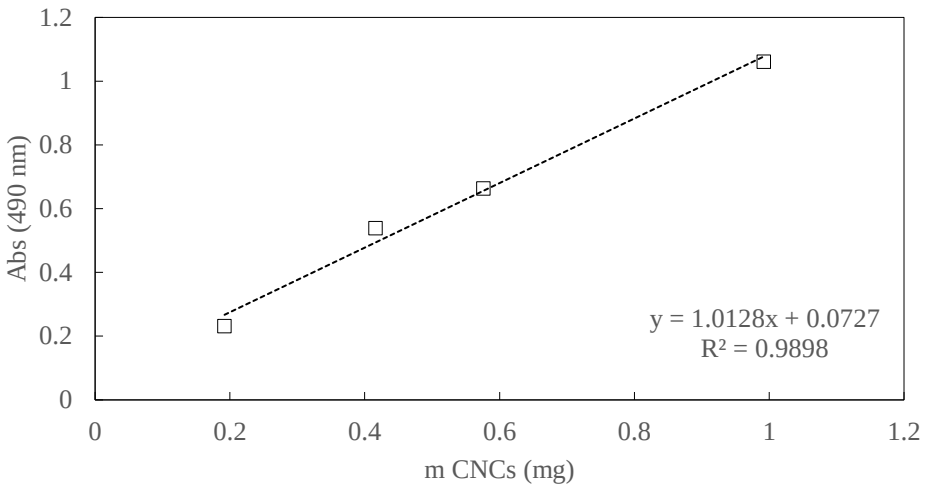

Figure I-45. Calibration curves of CNCs in water.

C. Pickering emulsification and RSV incorporation

Emulsification was achieved by mixing 0.4 mL of hexadecane (with or without RSV) with 1.6 mL of water-dispersed CNCs containing NaCl or not (O/W ratio = 20/80 v/v), and applying sonication for 2 min in the same conditions as in the preparation of CNCs dispersion (*Figure I-46*). Various concentrations of NaCl were used (from 5 to 75 mM).

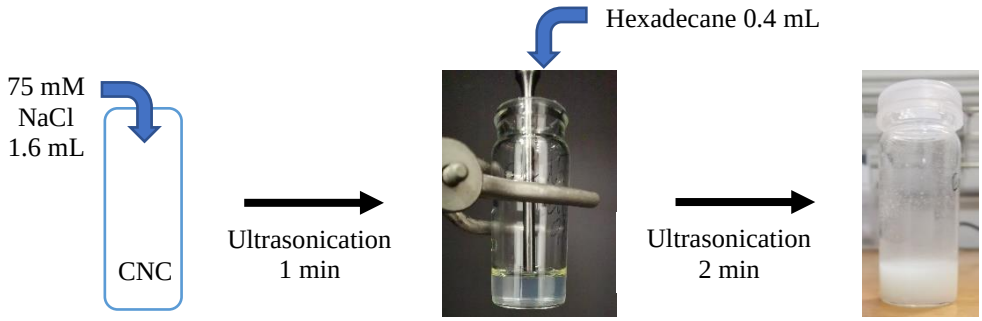

Figure I-46. Schematic illustrations of dispersion of CNCs in water and emulsification of hexadecane in water.

The incorporation of RSV in the emulsions was performed by solubilizing the molecule in hexadecane prior to emulsification, using an ultrasonic bath (30 min), in the absence of light,

and at 20 °C. These precautions were taken because RSV is prone to isomerization when exposed to ultraviolet or visible light (Neves et al., 2012), and to degradation at higher temperatures (Zupančič et al., 2015). Several RSV concentrations were studied: (from 20 µg/mL and 425 µg/mL, corresponding to 8 and 170 µg in the 2 mL total emulsion volume, respectively). Furthermore, the degradation of RSV due to ultrasonic cavitation has been reported by Kumar *et al.* (Kumar et al., 2017), but we did not observe this issue in our conditions of emulsification.

D. Characterisation of the Pickering emulsions

1. Evaluation of the droplets size

The size distributions of the emulsion droplets were measured by laser light scattering, using the Mastersizer 3000 apparatus (Malvern Instruments, UK). Static light-scattering data were transformed into size distributions using Mie Theory The refractive index of the continuous phase was 1.33. It was fixed at 1.43, 1.419, 1.5, 1.467, 1.48, 1.449 and 1.458 for hexadecane, isododecane, squalene, sunflower oil, virgin linseed oil, coconut oil and palm oil, respectively. A small volume of sample was introduced in the dispersion unit containing water (dilution factor ≈ 200), under stirring at 1500 rpm. Each measurement was performed in triplicate.

The droplet size distributions were described in terms of their volume-averaged diameter, D(4,3), surface-averaged diameter, D(3,2), and uniformity, P, defined as (*Equation I-22*):

$$D(4,3) = \frac{\sum N_i D_i^4}{\sum N_i D_i^3}; \quad D(3,2) = \frac{\sum N_i D_i^3}{\sum N_i D_i^2}; \quad P = \frac{\sum X_i |\overline{D} - D_i|}{\overline{D} \sum D_i} \qquad \textit{Equation I-22}$$

where $\overline{D}$ is the median diameter, *i.e.* the value for which the cumulative undersized volume fraction is equal to 50%, and N_i is the total number of particles with diameter D_i.

2. Microscopic observations

To acquire qualitative information in terms of characteristic droplet size and aggregation state, optical micrographs of the emulsions were taken on a bright-field upright microscope (Zeiss Axioscope 40) equipped with an Axioscope 105 color camera. To facilitate the observation, emulsions were diluted in deionized water (dilution factor ≈ 3), placed onto a glass slide and covered with a glass cover slip.

The CNCs at the oil/water interface around the emulsion droplets were visualized under polarized light, using an Olympus BX51 optical microscope (Olympus, Japan) fitted with a digital color camera (Color View, Olympus, Japan). 10X and 40X objectives were employed.

Visualisation of the CNCs particles at the droplet surface were also performed using cryo-scanning electronic microscopy (cryo-SEM) analyses. The samples were cryofixed by slush nitrogen freezing with PP3010 T, (Quorum Technologies, United Kingdom). Then, the samples were placed in the preparation chamber at −140 °C for cryofracture, then sublimation (−95 °C, 4 min) and metallization by platinum sputtering (10 mA, 30s). The observations were performed at 3 kV using a GeminiSEM 300 (Zeiss, Germany).

E. Quantification of RSV by UV-vis spectroscopy

The quantification of RSV in the water phase (Chapter IV) was performed using a Cary 100 UV–vis spectrophotometer and 500 µL quartz cells (1 cm). Pickering emulsion were typically centrifuged at 1 000 rpm for 5 min at 20 °C, to induce creaming and separate the oil droplets from the aqueous phase without destabilizing the emulsion. The aqueous subnatant was then collected and analysed by UV-vis spectroscopy.

In the cases of Pickering emulsions with high concentration of RSV (above 300 µg/mL of hexadecane), the crystallisation of RSV in the aqueous phase was anticipated since the RSV concentration may exceed the saturation limit in water. In order to collect the totality of RSV, including the crystallised RSV, the aqueous subnatant was collected from below through the outlet of a syringe (*Figure I-47*) and diluted to be below the RSV solubility in water. The absence of crystals was checked under microscopy.

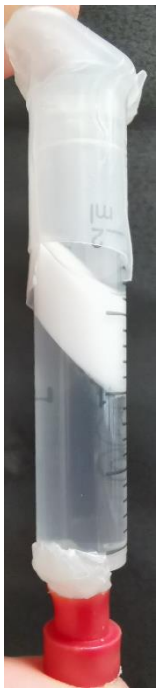

Figure I-47. Photograph of an emulsion after a centrifugation in a syringe. The aqueous subnatant was collected from below through the outlet of the syringe.

The RSV concentration in the aqueous subnatant was determined from the absorbency measured at 306 nm (Zupančič et al., 2015), based on a calibration curve constructed with aqueous solutions of known RSV concentrations (0, 2, 4, 6 and 8 µg/mL) (*Figure I-48*). These reference solutions were obtained by water dilution of a stock solution at 100 µg/mL, prepared by dissolving RSV in a 1/1 v/v mixture of methanol and water (methanol was added to facilitate the dissolution of RSV).

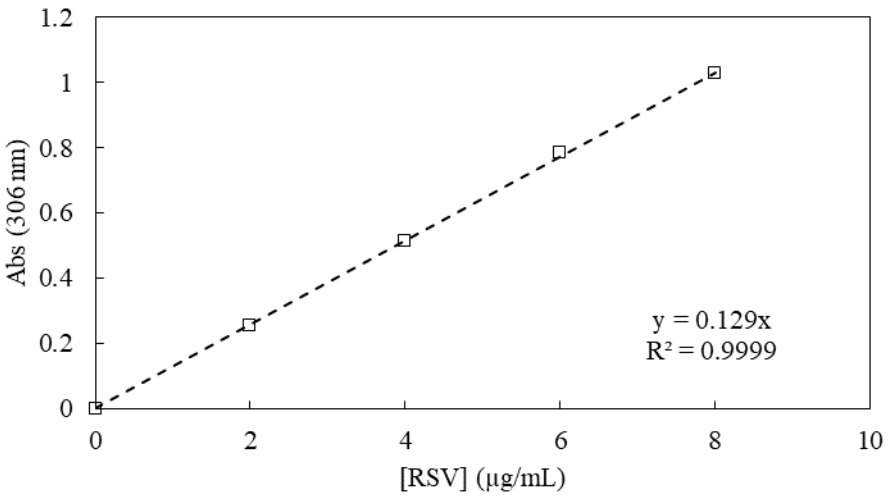

Figure I-48. Calibration curve for the determination of RSV concentration by UV-vis spectroscopy.

F. Evaluation of RSV uptake

The amount of RSV incorporated in the emulsion droplets (Chapter IV) was evaluated by measuring the RSV uptake (U) defined by *Equation I-23*.

$$U\ (\%) = \frac{M_{enc}}{M_{tot}} = \frac{M_{tot} - M_{aq}}{M_{tot}} \times 100\% \qquad \textit{Equation I-23}$$

where M_{enc} is the weight of RSV incorporated into the droplets, M_{tot} the weight of RSV initially introduced in hexadecane, and M_{aq} the weight of RSV measured in the water phase by UV-vis spectroscopy.

G. Release profiles of incorporated RSV and evaluation of the interfacial rate constant

The ability of the incorporated RSV to be released in the external water medium (Chapter IV, Part C) was investigated by the centrifugation method. (Abouelmagd et al., 2015) At discrete time intervals (t), centrifugation was applied to separate the droplets from the water phase. A

known volume of the aqueous phase (≈ 1.1 mL) was then withdrawn, replaced by the same volume of a fresh aqueous NaCl solution to renew the release medium, and analysed by UV-vis spectroscopy. The cumulative fractional release (CRF), defined as the cumulative amount of RSV released at time *t* (M_t) over that incorporated at time t = 0 (M_0), was then determined.

Washington and Evans proposed a mathematical model describing the release of an active when transport across the droplet interface is the rate limiting step (Washington and Evans, 1995). For long times, CFR can then be expressed as in *Equation I-24*:

$$\frac{M_t}{M_0} = 1 - exp\ (-\frac{3k_1 t}{R^2}) \qquad \textit{Equation I-24}$$

which can be rearranged into *Equation I-25*:

$$\frac{R^2}{3} ln(1 - \frac{M_t}{M_0}) = -k_1 t \qquad \textit{Equation I-25}$$

where k_1 is the interfacial rate constant, R the droplets radius. Hence, plotting the term on the left-hand side against time t should give a straight line for long times, the slope of which can be used to directly calculate k_1.

H. Release of interfacial RSV by addition of SDS

The release of RSV positioned at the droplets oil/water interface was triggered by adding SDS in the system (Chapter IV, Part B.2), and gently stirring the emulsion for two hours. The amount or RSV released was evaluated by re-measuring the U. For these investigations, 7 identical emulsions were prepared (2 mL), then 200 µL of SDS of increasing concentration (from 2 to 200 mM in water) was added in each emulsion.

I. Evaluation of lipid oxidation by the conjugated dienes method

1. Context

In this study, pristine and surface-modified CNCs were used to fabricate stable Pickering emulsions of linseed oil, a highly oxidable oil. The potential ability of these nanocelluloses to improve the oxidative stability of the linseed oil Pickering emulsions was investigated and the findings are reported in Chapter V.

Lipid oxidation in Pickering emulsions can be monitored by measuring primary or secondary oxidation products with different methods. The formation of peroxides with time (primary oxidation products) can be followed by measuring the peroxide value (PV), the iodine value (IV), the concentration of conjugated dienes (CD), or by a Rancimat test (Schaich et al., 2017). The determination of secondary oxidation products (mainly aldehydes) can be performed by measuring the p-anisidine value (pAV) or the thiobarbituric acid reactive substances value (TBARs) (Keramat et al., 2023).

Measuring CD values is one of the most used methods to evaluate the early stages of lipid oxidation of oils containing high levels of polyunsaturated fatty acids, such as linseed oil. The auto-oxidation of polyunsaturated lipids produces conjugated diene hydroperoxides (*Figure I-49*) (see Section 1.5.2.1), which can be determined quantitatively by their strong absorption at 233 nm.

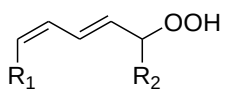

Figure I-49. Chemical structure of conjugated diene hydroperoxides.

In the current study, the measurement of CD was preferred over other methods (PV, IV and Rancimat test), because of its fastness and ease of use.

2. Protocols

a. Induction of oxidation by Fe(II)

The lipid oxidation in the Pickering emulsions was induced by the addition of two different iron solutions after the fabrication of the emulsions (Daoud et al., 2019). 10 µL of a 0.2 M $FeSO_4$ solution were added to 2 mL of emulsion to obtain a final Fe(II) concentrations of 10^{-3} M. 40 µL of a 0.5 M $FeSO_4$ solution were added to 2 mL of emulsion to obtain a final Fe(II) concentration of 10^{-2} M. The emulsions were stored in the absence of light under constant rotation at 5 rpm for various period of time (Rotator disk, Fisher Scientific).

b. Extraction of the lipid from the O/W emulsion

The determination of CD requires first to extract the lipid from the O/W Pickering emulsions (Velasco et al., 2008). Solvent extraction was performed using a mixture of isooctane/2-propanol (3:1) to break the emulsion and extract the oil (Cho et al., 2002). Practically, 0.2 mL of the oxidation-induced emulsion was added to 1 mL of isooctane/2-propanol (3:1) solution. The mixture was then homogenised using a vortex mixer for 1 min and left to stand for 1 min for phase separation.

c. Evaluation of CD by UV–Vis spectroscopy

CD were determined based on the AOCS official method Ti 1a-64 with some modifications (AOCS, 2009). 20 µL of the upper layer was diluted in isooctane. The sample was then filtered on a 0.45 µm PTFE membrane (Rotta et al., 2020). Absorbance spectra were recorded between 200 and 400 nm using a double beam UV–Vis spectrophotometer (Cary 100, Agilent, USA) with a data interval of 1 nm and a band path of 2 nm. Pure isooctane was used as a reference

(Daoud et al., 2019). The value of CD was expressed in millimoles of equivalents peroxide (LH) per kilogram of oil (mmol eq LH.kg^{-1} oil) using a molar extinction coefficient (ε) of 27,000M^{-1}·cm^{-1} at 233 nm (*Equation I-26*) (Lethuaut et al., 2002).

$$[CD]\left(\frac{mmol}{kg}\right) = \frac{Abs}{\varepsilon \times l \times d_{lin}} \times Dilution\ factor \qquad \textit{Equation I-26}$$

The overall procedures for the monitoring of lipid oxidation in emulsions are summarised in *Figure I-50*.

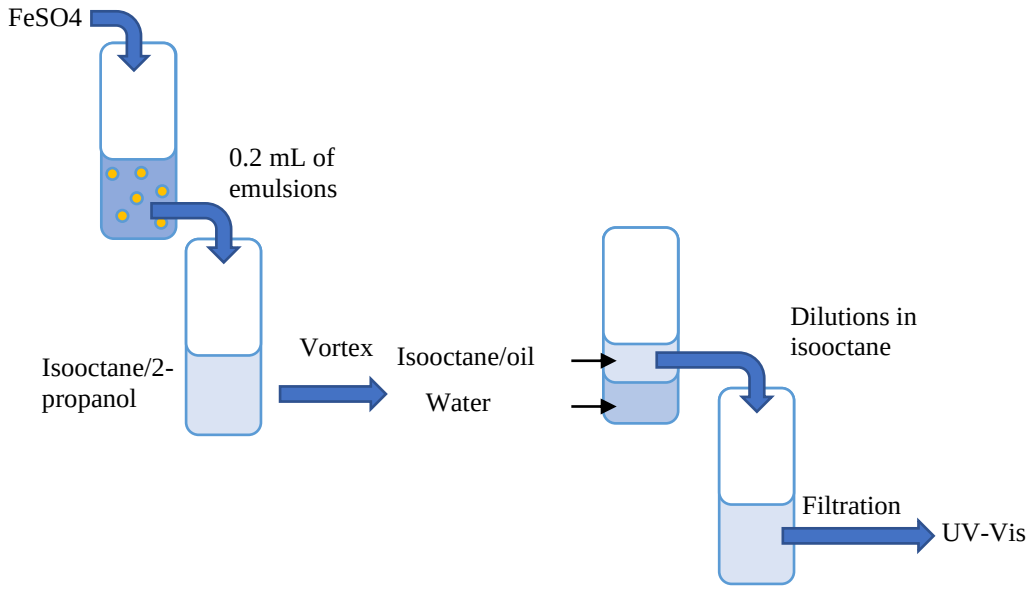

Figure I-50. Schematic illustrations of procedures to monitor the lipid oxidation.

References

Abouelmagd, S.A., Sun, B., Chang, A.C., Ku, Y.J., Yeo, Y., 2015. Release Kinetics Study of Poorly Water-Soluble Drugs from Nanoparticles: Are We Doing It Right? Mol. Pharmaceutics 12, 997–1003. https://doi.org/10.1021/mp500817h

Abrakhi, S., Péralta, S., Cantin, S., Fichet, O., Teyssié, D., 2012. Synthesis and characterization of photosensitive cinnamate-modified cellulose acetate butyrate spin-coated or network derivatives. Colloid Polym Sci 290, 423–434. https://doi.org/10.1007/s00396-011-2559-9

Alzahrani, F.M., Amari, A., Katubi, K.M., Alsaiari, N.S., Tahoon, M.A., 2022. The synthesis of nanocellulose-based nanocomposites for the effective removal of hexavalent

chromium ions from aqueous solution. Open Chemistry 20, 970–983. https://doi.org/10.1515/chem-2022-0215
AOCS, 2009. Spectrophotometric Determination of Conjugated Dienoic Acid Ti 1a-64.
Brand, J., Pecastaings, G., Sèbe, G., 2017. A versatile method for the surface tailoring of cellulose nanocrystal building blocks by acylation with functional vinyl esters. Carbohydrate Polymers 169, 189–197. https://doi.org/10.1016/j.carbpol.2017.03.077
Cho, Y.-J., McClements, D.J., Decker, E.A., 2002. Ability of Surfactant Micelles To Alter the Physical Location and Reactivity of Iron in Oil-in-Water Emulsion. J. Agric. Food Chem. 50, 5704–5710. https://doi.org/10.1021/jf020433g
Daoud, S., Bou-maroun, E., Dujourdy, L., Waschatko, G., Billecke, N., Cayot, P., 2019. Fast and direct analysis of oxidation levels of oil-in-water emulsions using ATR-FTIR. Food Chemistry 293, 307–314. https://doi.org/10.1016/j.foodchem.2019.05.005
Dubois, M., Gilles, K., Hamilton, J.K., Rebers, P.A., Smith, F., 1951. A Colorimetric Method for the Determination of Sugars. Nature 168, 167–167. https://doi.org/10.1038/168167a0
Dubois, Michel., Gilles, K.A., Hamilton, J.K., Rebers, P.A., Smith, Fred., 1956. Colorimetric Method for Determination of Sugars and Related Substances. Anal. Chem. 28, 350–356. https://doi.org/10.1021/ac60111a017
Dudefoi, W., Dhuiège, B., Capron, I., Sèbe, G., 2022. Controlled hydrophobic modification of cellulose nanocrystals for tunable Pickering emulsions. Carbohydrate Polymer Technologies and Applications 3, 100210. https://doi.org/10.1016/j.carpta.2022.100210
Goi, Y., Fujisawa, S., Saito, T., Yamane, K., Kuroda, K., Isogai, A., 2019. Dual Functions of TEMPO-Oxidized Cellulose Nanofibers in Oil-in-Water Emulsions: A Pickering Emulsifier and a Unique Dispersion Stabilizer. Langmuir 35, 10920–10926. https://doi.org/10.1021/acs.langmuir.9b01977
Hou, Y., Zhang, Z., Harrisson, S., Sèbe, G., 2024. SI-ATRP grafting of polymers from polydopamine-modified cellulose nanocrystals. Carbohydrate Polymers 341, 122346. https://doi.org/10.1016/j.carbpol.2024.122346
Keramat, M., Ehsandoost, E., Golmakani, M.-T., 2023. Recent Trends in Improving the Oxidative Stability of Oil-Based Food Products by Inhibiting Oxidation at the Interfacial Region. Foods 12, 1191. https://doi.org/10.3390/foods12061191
Kumar, R., Kaur, K., Uppal, S., Mehta, S.K., 2017. Ultrasound processed nanoemulsion: A comparative approach between resveratrol and resveratrol cyclodextrin inclusion complex to study its binding interactions, antioxidant activity and UV light stability. Ultrasonics Sonochemistry 37, 478–489. https://doi.org/10.1016/j.ultsonch.2017.02.004
Lethuaut, L., Métro, F., Genot, C., 2002. Effect of droplet size on lipid oxidation rates of oil-in-water emulsions stabilized by protein. J Amer Oil Chem Soc 79, 425. https://doi.org/10.1007/s11746-002-0500-z
Liebscher, J., Mrówczyński, R., Scheidt, H.A., Filip, C., Hădade, N.D., Turcu, R., Bende, A., Beck, S., 2013. Structure of Polydopamine: A Never-Ending Story? Langmuir 29, 10539–10548. https://doi.org/10.1021/la4020288
Liu, S., Chen, Y., Liu, C., Gan, L., Ma, X., Huang, J., 2019. Polydopamine-coated cellulose nanocrystals as an active ingredient in poly(vinyl alcohol) films towards intensifying packaging application potential. Cellulose 26, 9599–9612. https://doi.org/10.1007/s10570-019-02749-7
Liu, Y., Ai, K., Lu, L., 2014. Polydopamine and Its Derivative Materials: Synthesis and Promising Applications in Energy, Environmental, and Biomedical Fields. Chem. Rev. 114, 5057–5115. https://doi.org/10.1021/cr400407a

Neves, A.R., Lúcio, M., Lima, J.L.C., Reis, S., 2012. Resveratrol in medicinal chemistry: A critical review of its pharmacokinetics, drug-delivery, and membrane interactions. Current Medicinal Chemistry 19, 1663–1681. https://doi.org/10.2174/092986712799945085

Planes, M., Brand, J., Lewandowski, S., Remaury, S., Solé, S., Le Coz, C., Carlotti, S., Sèbe, G., 2016. Improvement of the Thermal and Optical Performances of Protective Polydimethylsiloxane Space Coatings with Cellulose Nanocrystal Additives. ACS Appl. Mater. Interfaces 8, 28030–28039. https://doi.org/10.1021/acsami.6b09043

Rotta, E.M., Giroux, H.J., Lamothe, S., Bélanger, D., Sabik, H., Visentainer, J.V., Britten, M., 2020. Use of passion fruit seed extract (Passiflora edulis Sims) to prevent lipid oxidation in dairy beverages during storage and simulated digestion. LWT 123, 109088. https://doi.org/10.1016/j.lwt.2020.109088

Saha, A.K., Brewer, C.F., 1994. Determination of the concentrations of oligosaccharides, complex type carbohydrates, and glycoproteins using the phenol-sulfuric acid method. Carbohydrate Research 254, 157–167. https://doi.org/10.1016/0008-6215(94)84249-3

Schaich, K.M., Xie, J., Bogusz, B.A., 2017. Thinking outside the classical chain reaction box of lipid oxidation: Evidence for alternate pathways and the importance of epoxides. Lipid Technology 29, 91–96. https://doi.org/10.1002/lite.201700025

Sèbe, G., Ham-Pichavant, F., Pecastaings, G., 2013. Dispersibility and Emulsion-Stabilizing Effect of Cellulose Nanowhiskers Esterified by Vinyl Acetate and Vinyl Cinnamate. Biomacromolecules 14, 2937–2944. https://doi.org/10.1021/bm400854n

Velasco, J., Marmesat, S., Holgado, F., Márquez-Ruiz, G., Dobarganes, C., 2008. Influence of two lipid extraction procedures on the peroxide value in powdered infant formulas. European Food Research and Technology 226, 1159–1166. https://doi.org/10.1007/s00217-007-0645-5

Washington, C., Evans, K., 1995. Release rate measurements of model hydrophobic solutes from submicron triglyceride emulsions. Journal of controlled release 33, 383–390.

Zupančič, Š., Lavrič, Z., Kristl, J., 2015. Stability and solubility of trans-resveratrol are strongly influenced by pH and temperature. European Journal of Pharmaceutics and Biopharmaceutics 93, 196–204. https://doi.org/10.1016/j.ejpb.2015.04.002

Chapter III. Formulation of the Pickering emulsions

A. Investigations with hexadecane as model oil

1. Conditions of emulsification

In preliminary experiments, O/W emulsions of hexadecane were prepared with or without salt (NaCl), and the evolution of the droplets size as a function of CNCs concentration was investigated. The emulsification was achieved by mixing 0.4 mL of hexadecane with 1.6 mL of water-dispersed CNCs containing NaCl or not (O/W ratio = 20/80 v/v), and applying sonication for 2 min. See Chapter II, Parts B and C for more details.

When no salt was added, large droplets were observed by microscopy right after preparation, but macroscopic phase separation occurred within one hour (Figure III-1**)**. Hence, no long-term stability could be obtained with pure water, in line with literature data (Capron et al., 2017; Bergfreund et al., 2019; Heise et al., 2022). The CNCs adsorption at the O/W interface is controlled first by the diffusion of the particles to the bare interface, secondly by the electrostatic energy barrier (Kutuzov et al., 2007; Dugyala et al., 2016; Dridi et al., 2018). Without salt, the electrostatic barrier is too high to reach a surface coverage sufficient for emulsion stability.

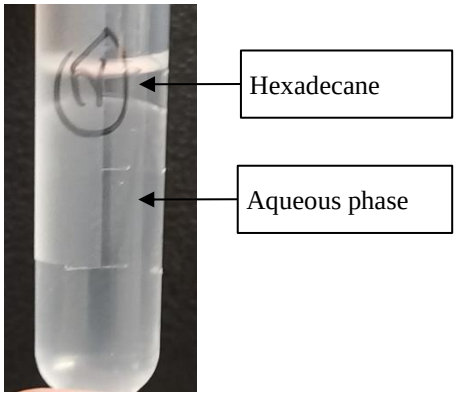

Figure III-1. Photograph of the O/W mixture one hour after sonication of hexadecane with the CNCs water suspension, in the absence of salt ([NaCl] = 0 mM; [CNCs] = 5.75 g/L of hexadecane; O/W ratio of 20/80 v/v).

When the same emulsion was prepared in the presence of various concentrations of NaCl (from 15 to 75 mM), stable emulsions were systematically obtained, no oil layer resulting from the coalescence of oil droplets being noted within 12 months. However, creaming occurred over time, due to the lower density of hexadecane and the effect of buoyancy forces on oil droplets (Sufi-Maragheh et al., 2019). As an illustration, the CNCs-stabilized emulsion prepared with 50 mM NaCl is presented in Figure III-2.

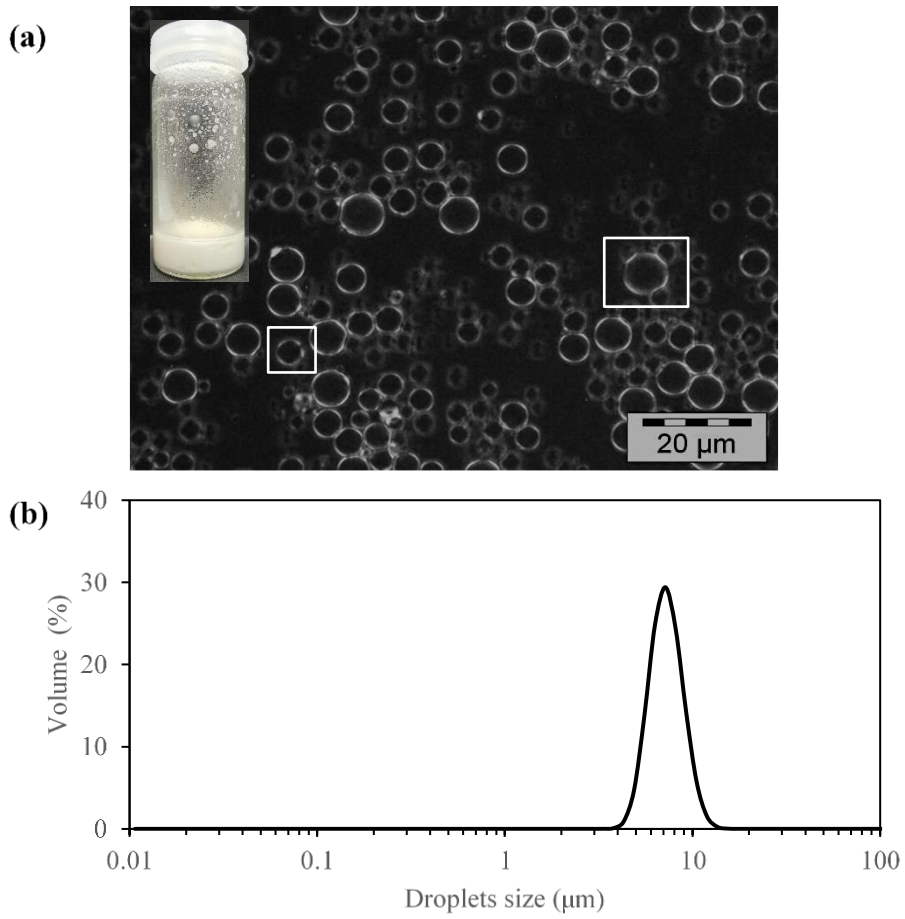

Figure III-2. (a) Micrography of a CNC-stabilized hexadecane-in-water emulsion observed under crossed polarizers and (b) size distribution of the droplets. [CNCs] = 8 mg/mL of hexadecane; [NaCl] = 50 mM; O/W = 20:80 v/v. Photograph of the emulsion in inset (top left).

Because of the birefringence of crystalline cellulose, observations under crossed polarized light allowed confirming that the CNCs were positioned on the droplets surface, (Figure III-2a). Some discontinuities were sometimes observed (white squares in Figure III-2), reflecting the uneven distribution of the CNCs on droplets surface. Size distribution was monomodal with a small P value (P= 0.157, Figure III-2b), as expected for Pickering emulsions.

2. Impact of the CNCs concentration

The impact of particles concentration on droplets size was investigated by static light scattering, through the measurement of the D(3,2), Sauter mean diameter. The inverse diameter measured at a constant NaCl concentration of 50 mM was plotted as a function of CNCs concentration in Figure III-3.

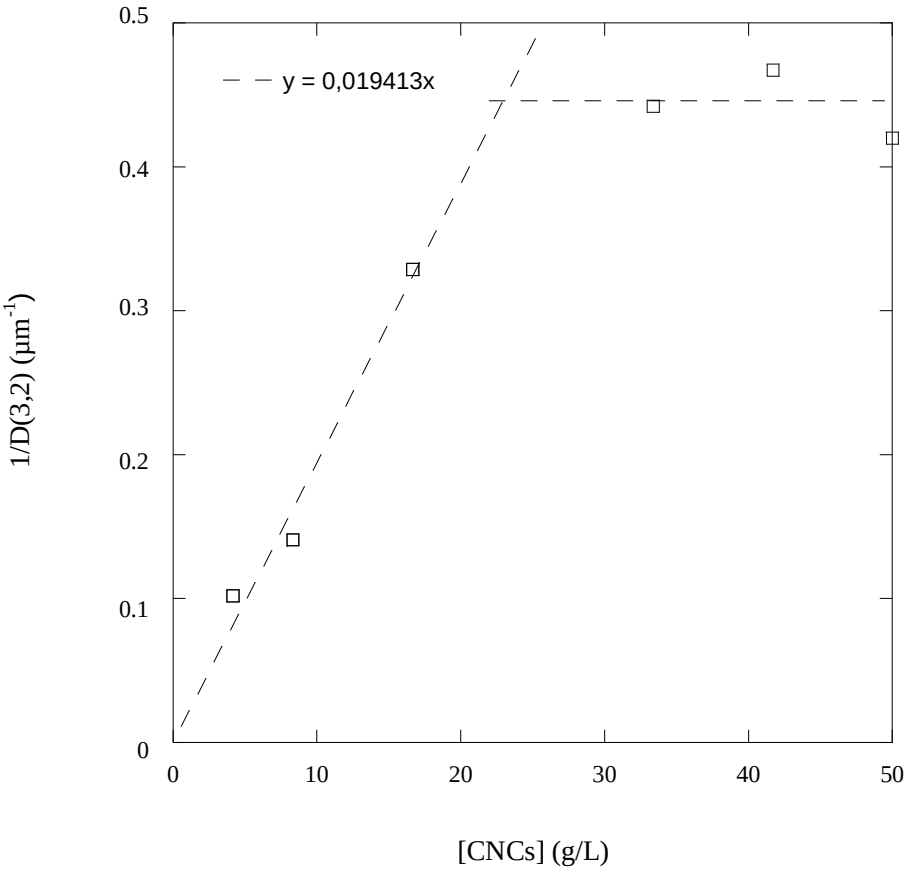

Figure III-3. Inverse D(3,2) diameter as a function of CNCs concentration (expressed in weight of CNCs per mL of oil phase), in the presence of 75 mM NaCl.

A linear dependence of 1/D(3,2) on CNCs concentration is observed at low particles concentration, until a plateau is reached when [CNCs] ≥ 20 g/L hexadecane, in line with the limited coalescence process expected for Pickering emulsions (Arditty et al., 2003). In the linear domain, droplets coalesce until a sufficient coverage by the particles is attained and coalescence is arrested. The droplets size change, but the interfacial coverage (C) is constant

in this domain. When the plateau is reached, the interfacial area stabilized by the particles is maximal and the droplets size is not anymore reduced by the addition of more particles.

The coverage percentage C and specific surface area S can be estimated from the slope of the limited coalescence domain using Equation I-5 and Equation I-7 (see Chapter I, Part A.5). Systems with lower C (and higher S) will require less particles to cover the same interfacial area, meaning that the interfacial coverage is lower in these systems. A C value of 116% (116 m^2/g for S) was inferred from the slope of Figure III-3, obtained with 50 mM NaCl.

3. Impact of ionic strength

S and C values were determined for each ionic strength, their salt concentration dependence being given in Figure III-4. Only the S error bars were reported in Figure III-4 (and the following ones), the error bars calculated with C being too large and imprecise in our experimental conditions (see Chapter I, Part A.5). The precise estimation of C is indeed highly dependent on the accuracy of the thickness of the CNCs, which is difficult to evaluate in our case, due to the variability of our material (length = 110 ± 48 nm; thickness = 4.8 ± 1.1 nm (Brand et al., 2017)).

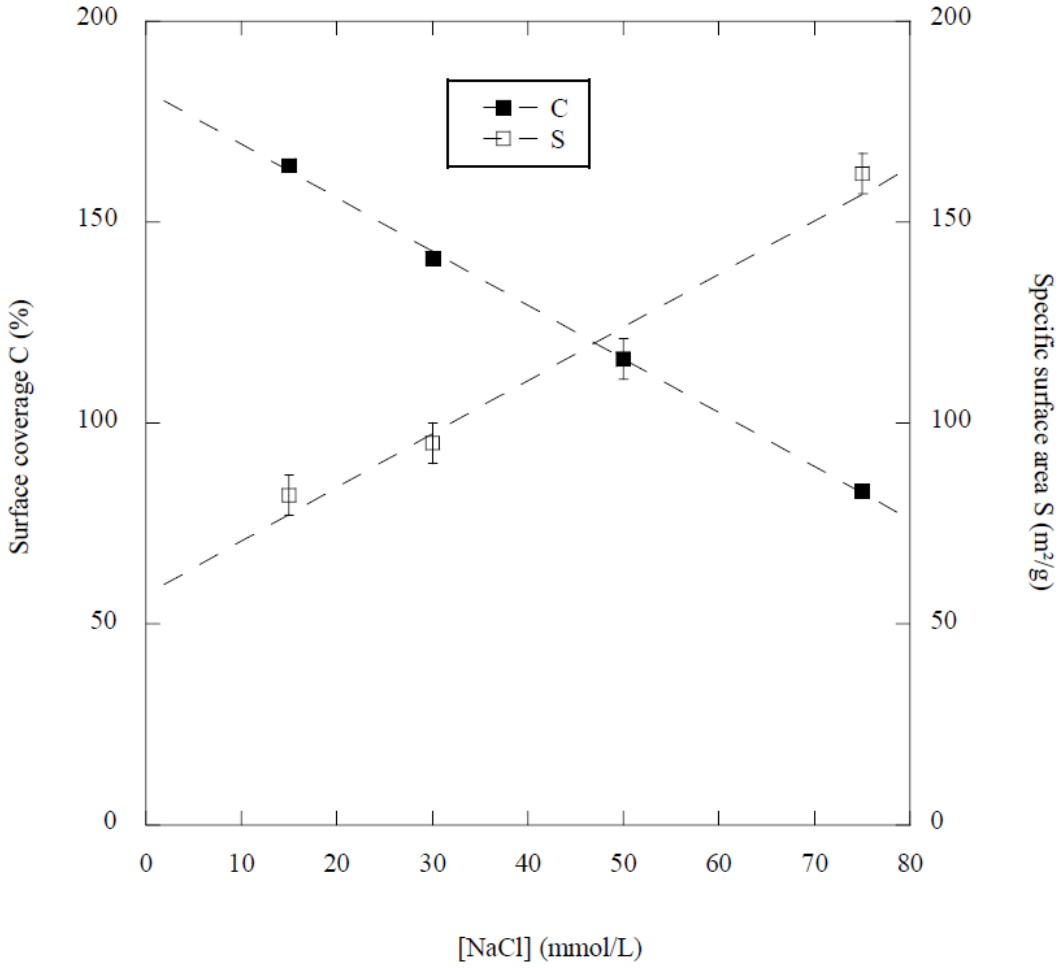

Figure III-4. NaCl concentration dependency of the surface coverage C (y_1 axis) and of the surface specific area S (y_2 axis). Errors bars on S were calculated from 3 different measurements.

The surface coverage by the particles around the droplets decreased progressively as more NaCl was added. This result could be surprising in view of the work of Bergfreund et al, who compared the surface pressure of various oil/water interfaces for 0.5 wt% CNCs adsorption, in the presence of 0 or 20 mM NaCl (Bergfreund et al., 2019), and concluded that C increased upon salt addition. Although a better coverage is expected with 20 mM NaCl compared with pure water – since no-long term stable emulsions can be formed without salt – the effect of salt variations has not been really studied in the publication. In a recent study, Heise et al. indirectly showed that C decreased with salt concentration, whilst they did not interpret this result in terms of surface coverage (Heise et al., 2022). They investigated the impact of NaCl

concentration (from 0 to 100 mM) on the droplets size of dodecane-in-water emulsions stabilized with TEMPO-oxidized CNCs, keeping constant the oil volume fraction (40/60, v/v) and the amount of CNCs (0.50 wt%) (Heise et al., 2022). They found that the droplets size decreased as the salt concentration increased, meaning that 1/D(3,2) increased, in line with what we observed in the 1/D(3,2) versus CNCs concentration curves (see Figure III-5) ; this implies that C decreased (S increased) with the salt concentration also in their conditions.

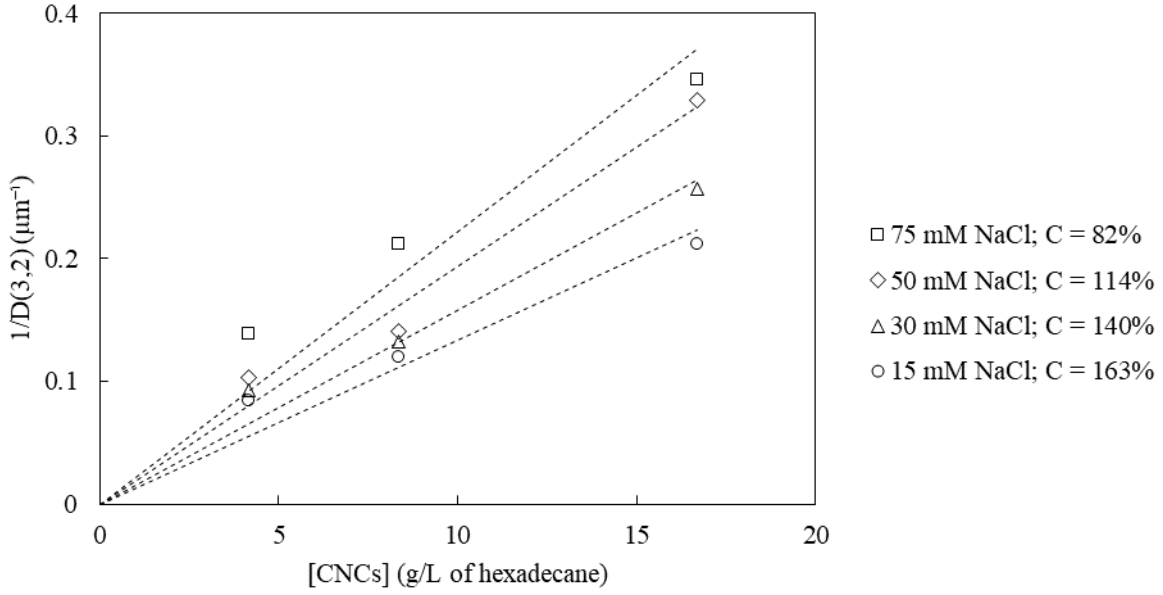

Figure III-5. Inverse diameter as a function of CNCs concentration for emulsions at different ionic strengths. The C obtained at the different salt concentrations is also reported.

The salt concentration is expected to impact strongly the aggregation state of the CNCs. Salt indeed reduces the Debye length, *i.e.* the thickness of the ions layer surrounding the nanoparticles, decreasing the range of electrostatic force, and allowing attractive forces such as van der Waals forces to operate. We believe that the decrease in C when more salt was added, resulted from an increasing aggregation of the CNCs. To verify this point, the state of aggregation of the CNCs dispersed in salty water was evaluated as a function of NaCl concentration, for a concentration of CNCs of 1 g/L, through the measurement of the

hydrodynamic radius (HR) by DLS (Figure III-6). An HR value of about 80 nm was measured without salt. The HR increased progressively with the salinity up to 50 mM NaCl (from 79 to 228 nm), before jumping to 787 ± 78 nm for 75 mM NaCl. Usually, aggregation of colloidal particles occurs at a given salt concentration, *i.e.* the critical coagulation concentration. Here, the progressive increase of the aggregates size up to 50 mM NaCl, could result from the heterogeneity of the rod-shaped CNCs (length = 110 ± 48 nm (Brand et al., 2017)) and thus, heterogeneity of the surface charge. At 75 mM NaCl, most of the CNCs should be aggregated, in view of the large value of HR.

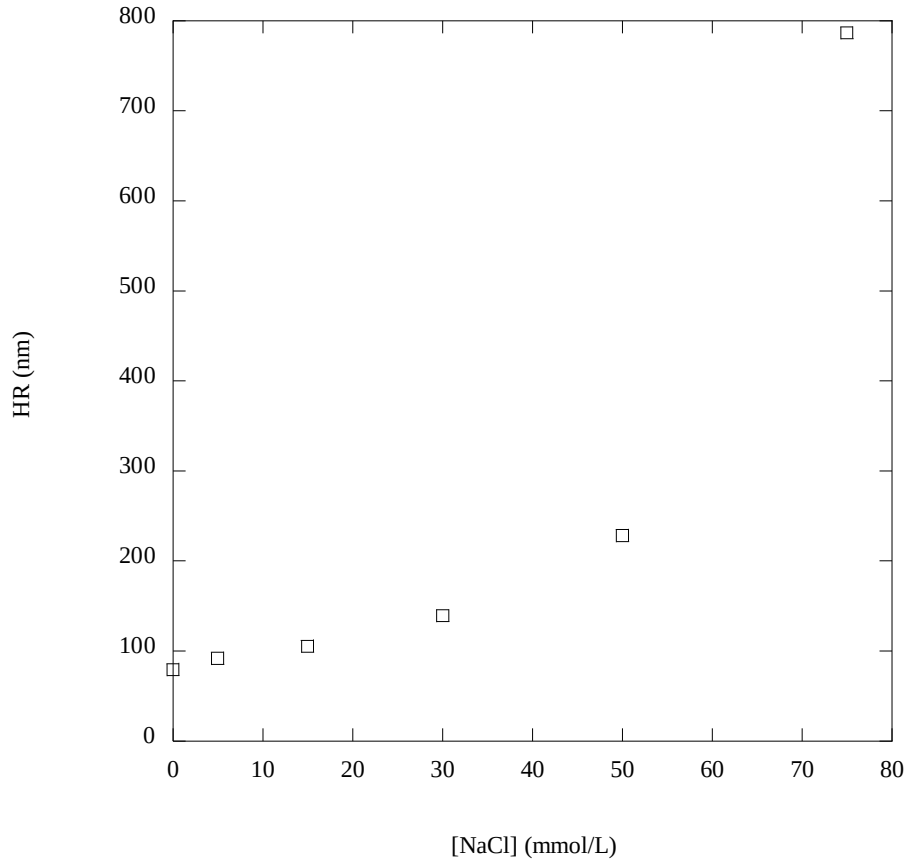

Figure III-6. Evolution of the hydrodynamic radius (HR) of CNCs dispersed in water as a function of NaCl concentration ([CNCs] = 1 g/L).

Hence, we assume that when the ionic strength increases, more CNCs are aggregated at the oil/water interface, leading to an increase in area devoid of CNCs, *i.e.* a lower interfacial

coverage. To further clarify this point, we later investigated how the ionic strength impacted the release kinetics of RSV (a model hydrophobic molecule), after its incorporation in the oil phase of the emulsions (see Chapter IV).

4. Impact of surface modification with vinyl octanoate

The CNCs used in this study possess accessible hydroxyl groups at their surface (sulphate ester groups excluded), which were previously estimated at 3.1 ± 0.1 mmol.g^{-1}, corresponding to 16.7% of the total number of hydroxyl groups found in the particle (Brand et al., 2017). The CNCs surface was rendered more hydrophobic by substituting part of the superficial hydroxyl groups with hydrophobic octanoyl moieties, through an acylation reaction based on the transesterification of vinyl esters and catalysed by potassium carbonate (see Chapter I, Part B.4.a.ii). The hydrophilic/hydrophobic balance at the CNCs surface was modulated by varying the surface degree of substitution (DS_{Surf}), which was achieved by varying the reaction time. Five reactions were performed at different reaction times (30, 35, 45, 60 and 90 min), and the different acylated products were denoted as CNC-Oct 30, CNC-Oct 35, CNC-Oct 45, CNC-Oct 60 and CNC-Oct 90, respectively. The preparation and characterisation of the octanoyle-modified CNCs is presented in detail in Chapter II, Part A.2.

a. Effect of surface degree of substitution (DS_{Surf})

The different octanoyl-modified particles were used to prepare hexadecane-in-water emulsions in the same conditions than with the unmodified CNCs, except that no salt was added. Only the CNC-Oct 30 particles led to stable emulsions with monodisperse droplets in our experimental conditions (Figure III-7) , the particles modified for longer times being probably too hydrophobic. We indeed showed in a previous study, that only the octanoyl-gafted CNCs

of low substitution levels could stabilise O/W emulsions (Dudefoi et al., 2022). The CNC-Oct 30 particles were then selected in subsequent investigations.

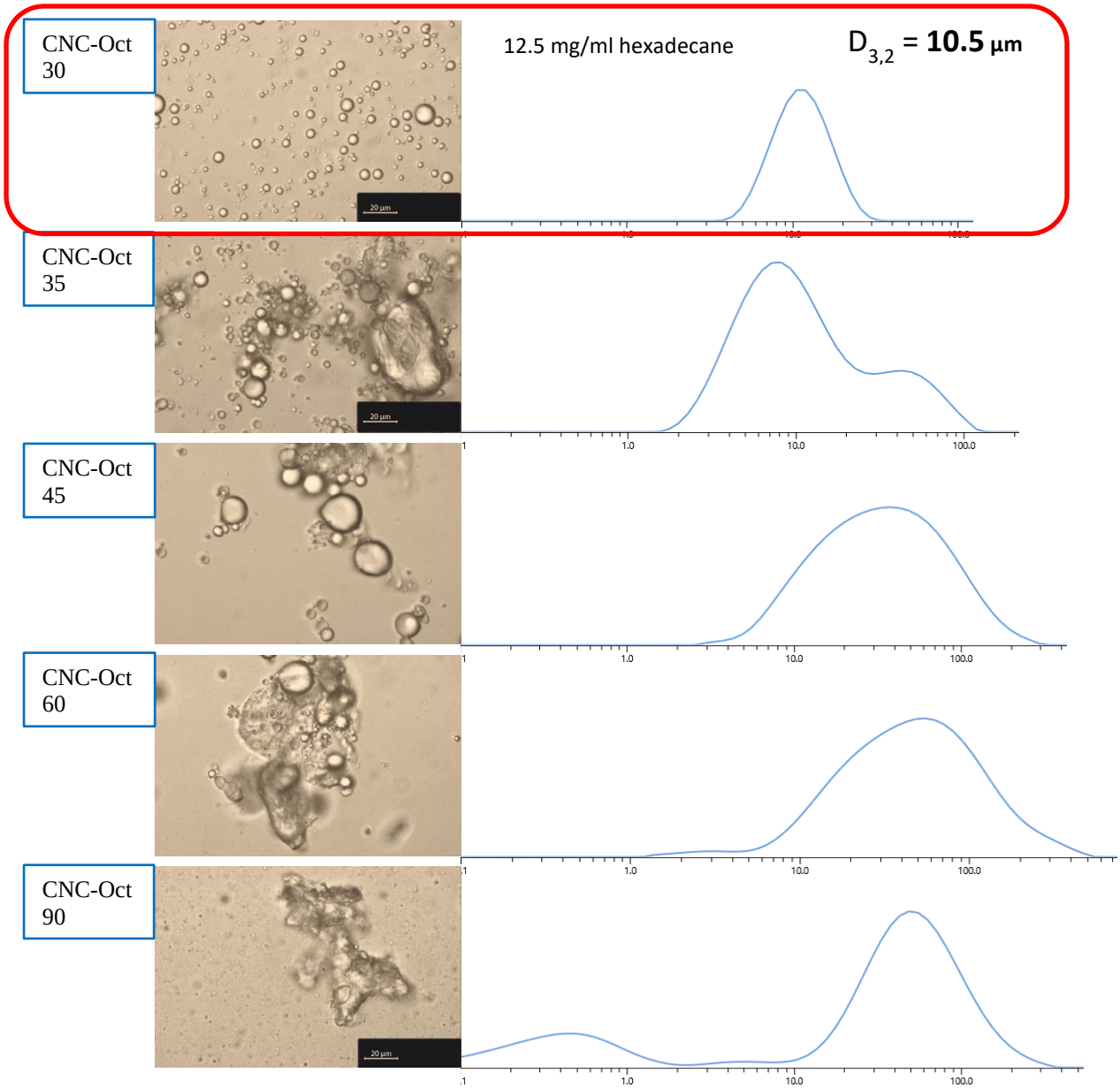

Figure III-7. Optical micrographs and droplets size distribution of the emulsions prepared with the CNC-Oct particle reacted for 30, 35, 45, 60 and 90 min.

b. Effect of particle's concentration and ionic strength

Different emulsions were prepared with the CNC-Oct 30 sample, by varying the particles concentration (from 0 to 40 g/L of hexadecane) at different ionic strengths (0, 30 & 75 mmol/L

NaCl). Stable Pickering emulsions were obtained in all cases, with the typical 1/D(3,2) *vs* particles concentration profile expected when the droplets diameter is controlled by the limited coalescence process (Figure III-8). Remarkably, stable emulsions could be obtained without salt, which was not possible when unmodified particles were used. The partial hydrophobisation of the CNCs may have increased the affinity of the particles for the oil, leading to a decrease in the kinetics energy barrier for CNCs adsorption at the O/W interface. The surface functionalization of the CNCs could also play the same role as salt for pristine CNCs. With silica as Pickering particle, it has been shown that the surface coverage is governed by electrostatic forces when the particle is hydrophilic (unmodified), while attractive hydrophobic forces are critical when the particle is hydrophobized (Simovic and Prestidge, 2004).

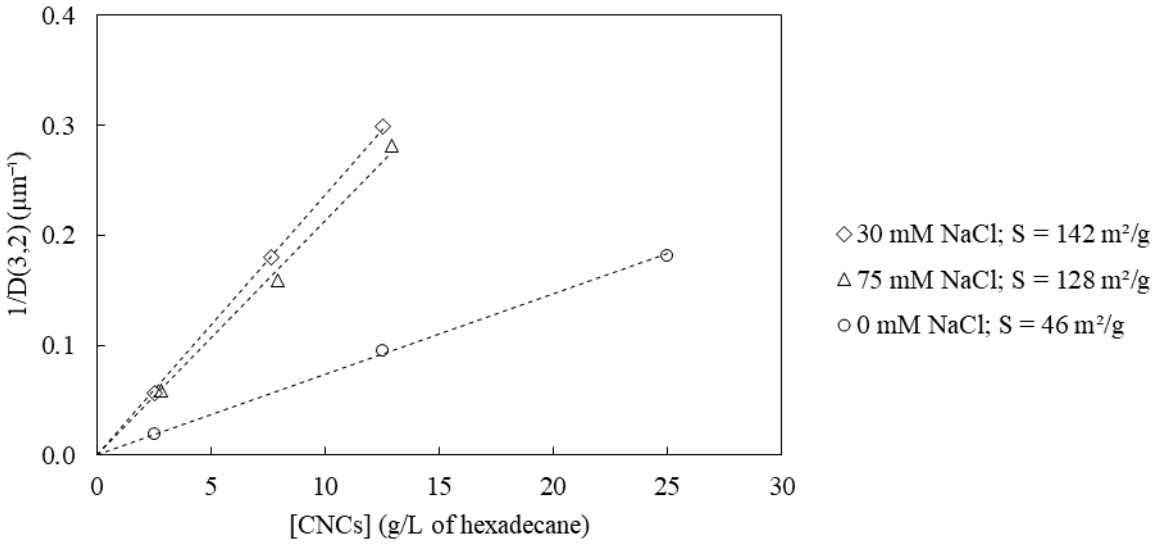

Figure III-8. Inverse diameter as a function of CNC-Oct 30 concentration for different ionic strengths (0, 30 and 75 mM of NaCl). The S obtained at the different salt concentrations is also reported.

Similarly to the unmodified CNCs, higher values of S (lower surface coverage) were obtained in the presence of salt, but the CNC-Oct 30 particles are slightly less sensitive to salt variations; maybe because of the lower absolute zeta potential (-32 mV as compared to -48 mV for

unmodified CNCs). The surface coverage C could not be estimated as the height of the CNC-Oct 30 particles was not evaluated.

B. Investigations with other oils

1. Stabilisation with unmodified CNCs

a. Impact of oil type on the surface specific area (S)

The ability of CNCs to stabilise O/W emulsions prepared with different oils was investigated. Six different oils *i.e.* isododecane, squalene, sunflower oil, virgin linseed oil, coconut oil and palm oil, were chosen for their potential applications in pharmaceutics, cosmetics and food industries. Additionally, virgin linseed oil was chosen because it contains high amounts of polyunsaturated fatty acids (ω-3 and ω-6 fatty acids), which makes it prone to oxidation (Tańska et al., 2018). Coconut and palm oils are also of interest to investigate the surface properties of the oil droplets by cryo-SEM, as these oils are in a solid state at 20 °C.

Regardless of the oil, stable emulsions were successfully produced by applying the same conditions as for the emulsification of hexadecane (75 mM NaCl; O/W = 20/80 v/v; see Chapter III, Part A). With linseed oil however, no clear limited coalescence domain could be identified when 1/D(3,2) was plotted as a function of CNCs concentration in these conditions, preventing the estimation of C and S for this system. The expected linear relationship was however obtained by changing the O/W ratio from 20/80 to 10/90 v/v; the C and S values were estimated from that graph for this system (two different salt concentrations were also investigated: 30 and 75 mM NaCl). Particular conditions were also applied for the emulsification of coconut and palm oil, due to their high melting point (23 °C for coconut oil (Firestone, 1997), 22 °C

for palm oil (Ramli et al., 2018)). These oils were homogenized at 40 ˚C to melt the crystals, and ultrasonication was applied without ice-cooling.

Figure III-9 gathers the microscopic images of the various emulsions prepared at different concentrations in CNCs, in which a decrease in droplets size with particles concentration is clearly observed.

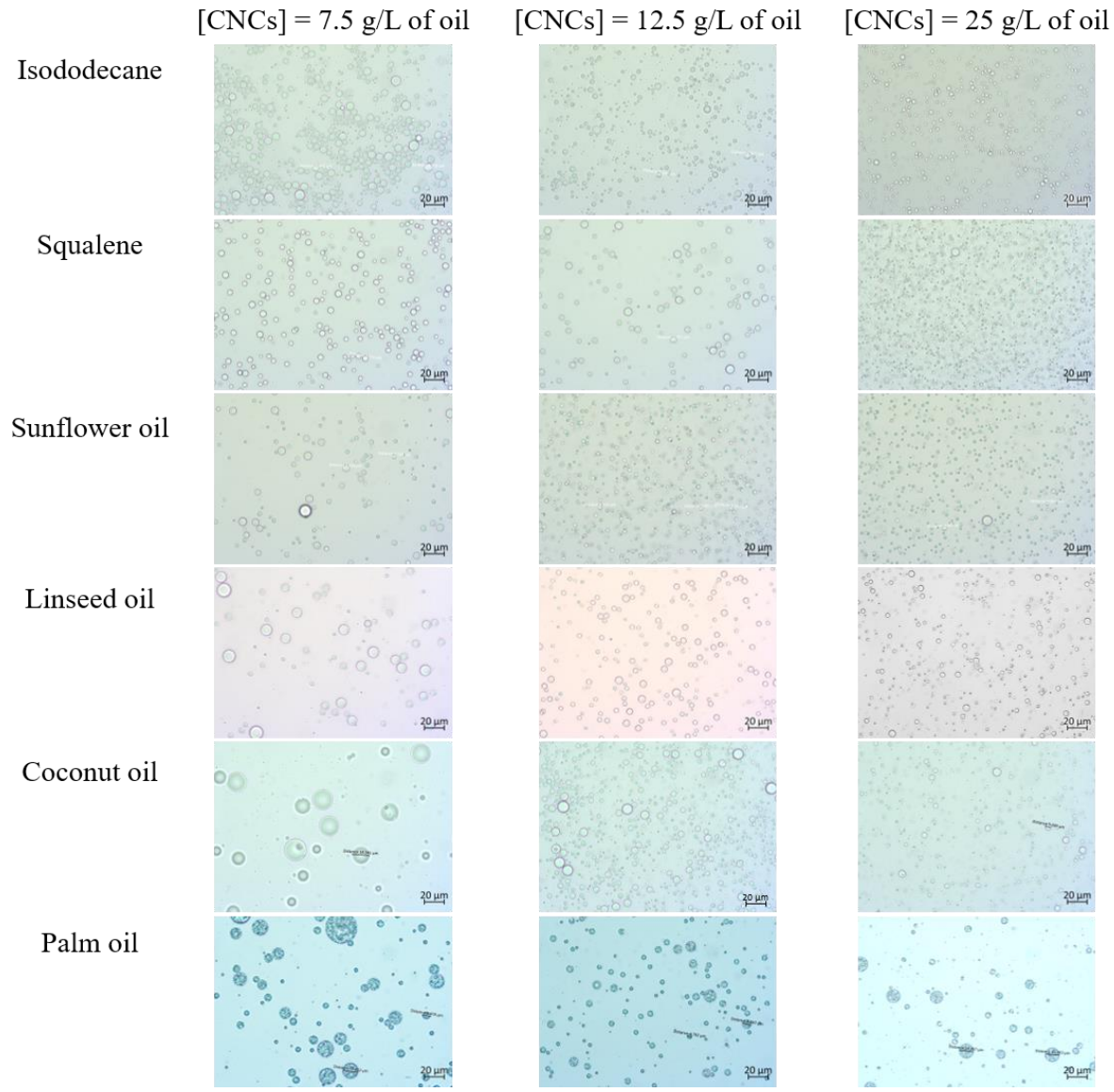

Figure III-9. Micrographs of the CNC-stabilized O/W emulsions prepared with different oils. [NaCl] = 75mM; O/W = 20:80 v/v, except for linseed oil for which O/W = 10:90 v/v.

The inverse Sauter diameter was plotted as a function of CNCs concentrations using an O/W ratio of 20/80 v/v in Figure III-10a (most oils) and an O/W ratio of 10/90 v/v in Figure III-10b (linseed oil). In all cases, a linear behaviour was observed in the low CNCs concentration range, indicating that all emulsions were controlled by the limited coalescence process. The surface coverage (C) and specific surface area (S) were measured for all emulsion systems and compared in Table III-1 with those obtained when hexadecane was used (Chapter III, Part A).

a)

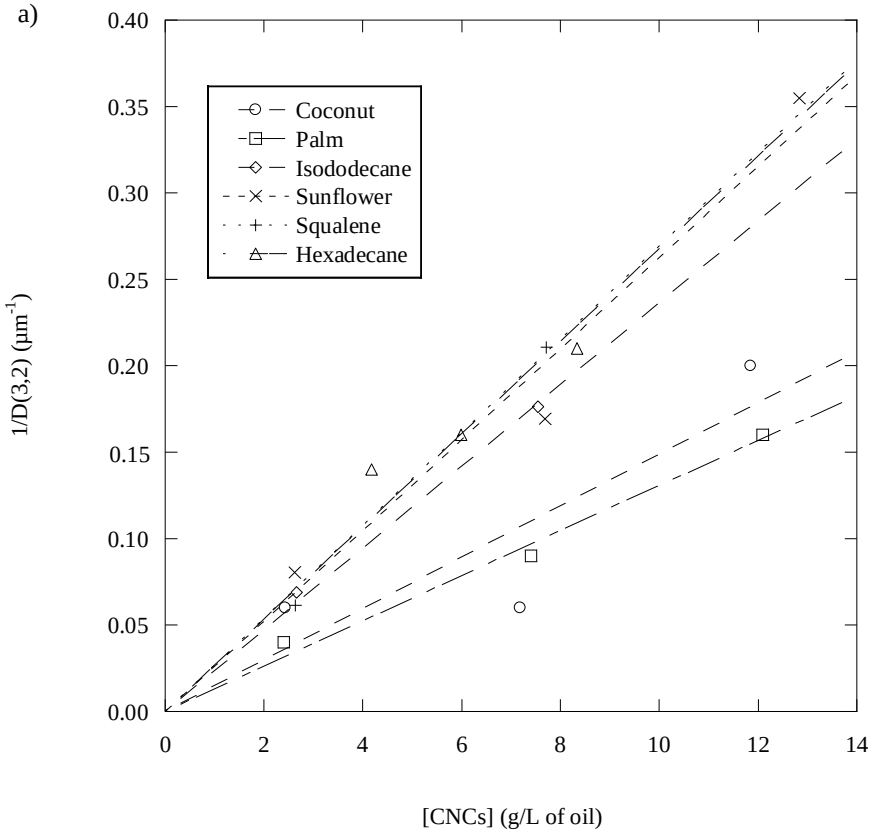
0.40
0.35
0.30
0.25
0.20
0.15
0.10
0.05
0.00
0
2
4
6
8
10
12
14
Coconut
Palm
Isododecane
Sunflower
Squalene
Hexadecane
1/D(3,2) (µm-1)
[CNCs] (g/L of oil)

b)

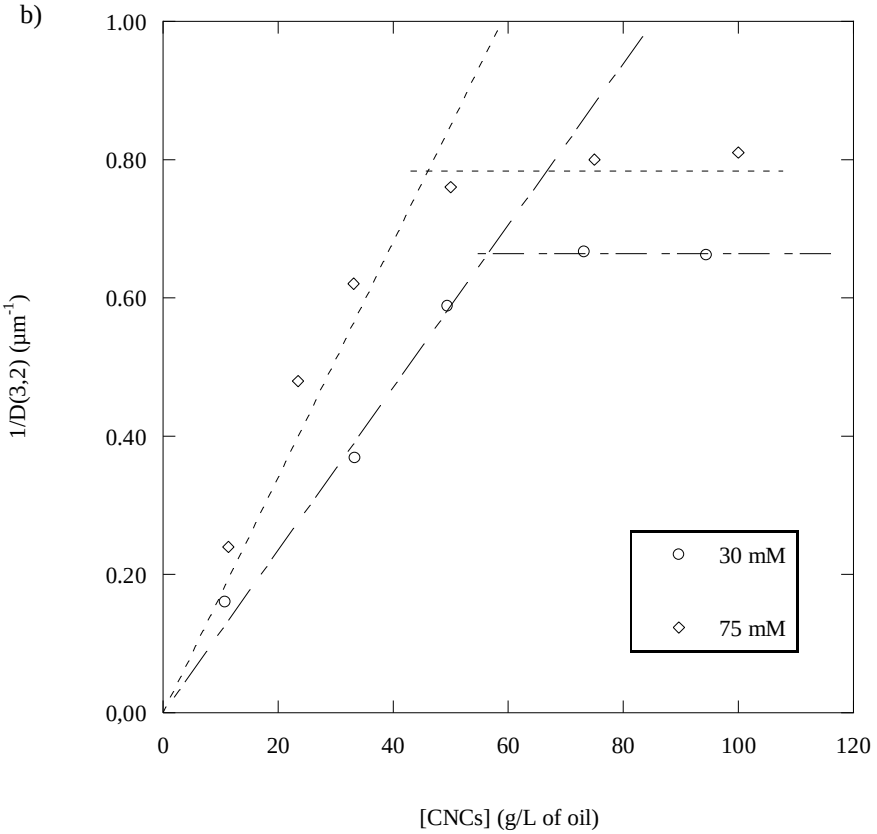
1.00
0.80
0.60
0.40
0.20
0,00
0
20
40
60
80
100
120
30 mM
75 mM
1/D(3,2) (µm-1)
[CNCs] (g/L of oil)

Figure III-10. Inverse Sauter diameter as a function of CNCs concentration (a) for different oils using a O/W ratio of 20/80 (v/v) and a NaCl concentration of 75 mmol/L, (b) for linseed oil using an O/W ratio of 10/90 for different ionic strengths (30 and 75 mmol/L NaCl).

Table III-1. Surface coverage (C) and specific surface area (S) values obtained for all the emulsion systems and CNCs type.

Oils	**CNCs**	**[NaCl] (mM)**	**C (%)**	**S (m^2/g)**
Hexadecane	Unmodified	75	82	162
		50	115	116
		30	141	95
		15	163	82
Virgin linseed oil		75	116	116
		30	187	72
Squalene		75	83	161
Sunflower oil		75	84	158
Isododecane		75	95	140
Palm oil		75	179	75
Coconut oil		75	184	73
Hexadecane	CNC-Oct 30	75	Not determined	128
		30	Not determined	142
		0	Not determined	44
Virgin linseed oil	CNC-Cin	75	Not determined	35
Virgin linseed oil	CNC-PDA	75	Not determined	10

For a given salt concentration (75 mM NaCl), hexadecane, sunflower oil, isododecane and squalene emulsions display similar droplets coverage, as the S and C values are in same order of magnitude (Table III-1). Clearly, coconut and palm oil distinguished themselves from the others, a much higher surface coverage (lower S) being measured with these oils (184 and 179 %, respectively). The oil viscosity could affect the initial size of the droplets during sonication and impact the S and C values. However, Table III-2 indicates that the viscosities of coconut and palm oil are comparable to those of sunflower and linseed oil at 45°C. Knowing that the ultrasonication produced heat and that the temperature was not controlled during emulsification, the influence of viscosity on S and C should be negligible.

Table III-2. Viscosities of the oils at 25°C et 45°C and interfacial tensions of the oils against water.

Oils	**Viscosity (mPa.s, 25°C)**	**Viscosity (mPa.s, 45 °C)**	**Interfacial tensions (mN/m)**
Hexadecane	4 ± 1 (Liu et al., 2018) 2.32 (Maan et al., 2013)	2 (Wang et al., 2016)	52 (De Aguiar et al., 2010)
Isododecane	1.2 (Sakanishi et al., 2014)	N/A	42.9 (Gneist and Bart, 2002)
Squalene	1.1 20°C (Brito et al., 2011)	N/A	25 (Hildebrandt et al., 2013)
Sunflower oil	54.9 (Sakanishi et al., 2014) 49 (Maan et al., 2013)	27 (Periyasamy et al., 2009)	24.8 (Bhatluri et al., 2015)
Coconut oil	N/A	24 40°C (Tipvarakarnkoon et al., 2008)	13.9 (Bhatluri et al., 2015)
Palm oil	N/A	38 40°C (Izhan et al., 2013)	8.0 ± 1.2 (at 60°C) (Ho and Chow, 2000)
Linseed oil	57 20°C (Blayo et al., 2001)	30 (Khan et al., 2006)	47.63 ± 0.03 (Drozłowska et al., 2020)

Another contributing factor could be the oil polarity, which is related to the O/W interfacial tension: an increasing oil polarity is associated with a lower interfacial tension (Bergfreund et al., 2019). The values of interfacial tension of the different oils were retrieved from literature and presented in Table III-2. Coconut oil and palm oil display the lowest interfacial tensions, and thus the highest polarities; both of them are indeed rich in medium-chain triglycerides. Bergfreund et al. postulated that the CNCs adsorption at the O/W interface strongly depends on the oil polarity; the more polar the oil, the more the CNCs are wetted in oil. As CNCs are deeper in the oil phase, it is then possible that the coalescence between droplets during the sonication process is more pronounced (less steric hindrance and steric repulsions between droplets). This would result in the formation of larger droplets for the same amount of CNCs, which implies a higher C value for these polar oils, in accordance with our findings. Another consequence would be a reduction in the energy barrier associated with the adsorption of CNCs at the oil/water interface, leading to a higher C value.

With linseed oil, two salt concentrations were used (Figure III-10b), and results of Table III-1 indicate a lower coverage when more salt was added, in line with what was observed with hexadecane.

b. Utilization of the coconut oil system to observe the CNCs organisation at the droplets surface by cryo-SEM

The organisation of CNCs at the O/W interface was investigated by visualizing them using cryo-scanning electronic microscopy (cryo-SEM) (Details in Chapter II, Part D.2). The visualisation of the CNCs from the hexadecane-in-water emulsions turned out to be difficult, as the droplets could not maintain their spherical shape during analyses (Figure III-11). When focusing on some of the intact droplets, we observed that their surface was not smooth, and presented a topography resembling that of "walnut shells".

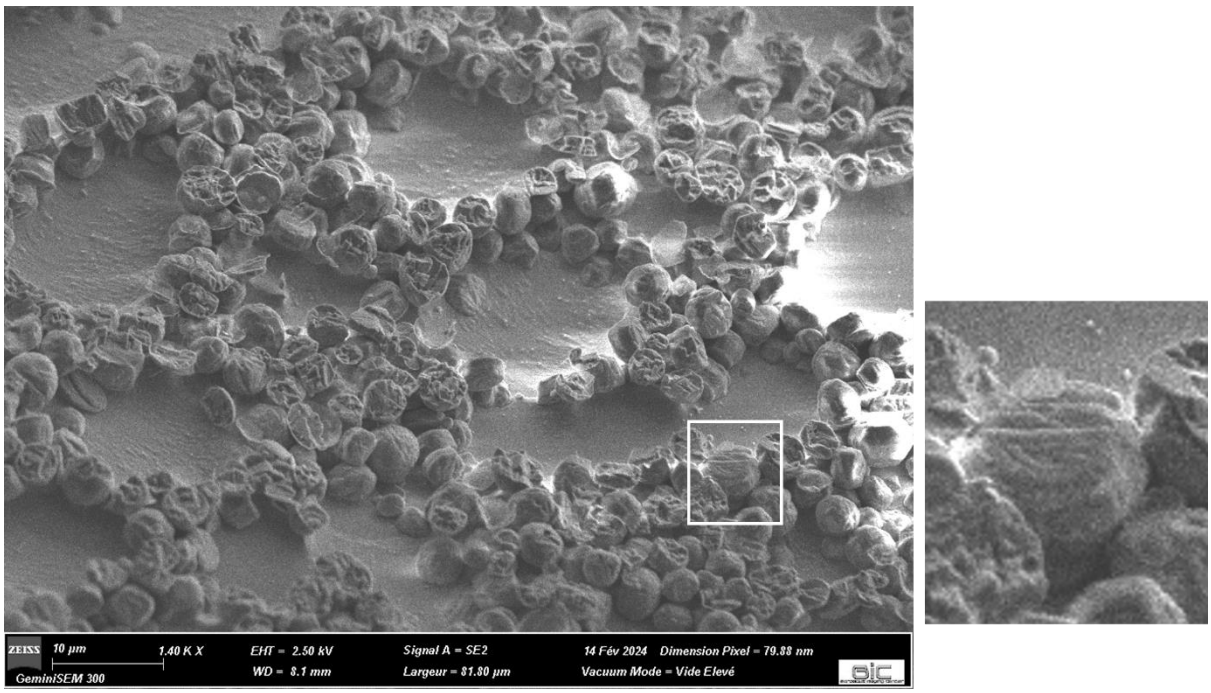

Figure III-11. Cryo-SEM image of an hexadecane-in-water emulsion stabilized with the CNCs ([CNCs] = 5.75 g/L of oil; O/W = 20:80 v/v; [NaCl] = 75 mM) and enlargement of the droplet in the white box (right).

To solve this problem, the cryo-SEM analysis was performed using the emulsion system based on coconut oil, which has the advantage to be solid at room temperature (the melting point of coconut oil is 23 °C). This property ensures that the oil droplets will not be affected by the vacuum during microscopic observations. Figure III-12 shows the cryo-SEM images of the coconut oil droplets stabilized by the CNCs. Densely-packed rod-shape CNCs are clearly visible on the droplets surface of Figure III-12a, b and c, in line with the high surface coverage measured from the limited coalescence domain (C = 184%). Some heterogeneities were however sometimes spotted, as evidenced on the picture of the large droplet analyzed in Figure III-12d, where both poorly-covered areas and densely packed domains are visible.

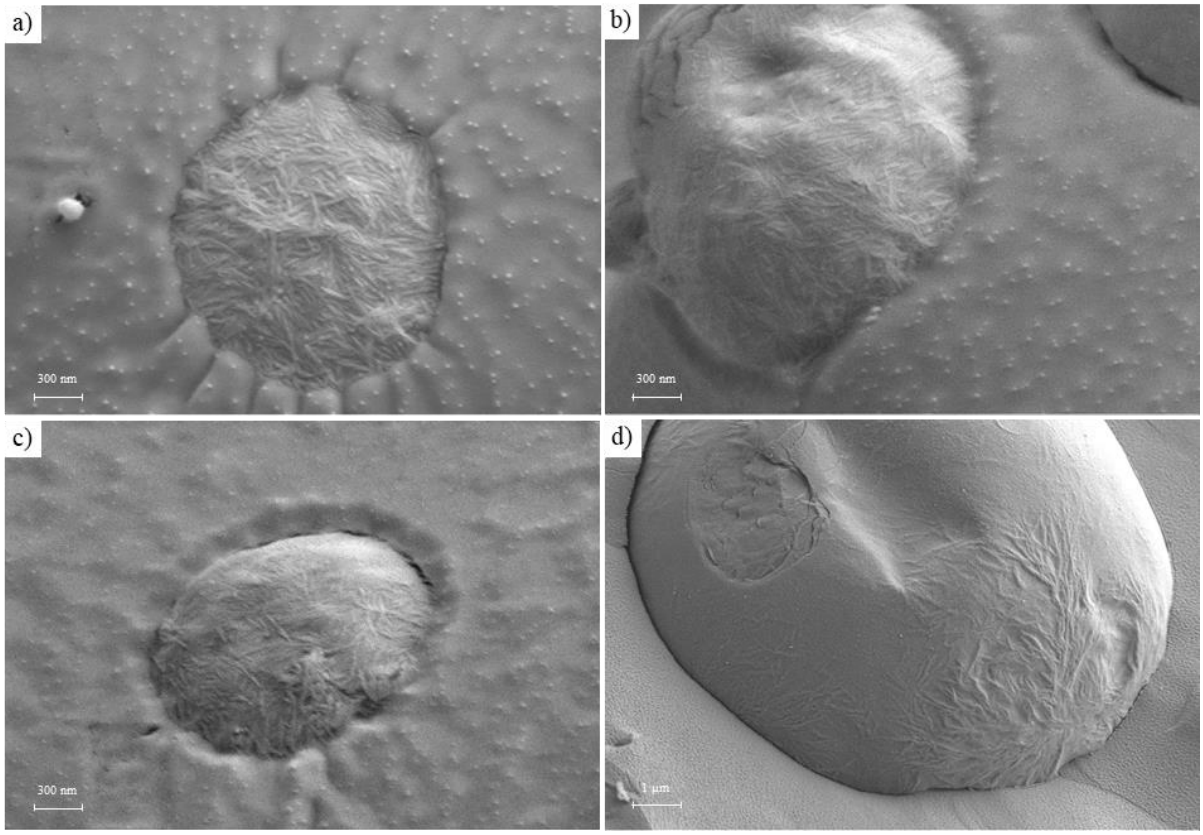

Figure III-12. Cryo-SEM images of the coconut oil droplets stabilized by the CNCs ([CNCs] = 7.2 g/L of oil; O/W = 20:80 v/v; [NaCl] = 75 mM).

2. Stabilisation with modified CNCs: the case of linseed oil

The ability of cinnamoyl- and polydopamine-modified CNCs (CNC-Cin and CNC-PDA, respectively) to stabilise linseed oil-in water emulsions was investigated, with the objective to later improve the oxidative stability of the oil (see Chapter V, Part B). Cinnamoyle groups are indeed reported to undergo reversible *trans-cis* isomerization and/or dimerization upon UV light irradiation, which may impart UV-protection, while polydopamine is an antioxidant with radical scavenging properties. The preparation and characterisation of the CNC-Cin and CNC-PDA particles are presented in detail in Chapter II, Part A.

Linseed oil emulsions were prepared with the CNC-Cin and CNC-PDA particles, using an O/W ratio of 20/80 and an NaCl concentration of 75 mM of NaCl. Stable emulsions were obtained in both cases (Figure III-13 and Table III-1), but the S values inferred from the slopes (35 $m^2.g^{-1}$ for CNC-Cin, 10 $m^2.g^{-1}$ for CNC-PDA) were significantly lower than when the unmodified particles were used (116 $m^2.g^{-1}$), suggesting a higher coverage at the droplets surface. These S values are quite different from those obtained with the octanoyle-modified CNCs after emulsification of hexadecane in the same conditions (128 $m^2.g^{-1}$ in Figure III-9), yet the zeta potentials of the particles were quite similar (-34.4 mV for CNC-Cin; -38.5 mV for CNC-PDA; -32 mV for CNC-Oct). The difference in surface coverage may therefore be related to the chemical structure of the grafted moieties, which differ significantly (aromatic for CNC-Cin and CNC-PDA, aliphatic for CNC-Oct), and/or to the high difference in oil viscosities (Table III-2). Further investigations are required to clarify this point.

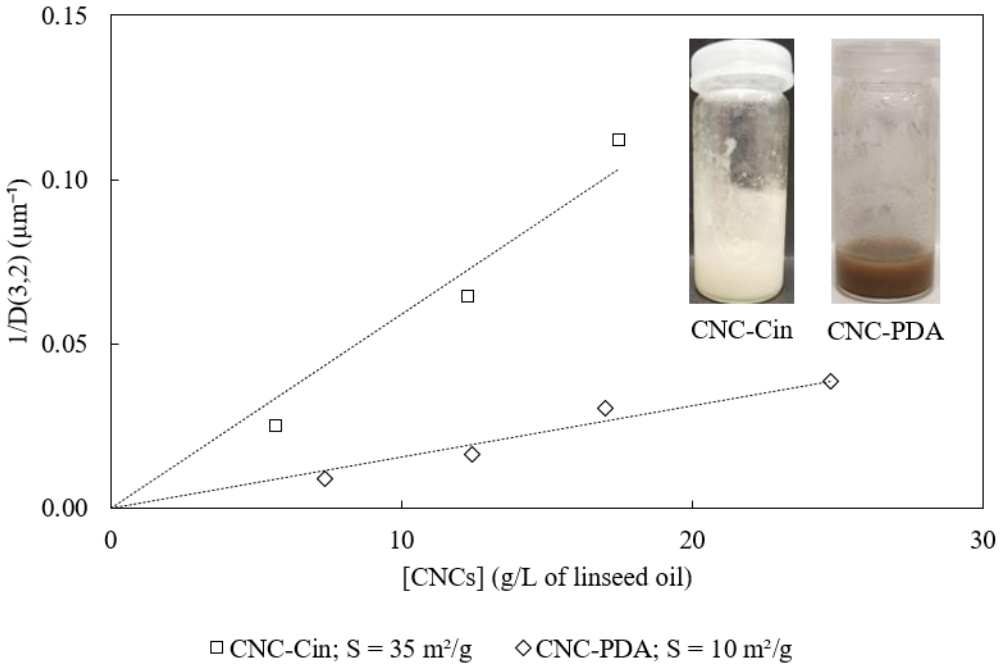

Figure III-13. Inverse diameter as a function of particles concentration for the emulsions stabilized by the CNC-Cin and CNC-PDA particles (O/W = 20/80 v/v; [NaCl] = 75 mM), and S values obtained from the slopes. Inset: photographs of the emulsions stabilized with 12.4 g/L of oil.

The surface coverage C was not estimated, as the height of the CNC-Cin and CNC-PDA particles was not known. The lower S values measured with the CNC-Cin and CNC-PDA samples have not been explained at this stage of the study. Additional experiments are required to clarify this point.

C. Conclusions

In this chapter, stable oil-in-water (O/W) Pickering emulsions were successfully prepared with unmodified CNCs, in the presence of NaCl solubilised in the aqueous phase. Regardless of the oil investigated – namely hexadecane, isododecane, squalene, sunflower oil, virgin linseed oil, coconut oil and palm oil – a linear dependence of 1/D(3,2) on CNCs concentration was observed at low particles concentration, in line with the limited coalescence process expected

for Pickering emulsions. The surface coverage by the particles around the droplets was estimated by calculating the coverage percentage C and specific surface area S, based on the slope of the limited coalescence domain. Preliminary results with hexadecane as model oil showed a linear dependency of C and S with the ionic strength, demonstrating that the surface coverage can be monitored by the NaCl concentration. We presume at this stage, that when the ionic strength increases, more CNCs are aggregated at the oil/water interface, leading to an increase in area devoid of CNCs, *i.e.* a lower interfacial coverage. Most of the oils investigated presented a similar behavior in terms of surface coverage when emulsified in the same conditions, except coconut and palm oils, for which a higher surface coverage (lower specific surface area S) was noted. This difference was attributed to the higher polarity of both oils. The coconut oil emulsion (solid at room temperature) enabled visualizing the rod-shaped CNCs at the surface of the oil droplets, in the form of densely packed domains.

In another set of experiments, the CNCs surface was rendered more hydrophobic by substituting part of the superficial hydroxyl groups with hydrophobic octanoyle moieties. Only the particles of low substitution level could stabilise hexadecane-in-water emulsions in our experimental conditions, but compared with unmodified CNCs, the S and C values were less sensitive to variations in ionic strength, and stable emulsions could be obtained without salt. The ability of cinnamoyl- and polydopamine-modified CNCs (CNC-Cin and CNC-PDA, respectively) to stabilise linseed oil-in water emulsions was also investigated, with the objective to later improve the oxidative stability of this highly oxidable oil. Stable emulsions were obtained in both cases, but the S values measured were significantly lower than when the unmodified particles were used, suggesting a higher coverage at the droplets surface.

References

Arditty, S., Whitby, C.P., Binks, B.P., Schmitt, V., Leal-Calderon, F., 2003. Some general features of limited coalescence in solid-stabilized emulsions. Eur. Phys. J. E 11, 273–281. https://doi.org/10.1140/epje/i2003-10018-6

Bergfreund, J., Sun, Q., Fischer, P., Bertsch, P., 2019. Adsorption of charged anisotropic nanoparticles at oil–water interfaces. Nanoscale Adv. 1, 4308–4312. https://doi.org/10.1039/C9NA00506D

Bhatluri, K.K., Chakraborty, S., Manna, M.S., Ghoshal, A.K., Saha, P., 2015. Separation of toxic heavy metals from its aqueous solution using environmentally benign vegetable oil as liquid membrane. RSC Adv. 5, 88331–88338. https://doi.org/10.1039/C5RA13260F

Blayo, A., Gandini, A., Le Nest, J.-F., 2001. Chemical and rheological characterizations of some vegetable oils derivatives commonly used in printing inks. Industrial Crops and Products 14, 155–167. https://doi.org/10.1016/S0926-6690(01)00079-6

Brand, J., Pecastaings, G., Sèbe, G., 2017. A versatile method for the surface tailoring of cellulose nanocrystal building blocks by acylation with functional vinyl esters. Carbohydrate Polymers 169, 189–197. https://doi.org/10.1016/j.carbpol.2017.03.077

Brito, L.A., Chan, M., Baudner, B., Gallorini, S., Santos, G., O'Hagan, D.T., Singh, M., 2011. An alternative renewable source of squalene for use in emulsion adjuvants. Vaccine 29, 6262–6268. https://doi.org/10.1016/j.vaccine.2011.06.067

Capron, I., Rojas, O.J., Bordes, R., 2017. Behavior of nanocelluloses at interfaces. Current Opinion in Colloid & Interface Science 29, 83–95. https://doi.org/10.1016/j.cocis.2017.04.001

De Aguiar, H.B., De Beer, A.G.F., Strader, M.L., Roke, S., 2010. The Interfacial Tension of Nanoscopic Oil Droplets in Water Is Hardly Affected by SDS Surfactant. J. Am. Chem. Soc. 132, 2122–2123. https://doi.org/10.1021/ja9095158

Dridi, W., Harscoat-Schiavo, C., Monteil, J., Faure, C., Leal-Calderon, F., 2018. Monodisperse Oil-in-Water Emulsions Stabilized by Proteins: How To Master the Average Droplet Size and Stability, While Minimizing the Amount of Proteins. Langmuir 34, 9228–9237. https://doi.org/10.1021/acs.langmuir.8b02029

Drozłowska, E., Bartkowiak, A., Łopusiewicz, Ł., 2020. Characterization of Flaxseed Oil Bimodal Emulsions Prepared with Flaxseed Oil Cake Extract Applied as a Natural Emulsifying Agent. Polymers 12, 2207. https://doi.org/10.3390/polym12102207

Dudefoi, W., Dhuiège, B., Capron, I., Sèbe, G., 2022. Controlled hydrophobic modification of cellulose nanocrystals for tunable Pickering emulsions. Carbohydrate Polymer Technologies and Applications 3, 100210. https://doi.org/10.1016/j.carpta.2022.100210

Dugyala, V.R., Muthukuru, J.S., Mani, E., Basavaraj, M.G., 2016. Role of electrostatic interactions in the adsorption kinetics of nanoparticles at fluid–fluid interfaces. Phys. Chem. Chem. Phys. 18, 5499–5508. https://doi.org/10.1039/C5CP05959C

Firestone, D., 1997. Physical and chemical characteristics of oils, fats and waxes.

Gneist, G., Bart, H.-J., 2002. Electrostatic Drop Formation in Liquid/Liquid Systems. Chem. Eng. Technol. 25, 899–904. https://doi.org/10.1002/1521-4125(20020910)25:9<899::AID-CEAT899>3.0.CO;2-Y

Heise, K., Jonkergouw, C., Anaya-Plaza, E., Guccini, V., Pääkkönen, T., Linder, M.B., Kontturi, E., Kostiainen, M.A., 2022. Electrolyte-Controlled Permeability in Nanocellulose-Stabilized Emulsions. Adv Materials Inter 9, 2200943. https://doi.org/10.1002/admi.202200943

Hildebrandt, E., Vrânceanu, M., Nirschl, H., Leneweit, G., 2013. Phospholipids as emulsifiers for micro/nano droplets suitable for biotechnological systems integration. La Houille Blanche 68–73.

Ho, C.C., Chow, M.C., 2000. The effect of the refining process on the interfacial properties of palm oil. J Americ Oil Chem Soc 77, 191–199. https://doi.org/10.1007/s11746-000-0031-7

Izhan, M.I., Rafiq, A.K.M., Syahrullail, S., 2013. Friction Resistance of Refined, Bleached and Deodorized (RBD) Palm Olein Using Modified Pin-on-disk Tribotester. Jurnal Teknologi 60. https://doi.org/10.11113/jt.v60.1437

Khan, A.R., Shama, R.S., Uddin, F., 2006. Effect of strong electrolytes on edible oils part III: viscosity of canola oil in 1,4-dioxane in the presence of HCl, NaOH and NaCl at different temperatures. Journal of Applied Sciences and Environmental Management 10. https://doi.org/10.4314/jasem.v10i1.17303

Kutuzov, S., He, J., Tangirala, R., Emrick, T., Russell, T.P., Böker, A., 2007. On the kinetics of nanoparticle self-assembly at liquid/liquid interfaces. Phys. Chem. Chem. Phys. 9, 6351. https://doi.org/10.1039/b710060b

Liu, L., Hu, Z., Sui, X., Guo, J., Cranston, E.D., Mao, Z., 2018. Effect of Counterion Choice on the Stability of Cellulose Nanocrystal Pickering Emulsions. Ind. Eng. Chem. Res. 57, 7169–7180. https://doi.org/10.1021/acs.iecr.8b01001

Maan, A.A., Schroën, K., Boom, R., 2013. Monodispersed water-in-oil emulsions prepared with semi-metal microfluidic EDGE systems. Microfluid Nanofluid 14, 187–196. https://doi.org/10.1007/s10404-012-1037-0

Periyasamy, N., Sathianathan, R.V., Krishnamoorthy, M., 2009. Viscosity Measurement Using Microcontroller to Study the Thermal Degradation of Edible Oil 102.

Ramli, N.A.S., Mohd Noor, M.A., Musa, H., Ghazali, R., 2018. Stability evaluation of quality parameters for palm oil products at low temperature storage. J Sci Food Agric 98, 3351–3362. https://doi.org/10.1002/jsfa.8839

Sakanishi, Y., Narusaka, Y., Itoh, M., Saeki, T., 2014. Rheology Control of Isododecane with Newly Synthesized Organogelators; 3,3',4,4'-Benzophenone Tetracarboxamide. J. Soc. Rheol., Jpn 42, 185–190. https://doi.org/10.1678/rheology.42.185

Simovic, S., Prestidge, C.A., 2004. Nanoparticles of Varying Hydrophobicity at the Emulsion Droplet−Water Interface: Adsorption and Coalescence Stability. Langmuir 20, 8357–8365. https://doi.org/10.1021/la0491807

Sufi-Maragheh, P., Nikfarjam, N., Deng, Y., Taheri-Qazvini, N., 2019. Pickering emulsion stabilized by amphiphilic pH-sensitive starch nanoparticles as therapeutic containers. Colloids and Surfaces B: Biointerfaces 181, 244–251. https://doi.org/10.1016/j.colsurfb.2019.05.046

Tańska, M., Mikołajczak, N., Konopka, I., 2018. Comparison of the effect of sinapic and ferulic acids derivatives (4-vinylsyringol vs. 4-vinylguaiacol) as antioxidants of rapeseed, flaxseed, and extra virgin olive oils. Food Chemistry 240, 679–685. https://doi.org/10.1016/j.foodchem.2017.08.007

Tipvarakarnkoon, T., Blochwitz, R., Senge, B., 2008. Rheological properties and phase change behaviors of coconut fats and oils.

Wang, Xiaojie, Wang, Xiaopo, Chen, J., 2016. Experimental investigations of density and dynamic viscosity of n -hexadecane with three fatty acid methyl esters. Fuel 166, 553–559. https://doi.org/10.1016/j.fuel.2015.11.008

Chapter IV. Incorporation of resveratrol in CNCs-stabilised emulsions and release study

The hexadecane-in-water Pickering emulsions fully characterised in the previous chapter (Chapter III, Part A) were subsequently loaded with resveratrol (RSV) and investigated with regards to its uptake (U) and release properties. RSV is a natural polyphenolic phytoalexin found in grapes, berry skins, soybeans, cherries, peanuts, plums and pomegranates, among others. The potential benefits of its encapsulation in Pickering emulsions have been demonstrated in a few recent studies (see Chapter I, Part D.2.c) but the utilisation of CNCs-based systems remains unexplored.

A. Incorporation of resveratrol

1. Protocol

RSV was initially dissolved in hexadecane and the emulsification steps were performed as described in Chapter II, Part C. The amount of RSV incorporated in the emulsion droplets was deduced from the quantity of RSV detected in the water phase, through the measurement of the absorbency at 306 nm by UV-vis spectroscopy (see Chapter II, Part E).

The limited solubility of RSV in the release medium (water in the current study) has to be taken into account when designing the protocol for the evaluation of RSV uptake and release kinetics. It is important to select an appropriate RSV concentration and volume of water, to ensure that the maximum concentration in the release medium does not exceed the solubility limit of RSV in this medium (reported to be between 19.6 and 50 μg/mL at 25 °C (Shi et al., 2008; Davidov-Pardo and McClements, 2014)). Therefore, an RSV concentration of 20 μg/mL relative to the oil phase was at first selected, the maximum concentration that the solute can reach in water in these conditions being 5 μg/mL. The O/W ratio was fixed to 20/80 v/v, as in Chapter III.

2. Partitioning of RSV between water & hexadecane

We first investigated how RSV partitioned between water and the oil phase, when no CNCs were present. A hexadecane solution containing RSV (20 µg/mL) was sonicated in the same conditions as for the preparation of the CNCs-stabilized emulsions, but without cellulose nanoparticles ([NaCl] = 75 mM). 90% of the RSV was detected in the water phase, indicating that the molecule has more affinity for water than for hexadecane. A weak stabilizing effect was also evidenced by optical microscopy, as some droplets were observed, which quickly destabilized after 30 min (Figure IV-1).

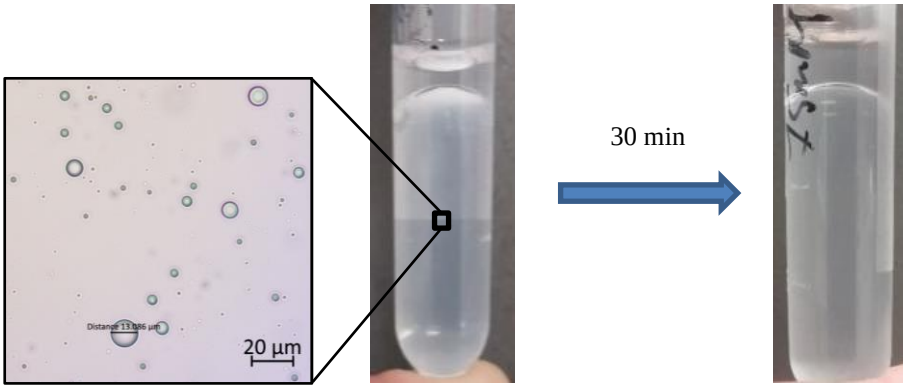

Figure IV-1. Photographs of the O/W mixture after sonication of the RSV-loaded hexadecane phase ([RSV] = 20 µg/mL) in the presence of the water phase ([NaCl] = 75 mM; O/W ratio of 20/80 v/v).

3. Interaction between resveratrol and the CNCs

In another preliminary study, we investigated the possibility for RSV to adsorb on the CNCs surface during emulsification. For that purpose, we measured the concentration of RSV remaining in the water phase after contact with a CNCs dispersion (we verified that the adsorbed RSV is not detected by UV-vis spectroscopy). For these experiments, an increasing

amount of RSV was stirred for 2 h in water, in the presence of 1.4 g/L CNCs and 75 mM NaCl. The weight ratio of RSV adsorbed on the CNCs (in µg/mg) was then plotted as a function of RSV concentration in Figure IV-2. The amount of RSV adsorbed on the CNCs increased linearly with the amount of RSV introduced initially, reaching a maximum ratio of 2.3 µg/mg in our experimental conditions. The linear dependency suggests that the CNCs surface was not saturated with the highest concentration of RSV used in this experiment. However, the limit of aqueous solubility of RSV in water was reached, it was therefore impossible to saturate the particles with RSV in these conditions.

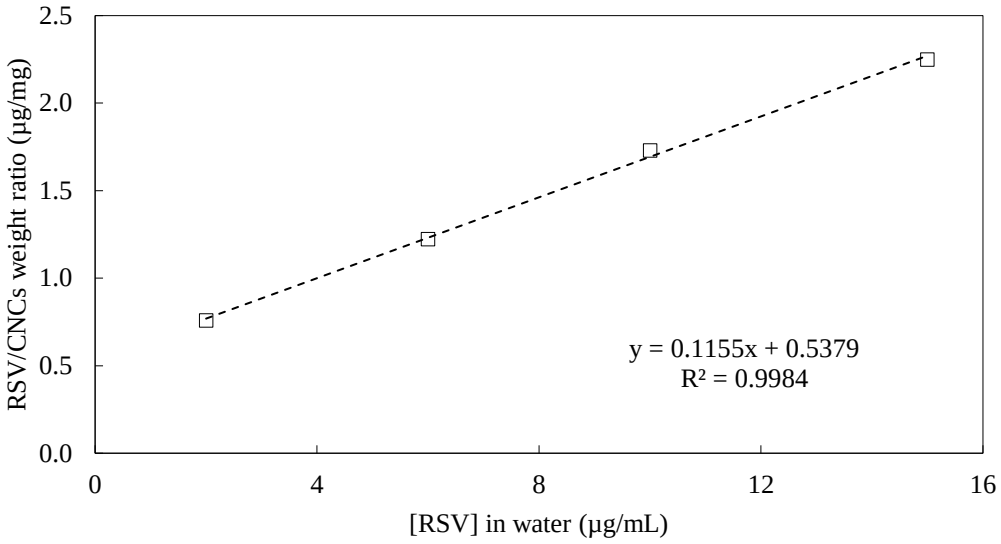

Figure IV-2. Weight ratio of RSV adsorbed on the CNCs (in µg/mg of CNCs) as a function of RSV concentration ([CNCs] = 1.4 g/L; [NaCl] = 75 mM).

4. RSV uptake and effect on the interfacial coverage

The amount of RSV incorporated in the emulsion droplets was evaluated by measuring the RSV uptake (U, see Chapter II, Part F). RSV uptake was measured as a function of droplets size for different surface coverages as illustrated in Figure IV-3. The droplets size (at a given

NaCl concentration) was varied by changing the CNCs concentration (0.05 – 0.24% w/v relative to hexadecane), while C was varied by using different salt concentrations (15, 30, 50 and 75 mmol/L).

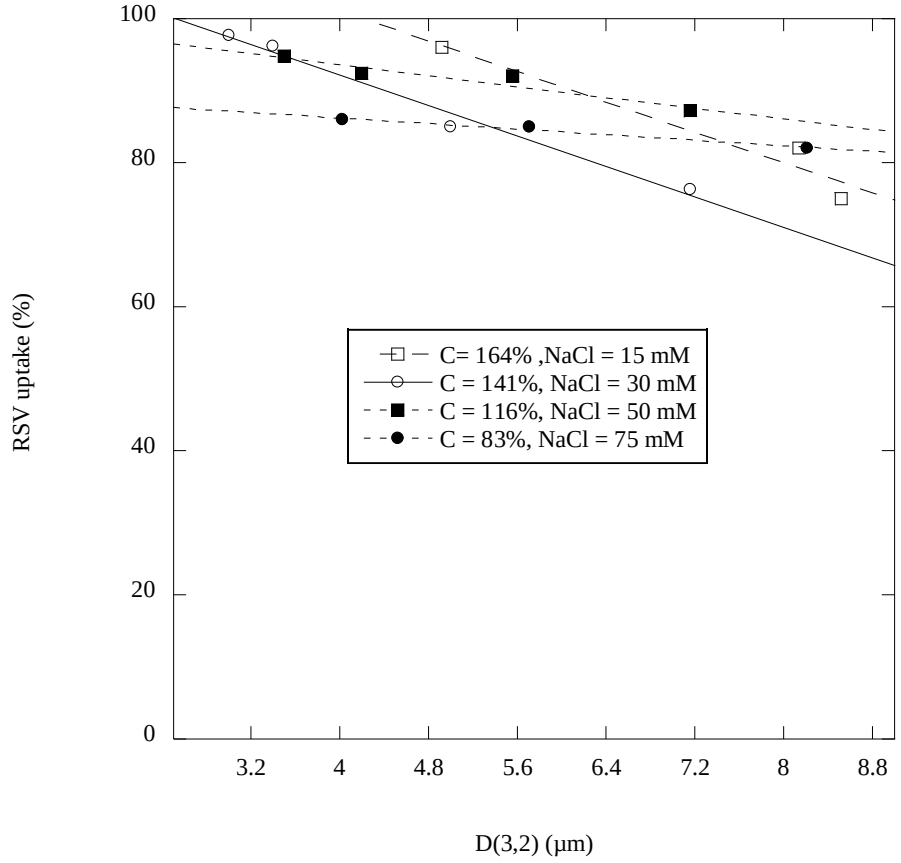

Figure IV-3. Evolution of the RSV uptake as a function of droplets size and NaCl concentration. Each point represents the mean of at least three measurements ± S.D. RSV concentration = 20 µg/mL.

The RSV uptake ranged from 76 ± 3 % to 98 ± 3 % depending on the conditions used, indicating that the method is quite efficient to incorporate RSV in the hexadecane droplets, in spite of its higher affinity for water (Chapter IV, Part A.2). In comparison, RSV uptakes ranging from 80 to 92% have been reported with modified bio-sourced particles such as starch (Matos et al., 2018), lignin (Dai et al., 2019) or chitosan (Zhang et al., 2017; Sharkawy et al., 2020). In Figure IV-3, no real trend could be inferred at constant droplet size.

For a given C on the other hand, a slight decrease in U with droplet size was observed. One possible explanation would be that the higher interfacial surface area of the smaller droplets favors the RSV uptake by trapping more RSV at the interface. The partial localization of RSV at the oil/water interface has been indeed demonstrated in many emulsion systems (Losada-Barreiro et al., 2014; Narkiewicz-Michalek et al., 2019; Díaz-Ruiz et al., 2021; Chen et al., 2023); it could be favoured in our case by the CNCs-RSV interactions revealed in Figure IV-2 (Chapter IV Part A.3).

The CNCs-stabilized emulsions loaded with RSV did not display any significant change in the RSV uptake during the first 6 hours (Figure IV-4), indicating that RSV was not released in the water phase within this duration. Similar results were reported by Matos et al. after encapsulation of RSV with octenyl succinic anhydride-modified starch (Matos et al., 2018), while a progressive release of RSV was noted in the very first hours with systems stabilized by poly(N-isopropylacrylamide)-grafted lignin (Dai et al., 2019), or chitosan/gum arabic particles (Sharkawy et al., 2020).

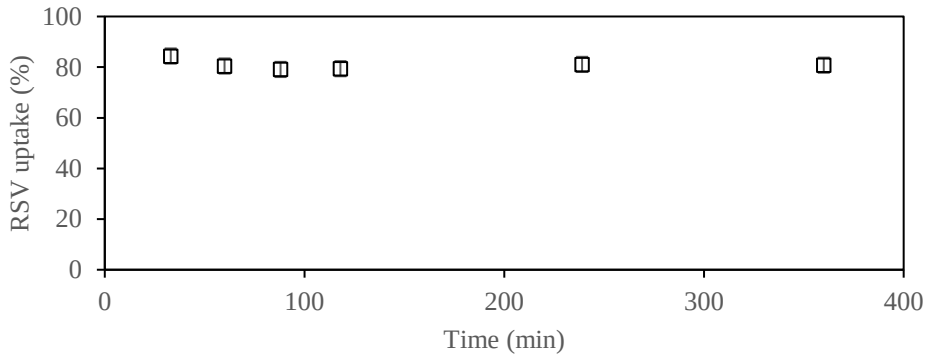

Figure IV-4. Evolution of the RSV uptake of a typical CNCs-stabilized hexadecane-in-water emulsion loaded with RSV within the first six hours. [CNCs] = 5.75 g/L oil, [NaCl] = 75 mM; [RSV] in hexadecane = 20 µg/mL; O/W ratio of 20/80 v/v). Error bars were estimated from 3 measurements.

For comparison purposes, RSV was also incorporated in a classical emulsion stabilized with sodium dodecyl sulfate (SDS), a common emulsifying agent. Emulsification was performed in the same conditions as with the CNCs ([RSV] in hexadecane = 20 µg/mL*;* O/W ratio = 20/80 v/v), using a 16 mM aqueous solution of SDS (see Chapter II, Part H). The RSV uptake measured just after emulsification was of only 15%, which is much lower than the 76 to 98 % obtained with the CNCs. This lower RSV uptake can be explained by the solubilization of part of the RSV molecules in the surfactant micelles found in the water phase.

B. Co-stabilising properties of resveratrol at the oil-water interface

1. Impact of resveratrol on the surface coverage

In the previous chapter, we hypothesized that part of the RSV could be positioned at the O/W interface, which could impact the stabilizing properties of the emulsions. To further clarify this point, we investigated the influence of RSV on the surface coverage, its modification being expected if RSV molecules are really present at the interface. Hence, the surface coverages were re-measured in the presence of increasing concentrations of RSV, and were compared with those of Figure III-5 (obtained without RSV) in Table IV-1.

Table IV-1. Comparison between the surface coverage (C in %) at different NaCl concentrations with or without RSV ([CNCs] = 0 - 25 g/L of hexadecane).

[NaCl] (mM)		**0**	**5**	**15**	**30**	**50**	**75**
[RSV] (µg/mL of hexadecane)	0	Not stable	n.d.	164	141	116	83
	20	220	103	81	76	78	82
	300	n.d.	n.d.	n.d.	n.d.	n.d.	69
	375	n.d.	n.d.	66	n.d.	n.d.	n.d.
	425	n.d.	n.d.	62	n.d.	n.d.	n.d.

The graphs used to re-calculate the different C values from the slopes are presented in Figure IV-5 and Figure IV-6.

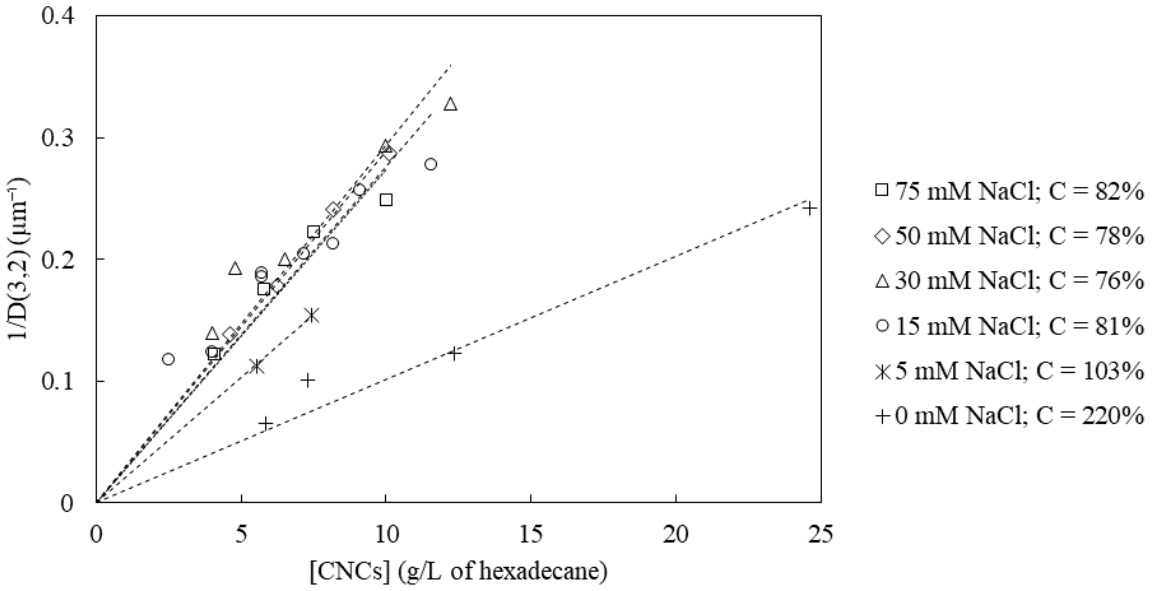

Figure IV-5. Inverse D(3,2) diameter as a function of CNCs concentration for the emulsions loaded with low concentrations of RSV (20 µg/mL of hexadecane) at different ionic strengths. The C obtained at the different salt concentrations are also reported.

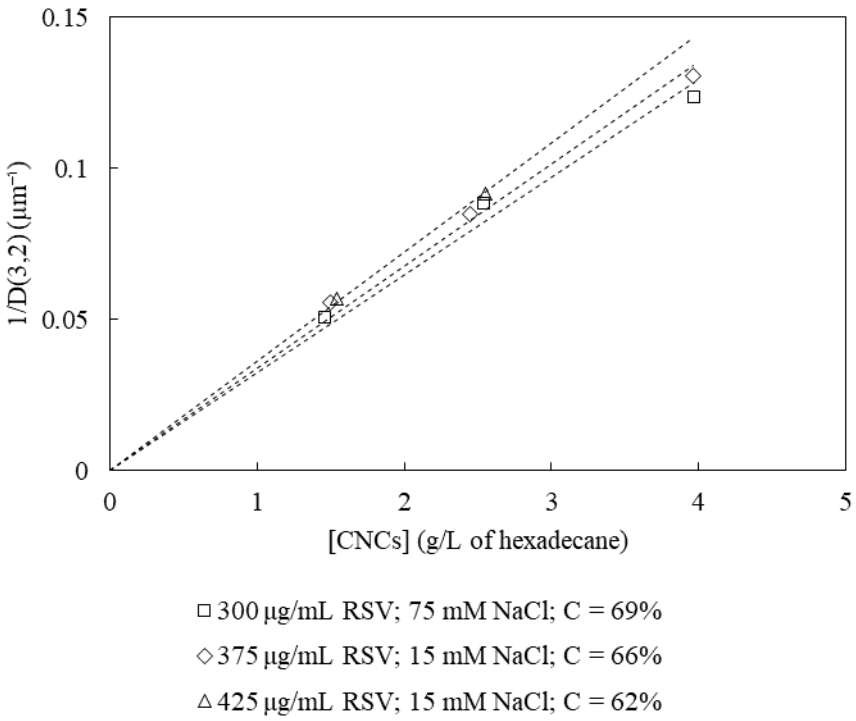

Figure IV-6. Inverse D(3,2) diameter as a function of CNCs concentration for the emulsions loaded with high concentrations of RSV (300, 375 and 425 µg/mL of hexadecane) at different ionic strengths. The C obtained are also reported.

The emulsions loaded with RSV were all stable, even without salt, which is quite remarkable since NaCl was required in unloaded emulsions. A C value of 220% was measured without salt (with 20 µg/mL RSV), this value decreasing down to 76 % in the presence of 30 mM NaCl (Table IV-1). Hence, the incorporation of RSV provoked a decrease in the interfacial coverage by the CNCs, less particles being required to stabilize the same interfacial area. This first result is of importance as it demonstrates that RSV molecules act as co-stabilizing agent with the CNCs, probably by positioning at oil/water interface. RSV acts then as a surfactant. The same trend was noted when higher concentrations of RSV were incorporated in the oil phase for a given salt concentration (Table IV-1). Interestingly, when C and S were plotted as a function of RSV concentration, a linear tendency was found, independently of the ionic strength (Figure IV-7). Hence, the droplets surface coverage by the CNCs is not anymore correlated to the salt

concentration when a co-stabilizer is added into the emulsions. This result suggests that a strong affinity exists between RSV and CNCs, which overcomes the repulsive electrostatic repulsions between CNCs.

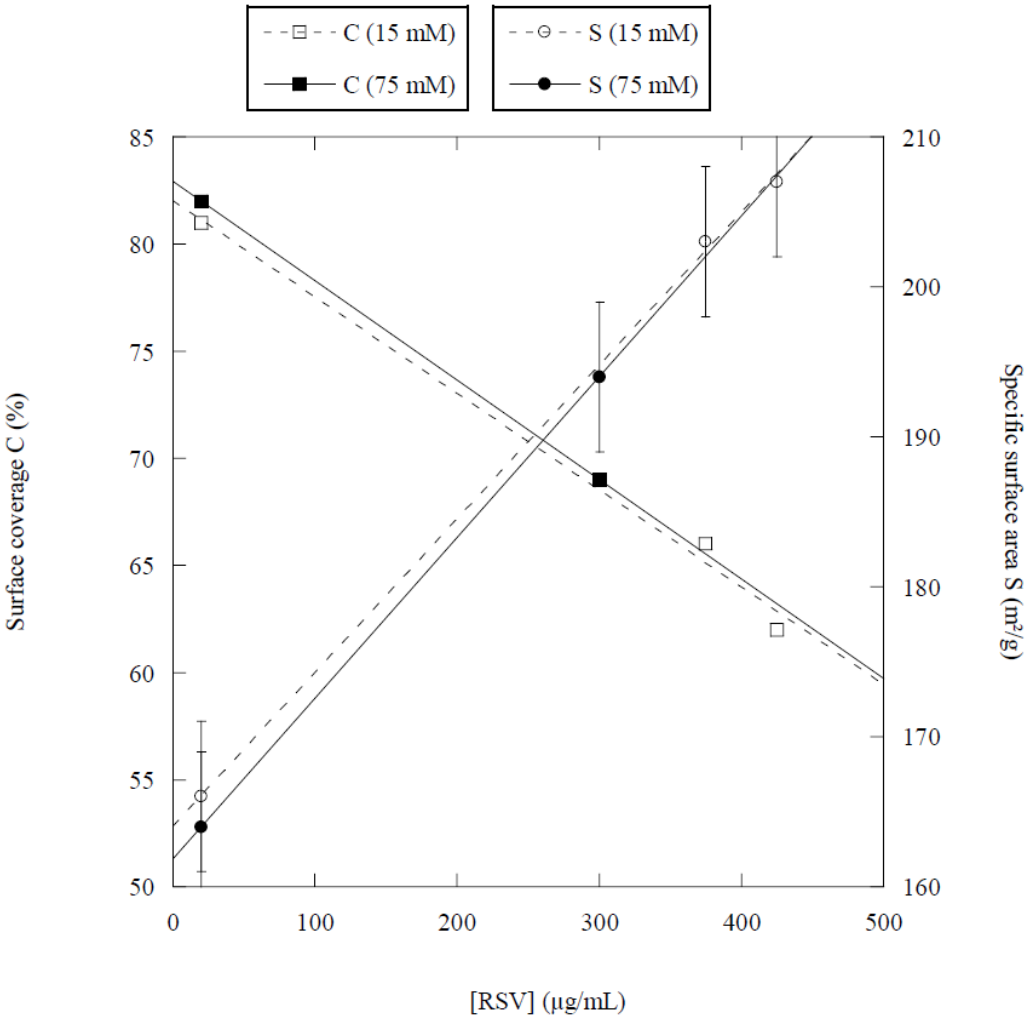

Figure IV-7. Evolution of the surface coverage C (y_1 axis) and of the surface specific area S (y_2 axis) as a function of RSV concentration for different NaCl concentrations (15 and 75 mM).

2. Triggered release of interfacial resveratrol by SDS

To further understand our system, we envisaged removing the interfacial RSV molecules by incrementally introducing SDS in the medium, just after emulsification. SDS is a surfactant

with a high hydrophilic to lipophilic balance, which makes it a better emulsifier compared to RSV. The addition of SDS is expected to replace the RSV positioned at the interface without modifying the droplets diameter, resulting in its release into the continuous phase.

Hence, 7 identical emulsions were prepared with 5.75 g/L of CNCs, and 200 µL of SDS of increasing concentration (from 2 to 200 mM in water) was subsequently added to each emulsion (see details in Chapter II, Part H). The evolution of RSV uptake was then plotted as a function of the SDS concentration in the aqueous phase (expressed in mmol/L of water) in Figure IV-8, the photos of the emulsions being presented in (Figure IV-9). The diameter of the droplets did not change after SDS addition in all experiments.

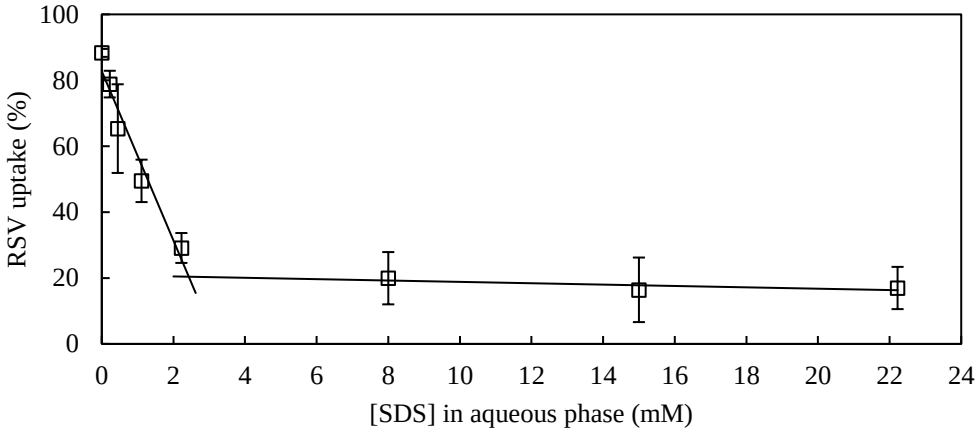

Figure IV-8. Evolution of RSV uptake as a function of SDS concentration in the aqueous phase, expressed in mmol/L of water. [CNCs] = 5.75 g/L of hexadecane; [NaCl] = 75 mM. Each point represents the mean of at least three measurements ± S.D.

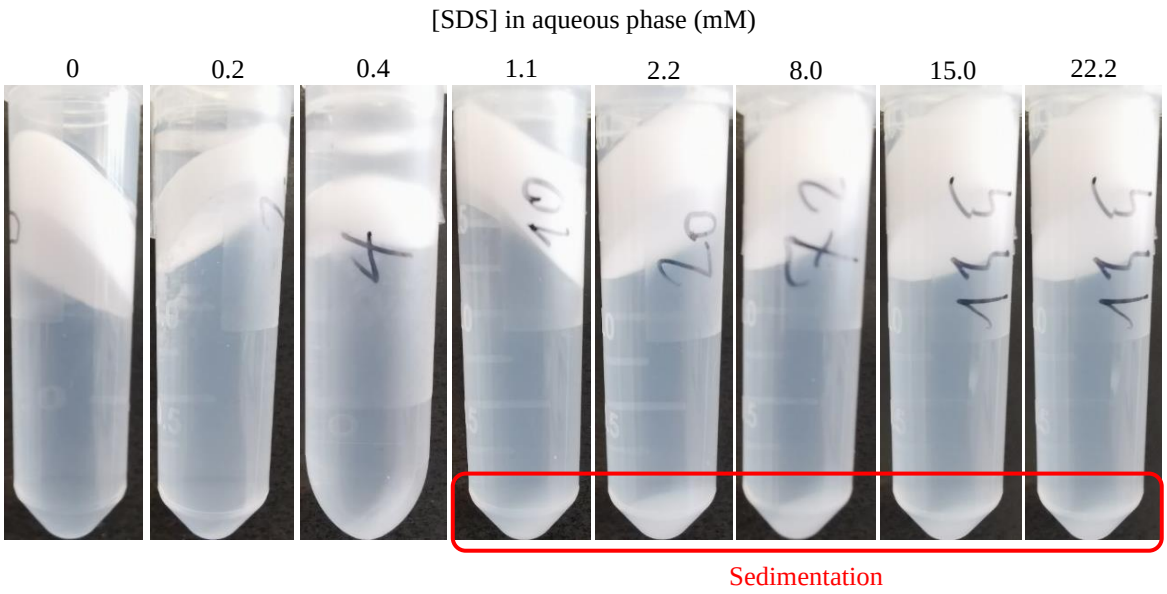

Figure IV-9. Photographs of the emulsions after addition of SDS and centrifugation.

A progressive decrease in RSV uptake was observed when more SDS was added, suggesting that RSV molecules were released in water as expected. A plateau was reached above ≈ 3 mM of SDS, indicating that about 20% of RSV could not be exchanged by SDS, regardless of its concentration in the medium. It is important to note at this stage that some sediments were visually observed for the emulsions in contact with high concentrations of SDS (1.1 – 22.2 mM in Figure IV-9), which we assigned to the release of CNC particles in the water phase. To verify this point, the CNCs in the water phase (CNC_{aq}) were quantified by the phenol-sulfuric acid method (see details in Chapter II, Part B) for the 7 emulsions investigated (Goi et al., 2019). CNC_{aq} was expressed in weight percent relative to the amount of CNCs initially introduced, and plotted as a function of SDS concentration in the aqueous phase in Figure IV-10.

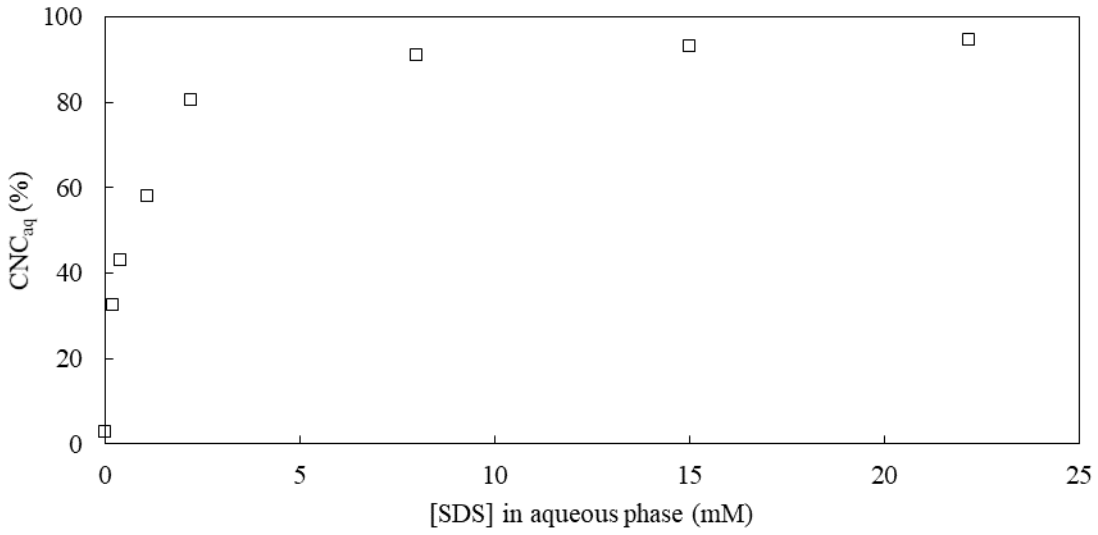

Figure IV-10. Evolution of the percentage of CNCs released in the water phase (CNC_{aq}) as a function of SDS concentration in the aqueous phase. [CNCs] = 5.75 g/L of hexadecane; [NaCl] = 75 mM.

Concomitantly to the RSV released, the incremental addition of SDS provoked indeed the progressive liberation of up to 94 ± 1% of the CNCs in the aqueous phase, likely because these particles were not directly anchored to the interface, being probably loosely bonded within aggregates. The weight ratio of "unreleased RSV" relative to "unreleased CNCs" (RSV_{un}/CNC_{un}), *i.e.* the RSV-to-CNCs ratio in the droplets, was plotted as a function of SDS concentration in Figure IV-11. Initially, this ratio was of about 3 µg RSV/mg of CNCs. When SDS was added, it increased up to 4 µg RSV/mg of CNCs, suggesting that more CNCs were released compared with RSV. This ratio progressively decreased to reach a plateau value for SDS concentrations above 8 mM. For these concentrations, a certain amount of CNCs (about 5 %) and RSV (about 18%) could not be detached by the treatment with SDS, regardless of its concentration in the medium. We hypothesized at this stage that the unreleased RSV could still be positioned at the interface (the concentration of RSV used in our experiments is indeed quite low), favouring the adsorption of the unreleased CNCs through the formation of complexes as demonstrated in Figure IV-2. The RSV/CNCs weight ratio in these complexes was estimated at 2.0 ± 0.1 µg/mg (Figure IV-11). The efficiency of CNCs complexes in stabilizing Pickering

emulsions has been demonstrated in recent studies (Akhlaghi et al., 2015; Angkuratipakorn et al., 2017).

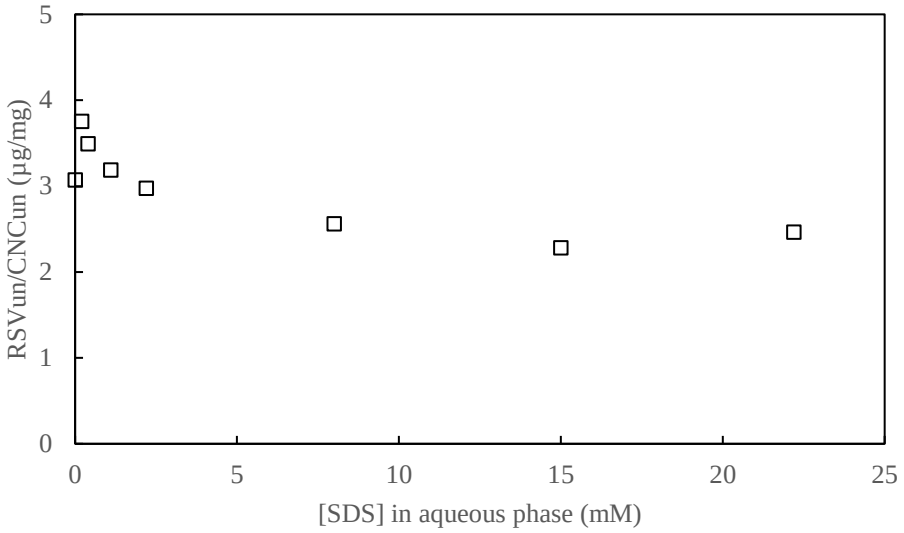

Figure IV-11. Weight ratio of "unreleased RSV" relative to "unreleased CNCs" (RSV_{un}/CNC_{un}) as a function of SDS concentration in the aqueous phase.

3. Tentative description of the interfacial organisation

A tentative interpretation of the previous results is given in Figure IV-12. We assume that CNCs aggregates were adsorbed at the oil/water interface and RSV was mostly located at the interface. For low concentrations of SDS, SDS molecules not only replaced some of the interfacial RSV molecules, but also provoked the detachment of loosely bonded CNCs from the multi-layered aggregates, *i.e.* those not directly anchored to the interface. At high SDS concentration, the interface was stabilized by both SDS and the undetached RSV/CNCs complexes (estimated ratio = 2.0 ± 0.1 µg/mg), which now form a thinner layer at the droplets surface.

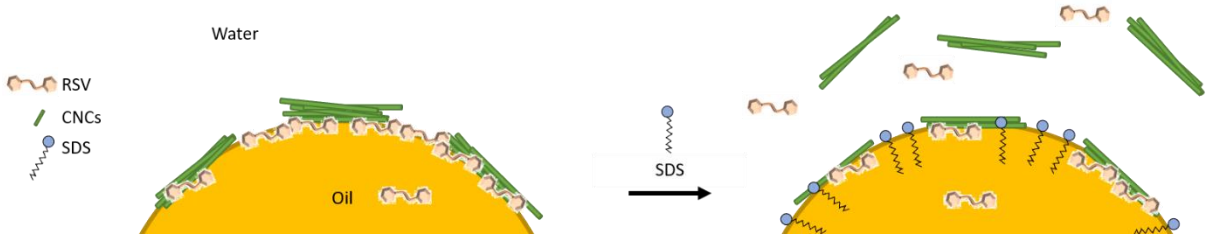

Figure IV-12. Schematic illustration of the possible organisation of CNCs and RSV at the interface after the addition of SDS.

C. Release profiles of incorporated RSV

1. Protocol

The ability for incorporated RSV to be released in the external water medium was investigated by the centrifugation method (see Chapter II, Part E): at discrete time intervals, centrifugation was applied to separate the droplets from the water phase, which was then withdrawn for UV-vis analysis and replaced with an equal volume of salty water to renew the release medium. Although the method is not appropriate for an exact evaluation of the release kinetics – even if already employed in some studies (Abouelmagd et al., 2015; Porta-i-Batalla et al., 2016) – it allowed comparing the released properties of emulsion systems displaying different surface coverage C, through the measurement of the cumulative fractional release (CFR) as a function of the times of centrifugations. Five emulsions with different C values were selected for this study (Emulsion 1 to 5 in Table IV-2) (see experimental details in Chapter II, Part E).

Table IV-2. Experimental details for the preparation of the emulsions used in the release experiments, with their characteristics and k_1 constants.

	Emulsion 1	Emulsion 2	Emulsion 3	Emulsion 4	Emulsion 5
[CNCs] (g/L oil)	4	4	4	4	5.75
[NaCl] (mM)	15	10	75	15	75
[RSV] (µg/mL)	425	300	300	375	20
C (%)	62	71	69	66	82
S (m^2/g)	217	189	194	203	164
D(3,2) (µm)	9	9	8.1	7.6	5.7
RSV uptake (%)	74 ± 3	91 ± 3	82 ± 3	77 ± 3	80 ± 3
k_1 (nm^2/s)	812	107	166	500	435 ± 10
R^2	0.973	0.965	0.997	1	0.999

Emulsions 1 to 4 are systems with droplet sizes large enough (D(3,2) > 7 µm) to cream easily during centrifugation, and having RSV concentrations high enough (300 to 425 µg/mL) to fill the core of the droplets, in addition to the RSV trapped at the interface. Emulsion 5 corresponds to the previous emulsion system with a low concentration of RSV (20 µg/mL). In all cases the volumetric fraction of hexadecane was set to 20%; the discrete time intervals for centrifugation were comparable but the concentration in NaCl and RSV differed.

2. Release profiles and interfacial rate constant

The CFR of emulsions 1 to 5 – defined as the cumulative amount of RSV released at time *t* (M_t) over that encapsulated at time t = 0 (M_0) – is plotted as a function of the time corresponding to the centrifugations in Figure IV-13a. The mathematical model proposed by Washington and Evans (Washington and Evans, 1995), see Equation II-5 in Chapter II Part E) was applied in

Figure IV-13b and used to evaluate the "pseudo" interfacial rate constant k_1 associated with the release of RSV (deduced from the slope in Figure IV-13b, and reported in Table IV-2).

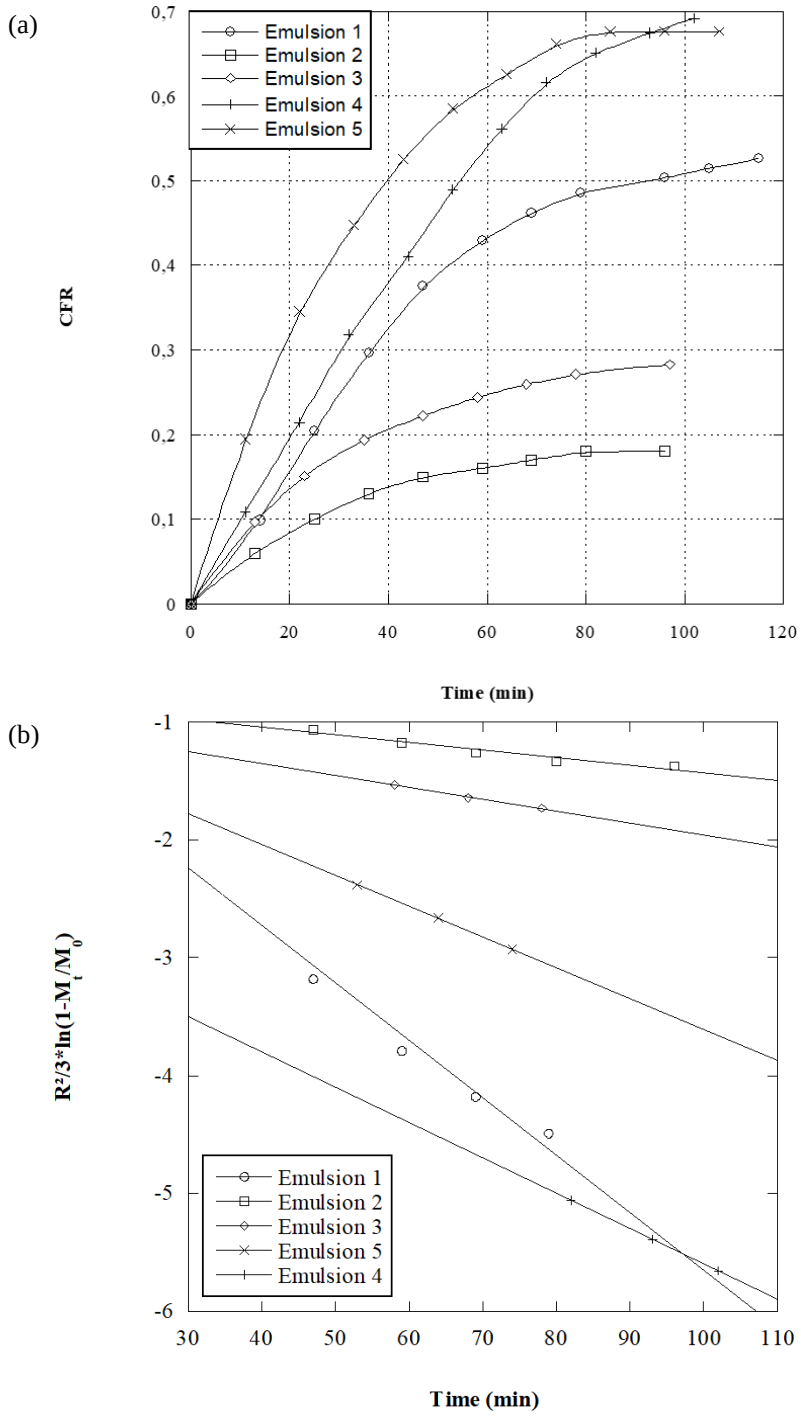

Figure IV-13. Release profiles measured by the centrifugation method for emulsions 1 to 5. (a) Cumulative fractional release (CFR) as a function of the times of centrifugations, with curves shown to guide the reader's eye. (b) Application of the model proposed by Washington et al. using Equation II-5. (Washington and Evans, 1995)

In Table IV-2, the RSV uptakes are in the same order of magnitude for the five emulsions (between 74 and 91%). When Emulsions 1 to 4 are compared, a faster release is observed (k_1 is higher) when C is smaller. This difference in release interfacial rates can be explained by a variation in the CNCs interfacial density, mainly due to a variation in the amount of interfacial RSV (co-stabiliser), since NaCl has a negligible effect on C in the presence of RSV. A lower interfacial coverage increases the probability of finding areas devoid of particles at the interface. Such voids give the incorporated materials a chance to diffuse out of the internal phase, as has been demonstrated for other Pickering emulsion systems (Yow and Routh, 2009; Dan, 2012; Fielding and Armes, 2012; Tan et al., 2014; Sufi-Maragheh et al., 2019). Hence, the smaller the C, the less hindrance for RSV to be released. The pseudo interfacial rate constant k_1 of Emulsions 1 to 4 was plotted as a function of C in Figure IV-14. Interestingly, a linear variation was found, demonstrating that the release rate at the interface was proportional to the droplets surface coverage.

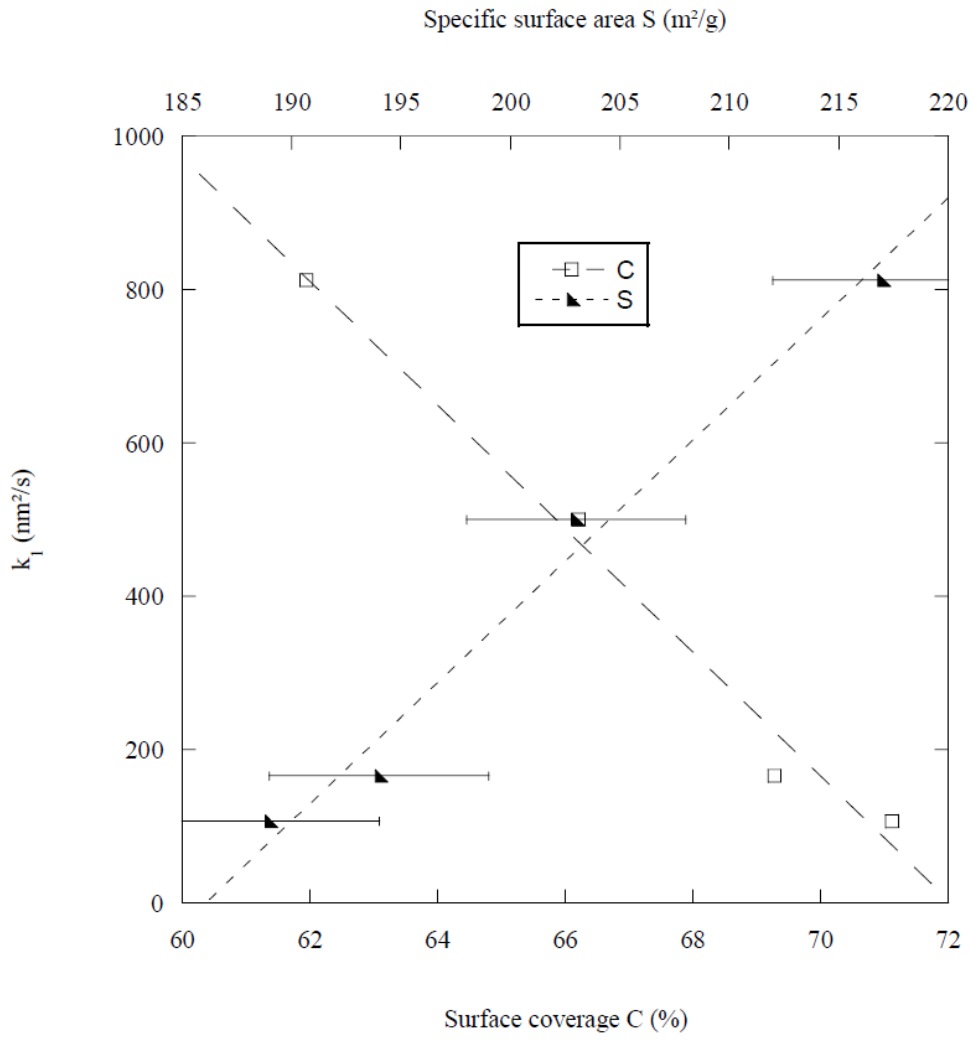

Figure IV-14. Evolution of k_1 as a function of the surface coverage C (y_1 axis) and of the surface specific area S (y_2 axis), based on Emulsions 1 to 4.

Emulsion 5 is the one used in the previous section, *i.e.* loaded with a much lower amount of RSV. Unlike with other emulsions, a plateau was reached for the last 3 centrifugations. Here, 23 ± 5% of RSV remained in the emulsion, in agreement with the results of Part B.2, where we showed that about 20% of RSV could never be detached from the droplets, presumably because of its strong association with part of the CNCs at the O/W interface. A different behavior was noted in terms of interfacial rate constant with Emulsion 5, since k_1 was larger than for the other emulsions, despite the higher C value. In that case, the RSV initial concentration was very low, suggesting that most of the RSV molecules were located at the O/W interface.

However, the model used here considers that the rate of release is limited by an interfacial barrier (Washington and Evans, 1995). It is then possible than this model is only valid for systems with high RSV concentrations, for which RSV is released from the core of the droplets.

Findings related to the release properties of RSV from Pickering emulsions stabilized by cellulose nanocrystals have been recently published (Mohd Noor et al., 2025).

D. Conclusions

In this chapter, hexadecane-in-water Pickering emulsions stabilized by CNCs in the presence of salt were used to incorporate RSV, selected as model hydrophobic molecule. The objective was to probe the impact of ionic strength on the droplet coverage by the CNCs and subsequent release of RSV. When RSV was incorporated in the internal phase, salt was not required anymore to stabilize the emulsion and the C value was now correlated to the RSV concentration instead of the ionic strength, the RSV molecules acting as co-stabilizers at the interface. Part of the RSV seemed to favour the anchoring of CNCs at the O/W interface, supposedly through the formation of complexes by intermolecular forces. Yet, most of the RSV trapped at the interface could be easily released on demand, by triggering its exchange with SDS. Release experiments with high RSV concentrations showed a linear dependency of the interfacial release rate with C, and as a consequence, with the surface coverage around the droplets; the lower the surface coverage, the quicker RSV was released.

References

Abouelmagd, S.A., Sun, B., Chang, A.C., Ku, Y.J., Yeo, Y., 2015. Release Kinetics Study of Poorly Water-Soluble Drugs from Nanoparticles: Are We Doing It Right? Mol. Pharmaceutics 12, 997–1003. https://doi.org/10.1021/mp500817h

Akhlaghi, S.P., Berry, R.M., Tam, K.C., 2015. Modified Cellulose Nanocrystal for Vitamin C Delivery. AAPS PharmSciTech 16, 306–314. https://doi.org/10.1208/s12249-014-0218-4

Angkuratipakorn, T., Sriprai, A., Tantrawong, S., Chaiyasit, W., Singkhonrat, J., 2017. Fabrication and characterization of rice bran oil-in-water Pickering emulsion stabilized by cellulose nanocrystals. Colloids and Surfaces A: Physicochemical and Engineering Aspects 522, 310–319. https://doi.org/10.1016/j.colsurfa.2017.03.014

Chen, Y., Cheng, H., Liang, L., 2023. Effect of Oil Type on Spatial Partition of Resveratrol in the Aqueous Phase, the Protein Interface and the Oil Phase of O/W Emulsions Stabilized by Whey Protein and Caseinate. Antioxidants 12, 589. https://doi.org/10.3390/antiox12030589

Dai, L., Li, Y., Kong, F., Liu, K., Si, C., Ni, Y., 2019. Lignin-Based Nanoparticles Stabilized Pickering Emulsion for Stability Improvement and Thermal-Controlled Release of *trans*-Resveratrol. ACS Sustainable Chem. Eng. 7, 13497–13504. https://doi.org/10.1021/acssuschemeng.9b02966

Dan, N., 2012. Transport through self-assembled colloidal shells (colloidosomes). Current Opinion in Colloid & Interface Science 17, 141–146. https://doi.org/10.1016/j.cocis.2012.03.003

Davidov-Pardo, G., McClements, D.J., 2014. Resveratrol encapsulation: Designing delivery systems to overcome solubility, stability and bioavailability issues. Trends in Food Science & Technology 38, 88–103. https://doi.org/10.1016/j.tifs.2014.05.003

Díaz-Ruiz, R., Laca, A., Sánchez, M., Fernández, M.R., Matos, M., Gutiérrez, G., 2021. Addition of Trans-Resveratrol-Loaded Highly Concentrated Double Emulsion to Yoghurts: Effect on Physicochemical Properties. IJMS 23, 85. https://doi.org/10.3390/ijms23010085

Fielding, L.A., Armes, S.P., 2012. Preparation of Pickering emulsions and colloidosomes using either a glycerol-functionalised silica sol or core–shell polymer/silica nanocomposite particles. J. Mater. Chem. 22, 11235–11244. https://doi.org/10.1039/C2JM31433A

Goi, Y., Fujisawa, S., Saito, T., Yamane, K., Kuroda, K., Isogai, A., 2019. Dual Functions of TEMPO-Oxidized Cellulose Nanofibers in Oil-in-Water Emulsions: A Pickering Emulsifier and a Unique Dispersion Stabilizer. Langmuir 35, 10920–10926. https://doi.org/10.1021/acs.langmuir.9b01977

Losada-Barreiro, S., Costa, M., Bravo-Díaz, C., Paiva-Martins, F., 2014. Distribution and Antioxidant Efficiency of Resveratrol in Stripped Corn Oil Emulsions. Antioxidants 3, 212–228. https://doi.org/10.3390/antiox3020212

Matos, M., Laca, A., Rea, F., Iglesias, O., Rayner, M., Gutiérrez, G., 2018. O/W emulsions stabilized by OSA-modified starch granules versus non-ionic surfactant: Stability, rheological behaviour and resveratrol encapsulation. Journal of Food Engineering 222, 207–217. https://doi.org/10.1016/j.jfoodeng.2017.11.009

Mohd Noor, M. A., Sèbe, G., Faure, C., 2025. Monitoring the interfacial release rate of resveratrol in Pickering emulsions stabilized by cellulose nanocrystals through the control of the surface coverage. Colloids and Surfaces A: Physicochemical and Engineering Aspects 704, 135429. https://doi.org/ 10.1016/j.colsurfa.2024.135429

Narkiewicz-Michalek, J., Szymula, M., Losada-Barreiro, S., Bravo-Diaz, C., 2019. Concentration of resveratrol at the oil–water interface of corn oil-in-water emulsions. Adsorption 25, 903–911. https://doi.org/10.1007/s10450-019-00108-3

Porta-i-Batalla, M., Eckstein, C., Xifré-Pérez, E., Formentín, P., Ferré-Borrull, J., Marsal, L.F., 2016. Sustained, Controlled and Stimuli-Responsive Drug Release Systems Based on Nanoporous Anodic Alumina with Layer-by-Layer Polyelectrolyte. Nanoscale Res Lett 11, 372. https://doi.org/10.1186/s11671-016-1585-4

Sharkawy, A., Casimiro, F.M., Barreiro, M.F., Rodrigues, A.E., 2020. Enhancing trans-resveratrol topical delivery and photostability through entrapment in chitosan/gum Arabic Pickering emulsions. International Journal of Biological Macromolecules 147, 150–159. https://doi.org/10.1016/j.ijbiomac.2020.01.057

Shi, G., Rao, L., Yu, H., Xiang, H., Yang, H., Ji, R., 2008. Stabilization and encapsulation of photosensitive resveratrol within yeast cell. International Journal of Pharmaceutics 349, 83–93. https://doi.org/10.1016/j.ijpharm.2007.07.044

Sufi-Maragheh, P., Nikfarjam, N., Deng, Y., Taheri-Qazvini, N., 2019. Pickering emulsion stabilized by amphiphilic pH-sensitive starch nanoparticles as therapeutic containers. Colloids and Surfaces B: Biointerfaces 181, 244–251. https://doi.org/10.1016/j.colsurfb.2019.05.046

Tan, H., Sun, G., Lin, W., Mu, C., Ngai, T., 2014. Gelatin Particle-Stabilized High Internal Phase Emulsions as Nutraceutical Containers. ACS Appl. Mater. Interfaces 6, 13977–13984. https://doi.org/10.1021/am503341j

Washington, C., Evans, K., 1995. Release rate measurements of model hydrophobic solutes from submicron triglyceride emulsions. Journal of controlled release 33, 383–390.

Yow, H.N., Routh, A.F., 2009. Release Profiles of Encapsulated Actives from Colloidosomes Sintered for Various Durations. Langmuir 25, 159–166. https://doi.org/10.1021/la802711y

Zhang, Y., Xu, X., Wang, Q., Zhang, H., Qian, A., Liu, T., Xia, Q., 2017. Preparation and characterization of colloidal particles synergistic with emulsifier stabilizing Pickering emulsion. Integrated Ferroelectrics 180, 24–36. https://doi.org/10.1080/10584587.2017.1336420

Chapter V. Oxidative stabilisation of linseed oil emulsions

The potential ability of unmodified and surface-modified CNCs to protect highly oxidizable oil-in-water emulsions against lipid oxidation is investigated in this chapter. Virgin linseed oil was chosen for this study because this organic oil contains elevated amount of polyunsaturated fatty acids (ω-3 and ω-6 fatty acids). Generally, oils and fats that contain polyunsaturated fatty acids are more vulnerable to oxidation during storage or heat treatment as they have multiple double bonds and reactive hydrogen atoms which makes them prone to oxidation (Tańska et al., 2018).

In addition to the unmodified CNC particles, the cinnamoyle- and polydopamine-modified CNCs were also tested, as they display interesting chemical properties. Cinnamate groups are indeed reported to undergo reversible *trans-cis* isomerization and/or dimerization upon UV light irradiation, which could impart UV-protection, while polydopamine is an antioxidant with radical scavenging properties (Chapter II, Part A).

A. Protocol

Linseed oil-in-water emulsions were prepared with the unmodified or modified CNCs, using an O/W ratio of 20/80 or 10/90 v/v, in the presence of NaCl (see Chapter III, Part B.1). The emulsions were then exposed to Fe(II) ions to accelerate lipid oxidation, and the oxidative stability was evaluated by measuring the evolution of the primary oxidation products, *i.e.* the conjugated dienes (CD) (see detailed protocol in Chapter II, Part I.2). The results were then compared with those obtained with conventional emulsions prepared with sodium dodecyl sulfate (SDS), a common emulsifying agent.

B. Oxidative stability of the emulsions stabilized with the unmodified CNCs

1. Evolution of the conjugated dienes (CDs) with time

a. In the presence of 10^{-3} M Fe(II) as accelerating agent

Preliminary experiments were performed by accelerating lipid oxidation with 10^{-3} M Fe(II). The linseed oil emulsion was prepared with an O/W ratio of 20/80 v/v, in the presence of 75 mM of NaCl. The estimated surface coverage (C) and interfacial surface area (S) for this system was 116% and 116 m^2/g, respectively (see Chapter III, Part B.1). The evolution of CDs during storage under protection from light, is plotted as a function of time in Figure V-1.

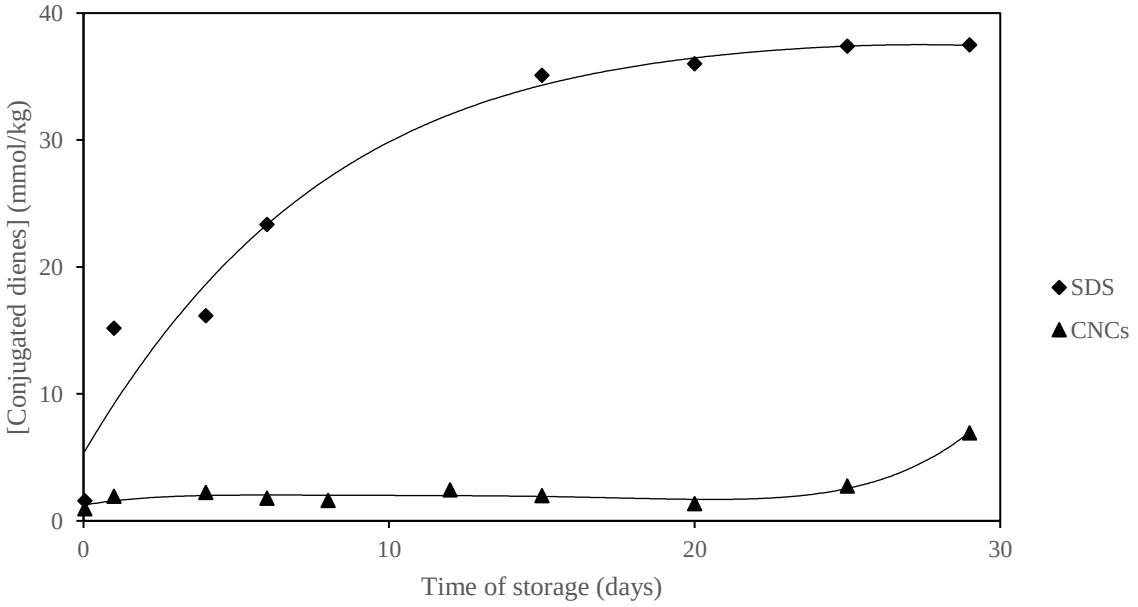

Figure V-1. Evolution of CDs with time during storage of linseed oil emulsions stabilized with SDS or the CNCs, in the presence of 10^{-3} M Fe (II) ions (expressed in mol per L of emulsion). [SDS] = 16 mmol/L; [CNCs] = 17.5 g/L of linseed oil; [NaCl] = 75 mM; oil/water ratio = 20% v/v.

With SDS (droplets diameter D(3,2) = 26 µm), a progressive increase in the CDs concentration was noted over time, until a maximum value of about 37 mmol/kg was reached after 15 days.

This significant increase is related to the high oxidizability of linseed oil and pro-oxidant effect of iron at the O/W interface.

Distinctively from the SDS-stabilised emulsion, the emulsion stabilised with the unmodified CNCs (droplets diameter D(3,2) = 6 µm) did not show any significant increase of CDs during the first 20 days, a maximum CD concentration of only 7 mmol/kg being noted after 29 days. Unlike SDS, the CNCs were able to significantly delay the oxidation of linseed oil, and this despite the higher oil/water interfacial area of this system (droplets are 5 times smaller), which yet increases the possibility of contact between the oil and O_2, or Fe(II) ions. Hence, the CNCs impeded somehow the formation of hydroperoxides (and as a consequence of CDs), expected after oxidation of the unsaturated fatty acids of linseed oil (Frankel, 2014). Compared with SDS, the CNCs are strongly adsorbed at the oil/water interface, with a greater adsorption energy. Since lipid oxidation is initiated at the O/W interface, CNCs are believed to protect the oil from oxidation by forming a physical barrier around the droplets, which should delay the permeation of oxygen molecules and Fe(II) ions into the oil phase. In addition, the negative charges at CNCs surface could have scavenged the Fe(II) ions by electrostatic interaction, as the number of sulfate ester groups in the system is close to the number of Fe(II) ions introduced in the water phase. The concentration of sulfate ester groups at the CNCs surface was estimated at 0.3 mmol/g of CNCs, based on the provider's data (sulfur content = 1.05 wt%), meaning that 2.1 µmol of negative charges are available in our emulsion system, while 1.6 µmol of Fe(II) are also present. Nevertheless, the physical barrier brought by the CNCs should be critical since SDS has also the capacity to scavenge the Fe(II) ions *via* its sulfate head group, yet the protection is low.

The mechanism proposed for the protection of linseed oil by the CNCs in our experimental conditions is summarized in Figure V-2.

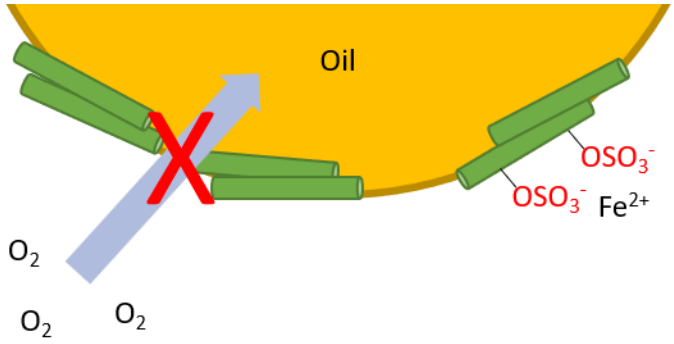

Figure V-2. Proposed mechanism for the protection of linseed oil by the CNCs at the O/W interface in our experimental conditions.

b. In the presence of RSV (with 10^{-3} M Fe(II) as accelerating agent)

Since RSV is a molecule displaying anti-oxidant properties (Davidov-Pardo and McClements, 2014), its impact on the oxidative stability of linseed oil emulsions was also studied. RSV was incorporated into the oil phase prior to emulsification ([RSV] = 20 µg/mL of linseed oil), and the oxidative stability of the emulsions stabilized with SDS or the CNCs was investigated in the same conditions as before. No significant modification of the droplets diameter was noted in the presence of RSV (D(3,2) = 23.5 µm with SDS; D(3,2) = 5.6 µm with the CNCs) The evolution of CDs with time for both emulsions is presented in Figure V-3 ; the results without RSV are also reported.

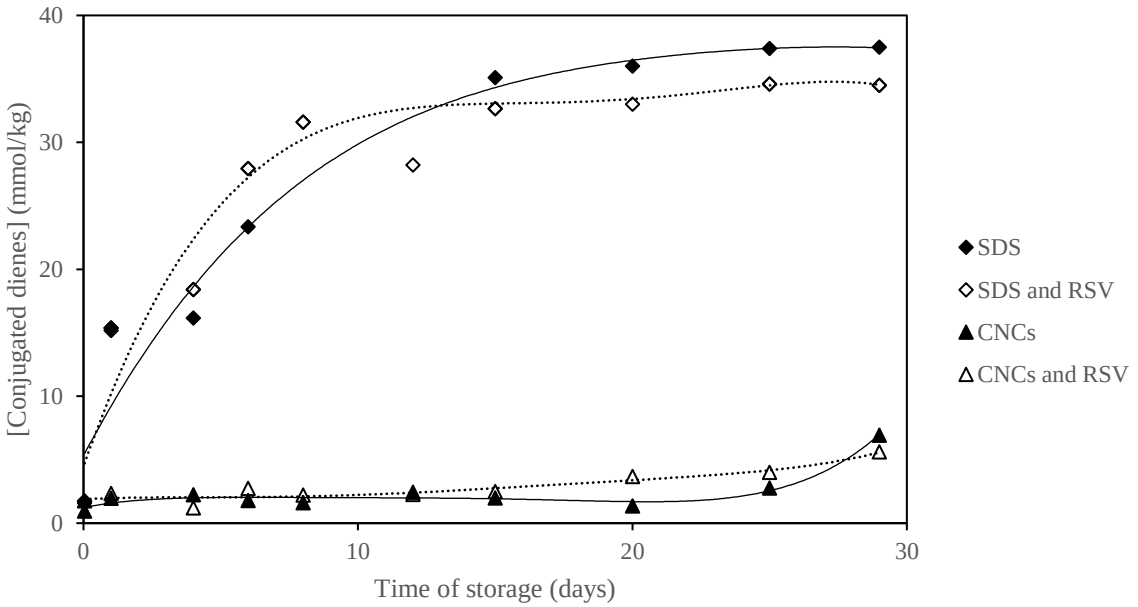

Figure V-3. Evolution of CDs with time during storage of SDS- and CNC-stabilized emulsions prepared with or without RSV, in the presence of 10^{-3} M Fe (II) ions (expressed in mol per L of emulsion). [SDS] = 16 mmol/L; [CNCs] = 17.5 g/L of linseed oil; [NaCl] = 75 mM; [RSV] = 20 µg/mL of linseed oil; oil/water ratio = 20% v/v.

Unexpectedly, the presence of RSV in both types of emulsion did not significantly impact the oxidative stability of linseed oil in our experimental conditions, which may be due to the low concentration of RSV used in these experiments.

c. In the presence of 10^{-2} M Fe(II) as accelerating agent

In order to further clarify the role of CNCs in influencing the rate of lipid oxidation, the oxidative stability of the emulsion stabilized with the CNCs was investigated again, but with ten times more Fe(II) as accelerating agent ([Fe(II)] = 10^{-2} M, expressed in mol per L of emulsion). This experiment was performed in the same conditions as before, and the results obtained were compared with those reported in Figure V-4.

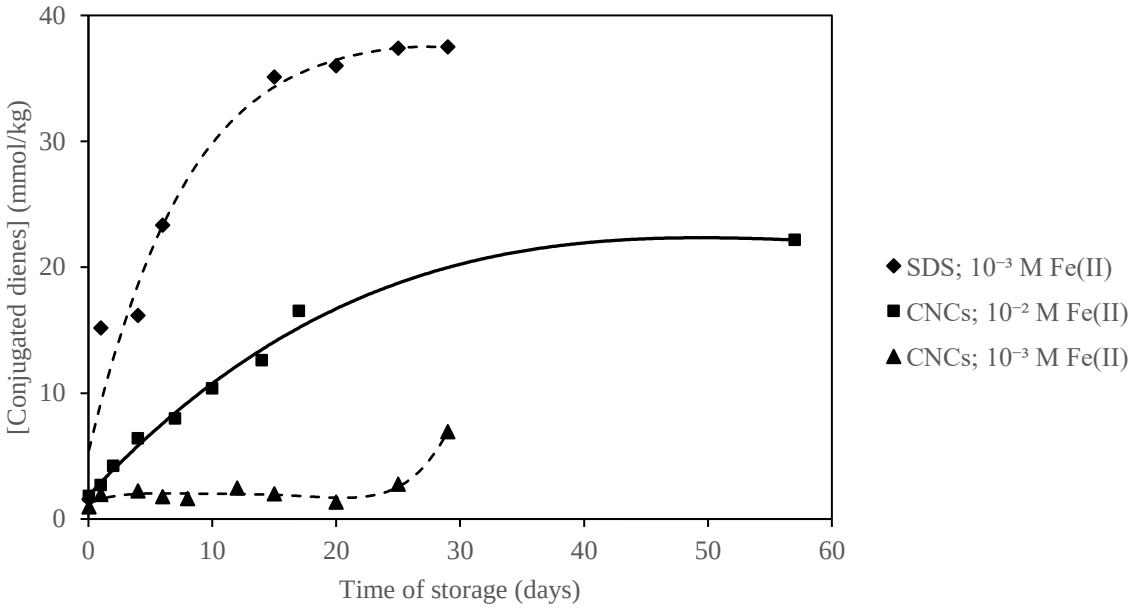

Figure V-4. Evolution of CDs with time during storage of the linseed oil emulsion stabilized with the CNCs, in the presence of 10^{-2} M Fe (II) ions (expressed in mol per L of emulsion). The results obtained with 10^{-3} M Fe (II) are also reported. [CNCs] = 17.5 g/L of linseed oil; [NaCl] = 75 mM; oil/water ratio = 20% v/v; [SDS] = 16 mmol/L.

The introduction of ten times more Fe(II) ions in the CNCs-stabilised emulsion led to a significant increase of CDs over time, suggesting that the probability of contact between the dispersed phase and Fe(II) was increased. The number of Fe(II) ions in our system is now 16 µmol, which is about 8 times more than the number of negative charges available at the CNCs surface (2.1 µmol). Hence, a significant amount of Fe(II) ions cannot be scavenged anymore by the CNCs sulfate ester groups, and can diffuse through the CNCs layer at the O/W interface (probably through the poorly covered areas), leading to the oil oxidation observed. Yet, the rate of oxidation remained much slower than in the case of the SDS-stabilized emulsion, exposed to 10 times less Fe(II) ions: the CD concentration after 57 days was 1.7 times lower than that measured with SDS after 29 days. Some protection is therefore imparted by the cellulosic shell.

In view of these results, a Fe(II) concentration of 10^{-2} M was used in subsequent experiments, as it allows a better highlight of the differences observed when certain parameters are changed.

2. Impact of droplets size and surface coverage

The oxidative stability of oil emulsions depends strongly on the properties of the O/W interface (Keramat et al., 2022), which is impacted by the droplets size (modification of the interfacial area), and the surface coverage around the droplets. Therefore, the impact of these two parameters was investigated.

For this purpose, different linseed oil emulsions differing in their composition were prepared, with the objective to produce systems with two different droplets size at comparable coverage percentage (C), and two different coverage at comparable droplets size (Table V-1).

Table V-1. Experimental details for the preparation of linseed oil emulsions with two different droplets diameter (D(3,2)) and coverage percentage (C).

	Oil/water ratio	**[CNCs] (g/L of oil)**	**[NaCl] (mM)**	**D(3,2) (μm)**	**C (%)**
Emulsion 1	10:90	35	75	1.6	116
Emulsion 2	20:80	17.5	75	6	116
Emulsion 3	10:90	50	30	1.8	187

a. Impact of droplets size

For this study, Emulsion 1 and 2 were compared. The evolution of CDs with time for both emulsions in the presence of 10^{-2} M Fe(II) is presented in Figure V-5. Let us note that the volume fraction of oil is taken into account when evaluating the conjugated dienes concentration, which is expressed in mmol per kg of oil.

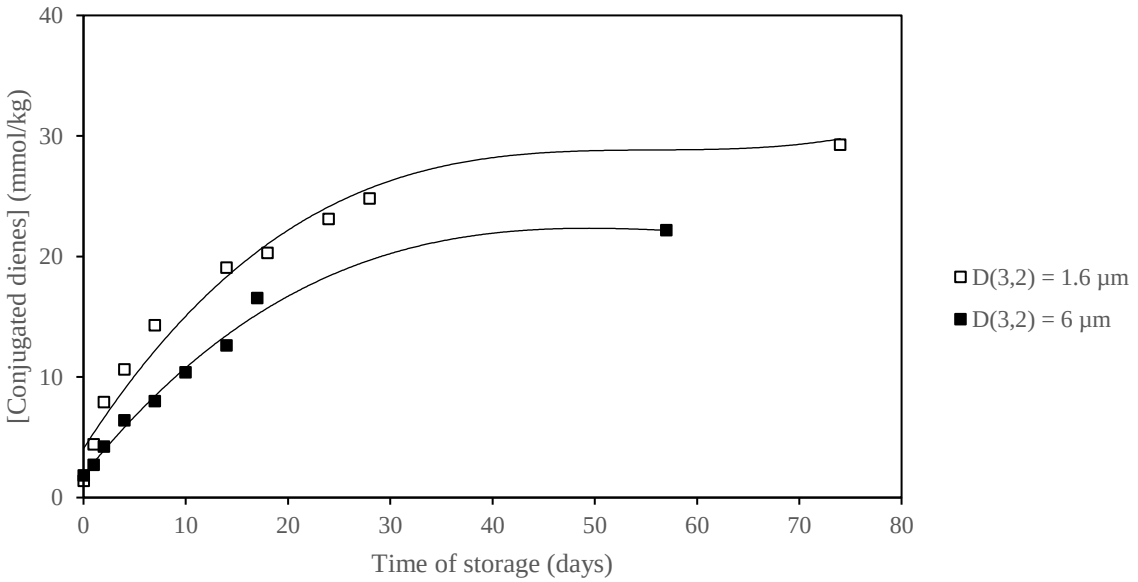

Figure V-5. Evolution of CDs with time during storage of the CNCs-stabilized linseed oil emulsions prepared with two different droplets size, in the presence of 10^{-2} M Fe (II) ions (expressed in mol per L of emulsion).

As expected, the emulsion with smaller droplets size (D(3,2) = 1.6 µm), *i.e.* with the larger interfacial area, displayed a higher lipid oxidation rate, the possibility of contact between linseed oil and Fe(II) ions, or O_2 dissolved in the water phase, being increased.

b. Impact of surface coverage

Here, Emulsion 1 and Emulsion 3 were compared (Table V-1). The evolution of CDs with time for both emulsions in the presence of 10^{-2} M Fe(II) is presented in Figure V-6.

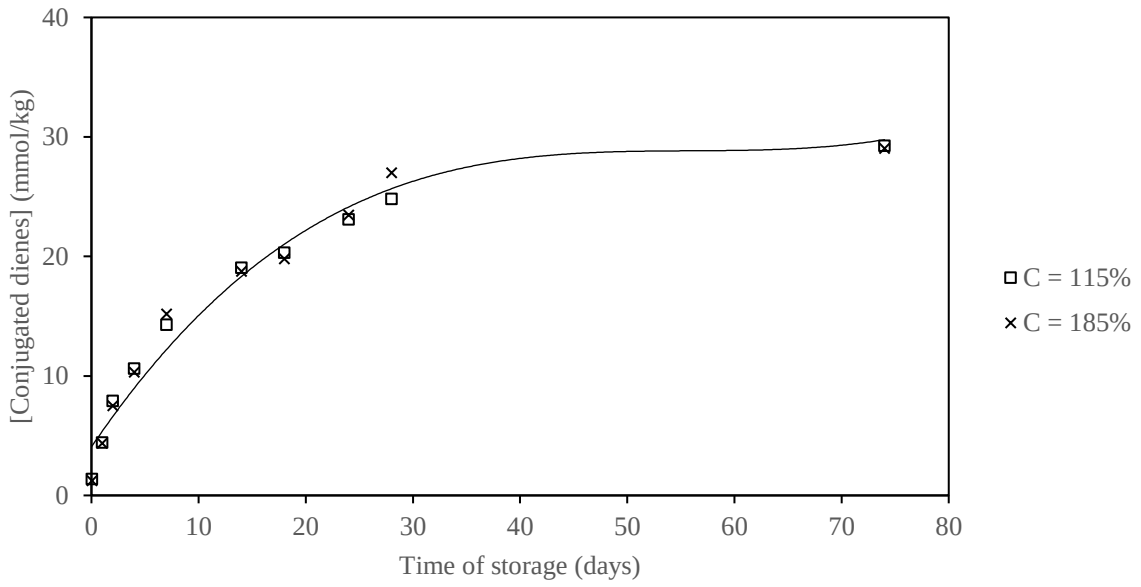

Figure V-6. Evolution of CDs with time during storage of the CNCs-stabilized linseed oil emulsions prepared with two different surface coverage (C), in the presence of 10^{-2} M Fe (II) ions (expressed in mol per L of emulsion).

Results show that the lipid oxidation rates of both emulsions are comparable, suggesting that the scavenging of Fe(II) ions by sulfate ester groups plays the major role in oil protection. The difference in surface coverage between the two systems (116 compared with 187%) does not significantly impact the rate of diffusion of O_2 and/or Fe(II) ions through the CNCs interfacial layer in our experimental conditions, probably because the cellulosic barrier is already effective at 116% coverage. It should be noted that the coverage percentage in these emulsions is much higher than in the systems used for the release studies with RSV (62 to 82% in Table IV-2).

C. Oxidative stability of the emulsions stabilized with chemically modified CNCs

1. Context of the study

We showed in the previous part, that linseed oil emulsions stabilized with unmodified CNCs have a better oxidative stability compared to those stabilized with SDS; yet oxidation still takes

place, although at a lower rate. To further improve the protective properties of the CNCs, we envisaged modifying their surface with functional groups displaying antioxidant or photoactive properties. Indeed, we reported in Chapter I Part E, that lipid oxidation takes place according to two different mechanisms: i) free radical autoxidation (with triplet-state oxygen) and ii) photosensitized oxidation. We reasoned at this stage, that the coating of the CNCs by polydopamine (Figure V-7a) – a biocompatible polymer with antioxidant and radical scavenging properties (Chapter II, Part A.4) – could limit the impact of the first mechanism, while the grafting of cinnamoyle moieties (Figure V-7b) – a photoactive group (Chapter II, Part A.3) – could limit the impact of the second one. Since polydopamine additionally displays UV-absorbing properties, some photoprotection is also expected with this compound. Unfortunately, due to lack of time, only the impact on the first mechanism was investigated, the experiments below being performed only under the protection of light.

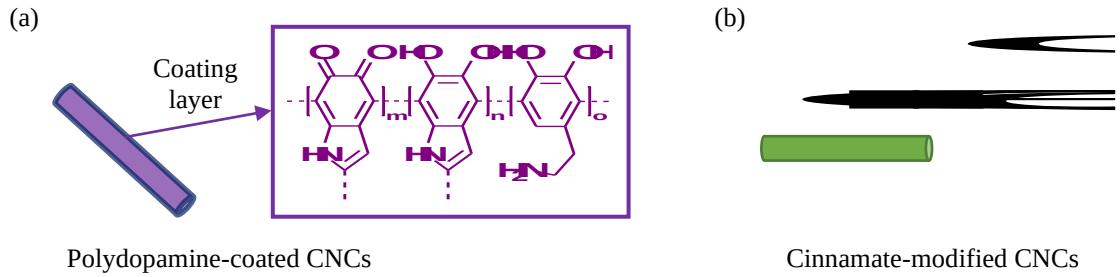

Figure V-7. Chemical structure of the CNCs surface after modification with polydopamine (a) and cinnamoyle moieties (b).

2. Impact of the polydopamine and cinnamoyl functionalization

The polydopamine and cinnamoyl-modified CNCs (CNC-PDA and CNC-Cin, respectively) were prepared according to the protocols described in Chapter II Part A. CNC-Cin-stabilized emulsions were prepared under the same conditions as with the unmodified CNCs in Chapter

V Section A.1.c ([CNCs] = 17.5 g/L of linseed oil; [NaCl] = 75 mM; oil/water ratio = 20% v/v; [Fe(II)] = 10^{-2} M), but the emulsions displayed bigger droplets sizes (D(3,2) = 25 µm instead of 6 µm). For the CNC-PDA-stabilized emulsions, the concentration of particles was reduced in order to produce droplets size in the same range as for the CNC-Cin-stabilized emulsions ([CNCs] = 12.5 g/L; D(3,2) = 25 µm).

The evolution of CDs with time for both emulsions is presented in Figure V-8, together with the results obtained with unmodified CNCs.

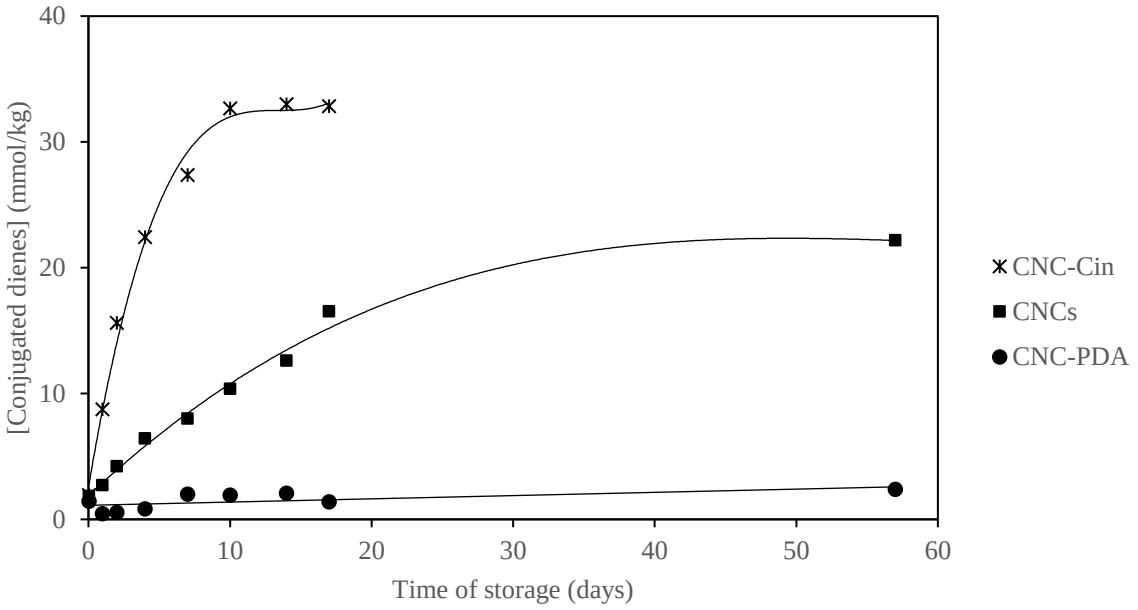

Figure V-8. Evolution of CDs with time during storage of the CNC-Cin, CNC-PDA and CNCs-stabilized linseed oil emulsions, in the presence of 10^{-2} M Fe (II) ions (expressed in mol per L of emulsion). [CNC-Cin] = 17.5 g/L of oil; [CNCs] = 17.5 g/L of oil; [CNC-PDA] = 12.5 g/L of linseed oil; [NaCl] = 75 mM; oil/water ratio = 20% v/v.

The evolution of CDs with time for the different emulsions showed very distinct trends. Interestingly, the emulsion stabilised with the CNC-PDA particles did not show any significant increase of CDs during storage, a maximum CD concentration of only 2 mmol/kg being noted after 57 days. This high oxidative stability was assigned to the radical scavenging and anti-

oxidant properties of polydopamine, thanks to the dihydroxyindole and dopamine units, which can retard lipid oxidation by reacting with oxygen (Figure V-9). Another contributing factor may be the size of the emulsion droplets, which are bigger and thus display a lower interfacial area, meaning that the possibility of contact between linseed oil and Fe(II) ions or O_2 is less. But this effect should be marginal as demonstrated in Figure V-5.

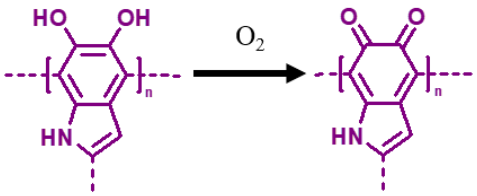

Figure V-9. Oxidation of dihydroxyindole or dopamine units to indolquinone.

With the CNC-Cin particles, a sharp increase in CDs concentration was noted during the first ten days, until a maximum value was reached at about 33 mmol/kg. Therefore, unlike polydopamine, the cinnamoyl moieties do not protect the oil from oxidation. Actually, it has been shown that the presence of hydroxyl groups in the benzene ring is essential for the cinnamoyl derivatives to display antioxidant and radical scavenging properties in line with the free radical autoxidation mechanism (Natella et al., 1999; Perinelli et al., 2022). The photoactive properties of the cinnamoyl group may have a positive impact on the photosensitized oxidation mechanism at stack when samples are irradiated by light, but all our experiments were performed under the protection of light. Compared to the unmodified CNCs, the partial protection by the cellulose particles is lost after the cinnamate grafting, which could result from the conversion of some hydroxyl groups into esters, a higher oxygen transmission rate being expected with the more hydrophobic cellulose esters (Wang et al., 2018).

D. Conclusions

In the first part of this chapter, we confirmed that the unmodified CNCs partially protected linseed oil emulsions from lipid oxidation in comparison to SDS, while the presence of RSV in our experimental conditions did not further improve the oxidative stability. We showed that emulsions with smaller droplets were more oxidized, but varying the CNCs surface coverage at the droplets interface did not affect the oxidative stability in our experimental conditions.

In the second part of this chapter, the protective properties of the CNCs were drastically improved by coating the nanoparticles with polydopamine, using a simple functionalisation process in water. This high oxidative stability was assigned to the radical scavenging and anti-oxidant properties of the dihydroxyindole and dopamine units introduced by the treatment. The grafting of photoactive cinnamate moieties on the other end, did not impart any protection in our experimental conditions, the oxidation profile being similar to the one obtained with SDS. Further experiments are however required to evaluate the impact of this grafting on the photosensitized oxidation mechanism at stack in the presence of light.

References

Davidov-Pardo, G., McClements, D.J., 2014. Resveratrol encapsulation: Designing delivery systems to overcome solubility, stability and bioavailability issues. Trends in Food Science & Technology 38, 88–103. https://doi.org/10.1016/j.tifs.2014.05.003

Frankel, E.N., 2014. Lipid oxidation. Elsevier.

Keramat, M., Kheynoor, N., Golmakani, M.-T., 2022. Oxidative stability of Pickering emulsions. Food Chemistry: X 14, 100279. https://doi.org/10.1016/j.fochx.2022.100279

Natella, F., Nardini, M., Di Felice, M., Scaccini, C., 1999. Benzoic and Cinnamic Acid Derivatives as Antioxidants: Structure−Activity Relation. J. Agric. Food Chem. 47, 1453–1459. https://doi.org/10.1021/jf980737w

Perinelli, D.R., Torregiani, E., Bonacucina, G., Cespi, M., Palmieri, G.F., Gabbianelli, R., 2022. Antioxidant Properties of Ester Derivatives of Cinnamic and Hydroxycinnamic Acids in Nigella sativa and Extra-Virgin Olive Oils-Based Emulsions. Antioxidants 11, 194. https://doi.org/10.3390/antiox11020194

Tańska, M., Mikołajczak, N., Konopka, I., 2018. Comparison of the effect of sinapic and ferulic acids derivatives (4-vinylsyringol vs. 4-vinylguaiacol) as antioxidants of rapeseed, flaxseed, and extra virgin olive oils. Food Chemistry 240, 679–685. https://doi.org/10.1016/j.foodchem.2017.08.007

Wang, J., Gardner, D.J., Stark, N.M., Bousfield, D.W., Tajvidi, M., Cai, Z., 2018. Moisture and Oxygen Barrier Properties of Cellulose Nanomaterial-Based Films. ACS Sustainable Chem. Eng. 6, 49–70. https://doi.org/10.1021/acssuschemeng.7b03523

General conclusions and perspectives

Throughout this thesis, oil-in-water (O/W) Pickering emulsions stabilized by unmodified and modified CNCs were prepared using different oils and salt concentrations, and investigated in terms of stability, surface coverage, encapsulation/release properties, and oxidative protection.

Regardless of the oil investigated – namely hexadecane, isododecane, squalene, sunflower oil, virgin linseed oil, coconut oil and palm oil – a linear dependence of the inverse droplet diameter on CNCs concentration was observed at low particles concentration, in line with the limited coalescence process expected for Pickering emulsions. The surface coverage by the particles around the droplets was estimated by calculating the coverage percentage C and specific surface area S, based on the slope of the limited coalescence domain. Preliminary results with hexadecane as model oil showed a linear dependency of C and S with the ionic strength, demonstrating that the surface coverage by the particles can be monitored by the NaCl concentration. When RSV was incorporated in the internal phase of the emulsion, salt was required anymore to stabilize the emulsion and the C value was now correlated to the RSV concentration instead of the ionic strength, the RSV molecules acting as co-stabilizers at the interface. Part of the RSV seemed to favour the anchoring of CNCs at the O/W interface, supposedly through the formation of complexes by intermolecular forces. Yet, most of the RSV trapped at the interface could be easily released on demand, by triggering its exchange with SDS. Release experiments with high RSV concentrations showed a linear dependency of the interfacial release rate with the surface coverage around the droplets; the lower the surface coverage, the quicker RSV was released.

When the surface of the CNCs was functionalized with hydrophobic octanoyle moieties, no salt was required to stabilize hexadecane-in-water emulsions, and the coverage by the particles was less sensitive to the variations in ionic strength. Stable linseed oil-in-water emulsions were

also obtained with cinnamoyl- and polydopamine-modified CNCs, but the coverage at the O/W interface differ in these systems (higher coverage).

Finally, we confirmed that the unmodified CNCs partially protected linseed oil emulsions from lipid oxidation in comparison to SDS. Emulsions with smaller droplets were more oxidized, but varying the CNCs surface coverage at the droplets interface did not affect the oxidative stability in our experimental conditions. The protective properties of the CNCs were drastically improved by coating the nanoparticles with polydopamine, using a simple functionalisation process in water. This high oxidative stability was assigned to the radical scavenging and anti-oxidant properties of the dihydroxyindole and dopamine units introduced by the treatment. The grafting of photoactive cinnamate moieties on the other end, did not impart any protection in our experimental conditions.

These promising outcomes could find application in formulations for food, pharmaceutical or cosmetics industries.

Based on the research and results in this thesis, the following recommendations are proposed for future studies:

(1) In Chapter III, Part B, we have successfully stabilised linseed oil emulsions with cinnamoyl- and polydopamine-modified CNCs, and showed that the surface coverage by these particles was much higher than when unmodified or octanoyle-modified CNCs were used. This difference in surface coverage was tentatively assigned to differences in chemical structure at the CNCs surface, and/or differences in oil viscosities, but additional experiments are required to clarify this point.

(2) We demonstrated in this thesis that the emulsification of linseed oil with unmodified CNCs, or even better with polydopamine-modified CNCs, improved significantly the oxidative stability of the oil, while the photoactive cinnamoyle-modified CNCs did not impart any protection. However, these experiments were performed under the protection of light, while lipid oxidation can take place according to two different mechanisms: i) free radical autoxidation (no light involved) and ii) photosensitized oxidation. Only the impact of the first mechanism was investigated up to now, and further investigations are required to evaluate the impact of light on our systems. In particular, a positive impact of the photoactive cinnamoyle-modified CNCs is expected in these conditions.

(3) The encapsulation and release properties of the hexadecane-in-water emulsions loaded with *trans*-RSV were investigated in the current thesis, but this molecule is highly photosensitive and rapidly isomerizes to *cis*-RSV when exposed to UV or visible light. It would be therefore important in future work, to investigate the photostability of the molecule encapsulated in the CNCs emulsions. Chemical functionalization of the CNCs could be also envisaged to further improve the stability of RSV if necessary.

(4) The encapsulation and release properties of CNC emulsions loaded with RSV were investigated using hexadecane as model oil, but the study should be now extended to other commercial oils used in industry.